

**CABLE STAYED BRIDGES: NONLINEAR ELASTIC DIMENSIONAL
ANALYSIS**

Walter F. Janzen

B. A. Sc. The University of British Columbia, 1978

A THESIS SUBMITTED IN PARTIAL FULFILLMENT OF
THE REQUIREMENTS FOR THE DEGREE OF
MASTER OF APPLIED SCIENCE

in

THE FACULTY OF GRADUATE STUDIES
DEPARTMENT OF CIVIL ENGINEERING

We accept this thesis as conforming
to the required standard

THE UNIVERSITY OF BRITISH COLUMBIA

April 1988

© Walter F. Janzen

In presenting this thesis in partial fulfilment of the requirements for an advanced degree at the University of British Columbia, I agree that the Library shall make it freely available for reference and study. I further agree that permission for extensive copying of this thesis for scholarly purposes may be granted by the head of my department or by his or her representatives. It is understood that copying or publication of this thesis for financial gain shall not be allowed without my written permission.

Department of CIVIL ENGINEERING

The University of British Columbia
Vancouver, Canada

Date APRIL 27, 1988

Abstract

Cable stayed bridges are the state of the art in long span bridges. Developments in cable response analysis and computer hardware and software have allowed engineers to design and build many cable stayed bridges. Bridges of many different configurations with longer and longer spans are being built. With the long spans and high axial loads in the deck, the stability of cable stayed bridges becomes a growing concern. Current analysis procedures use a parabolic approximation to the true catenary response of cables, which is quite accurate for tight cables; however, for near instability conditions with the accompanying large deflections and consequently loose cables, a catenary model is called for. Herein, a study is conducted on the elastic stability of cable stayed bridges utilizing a true catenary model of cable response. A dimensional analysis of cable stayed bridge stability is undertaken as well as deck maximum deflection and moment under service load conditions.

A computer program written by this author is the analysis tool used in this work. The program is given the acronym ULA which stands for Ultimate Load Analysis. ULA is a nonlinear plane frame program with catenary cable elements and an interactive graphics interface. The dimensional analysis is carried out by comparing the computer model of a cable stayed bridge to the theoretical model of a beam on an elastic foundation. Two preliminary simplified cable stayed bridge backspan models are studied first in order to develop the dimensionless ratios that are applicable to the bridge response and to gain an insight into the cable stayed bridge behaviour. The final model is that of an entire cable stayed bridge. Because of the multitude of parameters governing cable stayed bridge behaviour it is not possible to describe all cable stayed bridges. Instead, the dimensionless behaviour of a standard model is examined and the sensitivity of this standard to various parameter variations is given in the form of dimensionless charts.

Finally, a preliminary design and analysis aid is developed from the dimensionless charts and is then applied to two existing bridge designs.

Table of Contents

Abstract	ii
List of Tables	vii
List of Figures	viii
Nomenclature	xii
Special Subscript Notation	xiv
Acknowledgement	xv
1 Introduction	1
1.1 Development of Cable Stayed Bridges	1
1.2 Advantages of Multi-Cable Stayed Bridges	6
1.3 Scope of Thesis	7
2 Analysis System	9
2.1 Current Analysis Procedures	9
2.1.1 Deck Stability	10
2.1.2 Bridge Response	11
2.2 Proposed Analysis Procedure	13
2.3 Dimensional Analysis	15
2.4 Computer Models Analyzed	15
3 Simplified Backspan Model	18
3.1 The Model	18

3.2	Stability	20
3.2.1	Stability Dimensionless Ratios	21
3.2.2	Parameters and Ratios from Existing Bridge Designs	26
3.2.3	Results of Stability Analysis	28
3.3	Deflection and Moment	35
3.3.1	Deflection Dimensionless Ratios	35
3.3.2	Results of Deflection Analysis	39
3.3.3	Moment Dimensionless Ratios	44
3.3.4	Results of Moment Analysis	46
4	Backspan Model	53
4.1	The Model	53
4.2	Stability	55
4.2.1	Stability Dimensionless Ratios	55
4.2.2	Parameters and Ratios from Existing Bridge Designs	58
4.2.3	Results of Stability Analysis	59
4.3	Deflection and Moment	66
4.3.1	Results of Deflection Analysis	67
4.3.2	Results of Moment Analysis	71
5	Full Bridge Model	76
5.1	The Model	76
5.2	Stability	82
5.2.1	Stability Dimensionless Ratios	82
5.2.2	Parameters and Ratios from Existing Bridge Designs	85
5.2.3	Results of Stability Analysis	87
5.3	Deflection and Moment	98
5.3.1	Results of Deflection Analysis	101

5.3.2	Results of Moment Analysis	108
6	Application	116
6.1	The Model	116
6.2	Procedure	117
6.2.1	Stability	118
6.2.2	Deflection and Moment	118
6.3	Examples	119
6.3.1	Stability	119
6.3.2	Deflection and Moment	120
7	Conclusion	124
7.1	Further Research	125
	Bibliography	128
A	Catenary Cable	131
B	ULA Implementation of Catenary Cable	140
C	Data From Existing Cable Stayed Bridge Designs	144
C.1	Backspan Data from Bridge Designs for Simplified Backspan Model . . .	146
C.2	Backspan Ratios from Bridge Designs for Simplified Backspan Model . .	147
C.3	Backspan Data from Bridge Designs for Backspan Model	148
C.4	Backspan Ratios from Bridge Designs for Backspan Model	149
C.5	Bridge Data from Bridge Designs for Full Bridge Model	150
C.6	Bridge Ratios from Bridge Designs for Full Bridge Model	152
D	Maximum Deflection and Moment	153

List of Tables

6.1	Check on applicability.	119
6.2	Summary of stability analysis.	120
6.3	Summary of deflection analysis.	121
6.4	Summary of moment analysis.	122

List of Figures

1.1	First modern cable stayed bridges.	3
1.2	Cable bearings in towers.	4
1.3	Modern cable stayed bridge.	5
1.4	Truss model of cable stayed bridge.	5
2.5	Progressive computer models of cable stayed bridges. (Models drawn to different scales.)	17
3.6	Simplified backspan model.	20
3.7	Derivation of elastic foundation modulus.	23
3.8	Stability failure of simplified backspan model.	29
3.9	Stability factor of safety with uplift pressure.	30
3.10	Stability of simplified backspan model (F/F_H).	33
3.11	Stability of simplified backspan model.	33
3.12	Stability of simplified backspan model— n varied.	34
3.13	Examples of deflection decay in a beam on an elastic foundation.	36
3.14	Dimensionless plot of Hetényi's deflection.	39
3.15	Deflection of standard simple backspan model.	40
3.16	Magnification of maximum deflection.	41
3.17	Dimensionless deflection versus dimensionless cable tautness.	42
3.18	Dimensionless deflection versus dimensionless decay length.	43
3.19	Dimensionless deflection versus dimensionless load.	44
3.20	Dimensionless plot of Hetényi's moment.	46
3.21	Moment of standard simple backspan model.	47
3.22	Bridge deck construction methods.	48

3.23	Magnification of maximum moment.	49
3.24	Dimensionless moment versus dimensionless cable tautness.	51
3.25	Dimensionless moment versus dimensionless decay length.	51
3.26	Dimensionless moment versus dimensionless load.	52
4.27	Backspan model.	54
4.28	Free-body diagram of a cable-deck connection.	55
4.29	Stability failure of backspan model.	60
4.30	Stability factor of safety of backspan model.	61
4.31	Critical simplified backspan section.	62
4.32	Critical backspan section.	63
4.33	Stability of backspan model.	65
4.34	Stability of backspan model— l_D/l_B varied.	65
4.35	Deflection of standard backspan model.	68
4.36	Magnification of maximum deflection.	69
4.37	Dimensionless deflection versus dimensionless decay length.	70
4.38	Dimensionless deflection versus dimensionless cable tautness.	70
4.39	Dimensionless deflection versus dimensionless load.	71
4.40	Moment of standard backspan model.	72
4.41	Magnification of maximum moment.	73
4.42	Dimensionless moment versus dimensionless decay length.	74
4.43	Dimensionless moment versus dimensionless cable tautness.	74
4.44	Dimensionless moment versus dimensionless load.	75
5.45	Bridge model (half shown—symmetric, except right bearing is a fixed pin).	77
5.46	Free body diagram of bridge model (half shown—symmetric).	80
5.47	Axial influence lines and load cases for instability.	88
5.48	Stability failure of standard bridge model—load cases 1 and 2.	89

5.49	Stability failure of standard bridge model—load cases 3 and 4.	90
5.50	Stability factor of safety of bridge model.	92
5.51	Critical deck section for each load case.	94
5.52	Stability of full bridge model.	95
5.53	Critical deck section for varying F/F_H	96
5.54	Factor of safety vs F/F_H	97
5.55	Stability of full bridge model— l_D/l_B varied.	98
5.56	Stability of full bridge model— $A_{C_a}/\sum A_C$ varied.	99
5.57	Stability of full bridge model— $E_T I_T/EI$ varied.	99
5.58	Load cases for maximum backspan and mainspan deflection.	102
5.59	Maximum backspan deflection (magnified 200 times) of standard full bridge model.	102
5.60	Maximum mainspan deflection (magnified 200 times) of standard full bridge model.	103
5.61	Magnification of maximum deflection.	104
5.62	Dimensionless deflection versus dimensionless decay length.	105
5.63	Dimensionless deflection versus dimensionless cable tautness.	106
5.64	Dimensionless deflection versus dimensionless load.	106
5.65	Dimensionless deflection versus dimensionless cable area.	107
5.66	Dimensionless deflection versus dimensionless tower stiffness.	107
5.67	Load cases for maximum backspan and mainspan moment.	108
5.68	Maximum backspan moment of standard full bridge model.	109
5.69	Maximum mainspan moment of standard full bridge model.	110
5.70	Magnification of maximum moment.	111
5.71	Dimensionless moment versus dimensionless decay length.	112
5.72	Dimensionless moment versus dimensionless cable tautness.	113
5.73	Dimensionless moment versus dimensionless load.	114

5.74 Dimensionless moment versus dimensionless cable area.	115
5.75 Dimensionless moment versus dimensionless tower stiffness.	115
7.76 Plastic stability failure of bridge model.	127
7.77 Plastic hinge failure of bridge model.	127
A.78 Catenary cable element.	131
A.79 Catenary cable.	132
A.80 Pin ended member equivalent to catenary cable.	135
A.81 Elongation of catenary cable.	135
A.82 Bar extension under a change in tension.	138
A.83 Relative motion perpendicular to cable chord.	138
B.84 Behaviour of catenary cable under load changes.	140

Nomenclature

A_C	cable cross sectional area
A_{C_a}	total anchor cable cross sectional area
E	deck elastic modulus
E_C	cable elastic modulus
E_T	tower elastic modulus
F	axial load in deck at tower due to dead load
F_H	buckling load for a beam-column on an elastic foundation
f	dimensionless cable tautness
H	horizontal cable force
h	cable height
h_T	tower height
I	deck moment of inertia
I_T	tower moment of inertia
k	elastic foundation modulus
L	cable horizontal projected length
l_B	backspan length
l_D	backspan decay length
l_M	mainspan length
M_B	maximum backspan moment
M_M	maximum mainspan moment
M_H	Hetenyi's beam on an elastic foundation moment
N	number of deck intervals in the backspan
N_C	number of cables in the backspan or half the mainspan
n	number of half-waves in a buckled shape

P	axial load in tower at base due to dead load
P_T	Tang's critical axial load in the deck
S	cable chord length
s	cable spacing at deck or length of deck interval
s'	cable spacing at tower
T	dead load cable tension in the chord direction
T_s	service (dead plus live) load cable tension
w_C	weight per unit length of cable
w_D	uniformly distributed dead load
w_L	uniformly distributed live load
α	dummy variable
β	dummy variable
β_T	Tang's elastic foundation constant
γ	dummy variable
γ_C	cable density
Δ	cable elongation in the chord direction
δ	deck vertical deflection
δ_B	maximum backspan deflection
δ_M	maximum mainspan deflection
δ_H	maximum deflection of a beam-column on an elastic foundation
λ	load level
σ_C	cable stress
θ	cable chord angle of inclination to deck

Special Subscript Notation

<i>avg</i>	average
<i>c</i>	critical
<i>cen</i>	centroid
<i>eff</i>	effective
<i>sec</i>	secant
<i>tan</i>	tangent
⌒	half-wave
□	standard model
*	value from computer analysis (superscript)

Acknowledgement

I would like to thank Dr. Roy Hooley for his support and direction throughout this research.

This work would not have been possible without the funding provided by the National Sciences and Engineering Research Council of Canada.

I would like to thank the University of British Columbia for providing an excellent research environment, and I thank the Civil Engineering Department for their help and for the provision of excellent computer analysis tools by way of their Computer Graphics Laboratory.

I would especially like to express my gratitude to the two ladies in my life. I thank my mother for her confidence in me and my wife for her patience and support.

Chapter 1

Introduction

1.1 Development of Cable Stayed Bridges

The concept of supporting a beam with stays is not a new one. Egyptians used the idea for their sailing ships and in some tropical regions vines attached to trees were used to support walkways. Several cable stayed bridges were built in Europe from 1784 to 1824 using timber, wire, chain and iron bar stays. However, the development of cable stayed bridges stopped there due to the collapse of several bridges. It was Navier who reported on these failures and made the comment that suspension bridges were preferable. This suggestion of Navier's was enough to cause bridge engineers to abandon the cable stayed bridge concept [1,2].

The use of stay cables was not entirely abandoned, as several suspension bridges had inclined ropes in addition to vertical hangers. However, the low strength of the stays precluded prestressing, so the stays were installed in a slack condition. These stays would simply elongate due to sag reduction when loaded, thus were ineffectual under service loads. It was not until 1938 that stay cables were again used in a bridge design as main load carrying members. Dischinger had the task of designing a railway bridge over the Elbe River and he found that the deflections of a suspension bridge could be significantly reduced if tight wires were used as supplemental stays.

After World War II, the rebuilding of Germany's bridges brought the cable stayed bridge back into favour, largely due to the need for economy of steel. Earlier cable stayed bridges failed due to inferior materials and a misunderstanding of the structural behaviour of the cables. Now, with better materials and armed with Dischinger's

findings, which were published in 1949 [3], cable stayed bridges were proposed for the reconstruction of bridges over the Rhine River.

The first modern cable stayed bridges were essentially beam bridges with only 2 to 6 stays in the main span as shown in Figure 1.1. The spans between cable supports were between 30 and 60 meters, with the cables acting as major supports, taking the place of piers. This reduced the bending stresses in the deck, allowing smaller cross sections; hence, a saving in steel. With the limited number of stays along the span, the cables had to carry major portions of the bridge dead load and live load, thus the cables were very large and the connections to the deck and anchor were quite complicated. To reduce tower moments, special roller and rocker bearings were built which allowed the cables to pass through the tower, as shown in Figure 1.2. Along with the heavy members and elaborate bearings, the construction of these bridges still required falsework.

Several arrangements of cable layout and tower shape were used as can be seen in Figure 1.1. Radiating cable layouts with the cables converging to one area on the tower, and harp designs with the cables parallel to each other were used in conjunction with single plane cable, double plane cable and double inclined plane cable systems (A-frame towers). These configurations were used in single tower and multi-tower bridges. The deck was sometimes rigidly supported at the tower and in other designs the deck passed through the tower with only side bearings provided. Fixed-base and pinned-base towers were both used.

As experience was gained in the design and construction of cable stayed bridges it was found that most difficulties disappeared if a larger number of stays was used such that the cable spacing at the deck was from 8 to 15 meters [4]. With this many cables, it was no longer possible to connect all the cables at one point for a radiating layout and complicated tower bearings for harp bridges had to be abandoned.

Figure 1.3 shows a modern cable stayed bridge with a fan shape arrangement of cables. In this system, the deck behaves more like the bottom chord of a truss, rather

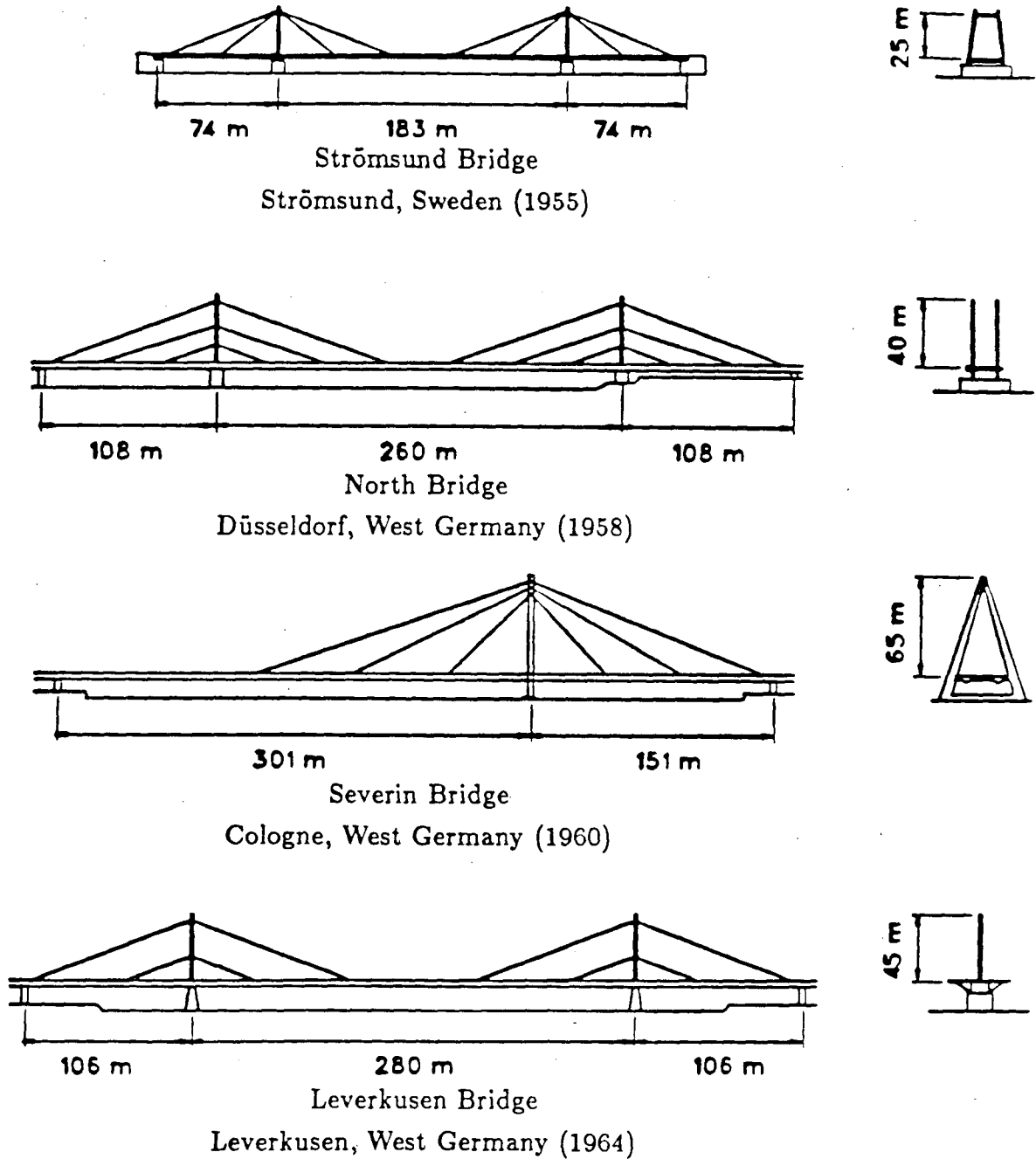


Figure 1.1: First modern cable stayed bridges.

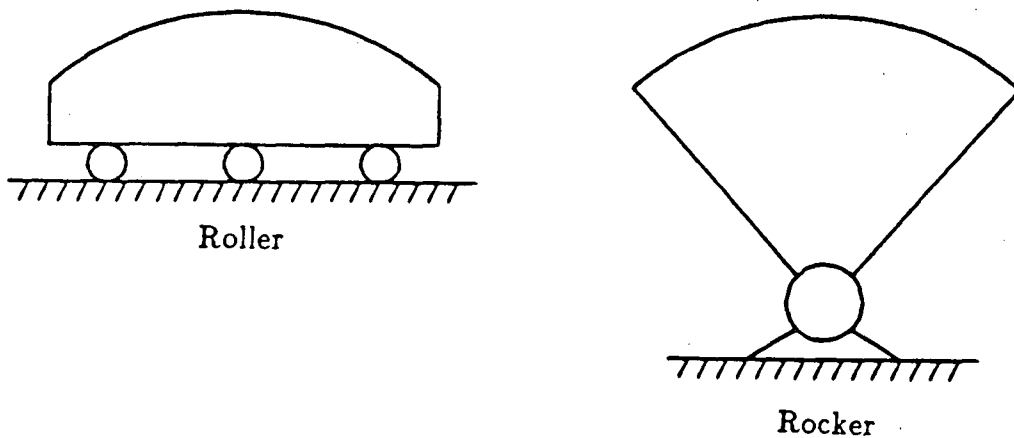
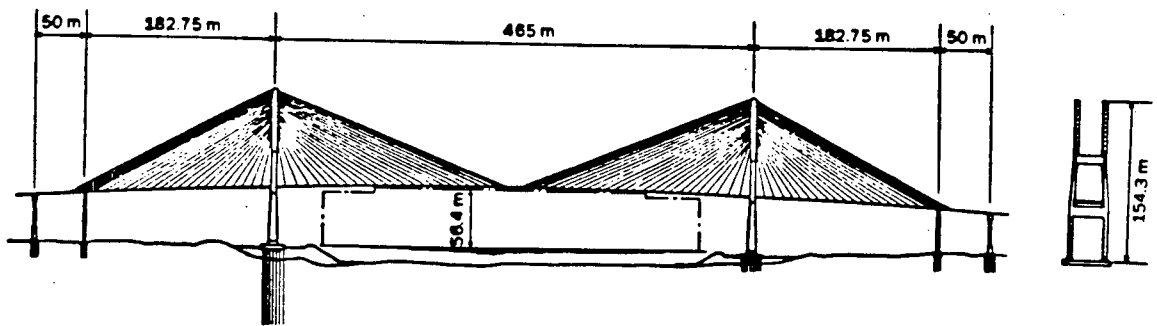


Figure 1.2: Cable bearings in towers.

than a simply supported beam. This analogy is outlined in Figure 1.4. The basic element (a) is a pin connected truss made of four members, and the weight W is supported entirely by axial stress. The weight can be applied in different positions along the deck, and to accommodate this, extra members are built into the truss (b). A complete bridge can be modelled as a pin connected truss (c) and all loads on the deck panel points are supported by axial stress. With the deck modelled as a continuous beam rather than pin connected beams, the structure still behaves as a truss with only secondary bending stresses in the deck. The final extension of the truss model is to distribute the cable connections along the towers (d). This induces primary bending stress into the structure to produce a frame not a truss; however, the bridge can be made nearly moment free for dead load.

The evolution toward modern cable stayed bridges was made possible by the development of orthotropic steel and concrete decks that could bear large axial forces, together with the advent of the computer. With the nonlinear cable behaviour modelled in a computer program and with the tremendous computing power available, the analysis of multi-cable stayed bridges became easy.



Alex Fraser Bridge
Vancouver, British Columbia, Canada (1986)

Figure 1.3: Modern cable stayed bridge.

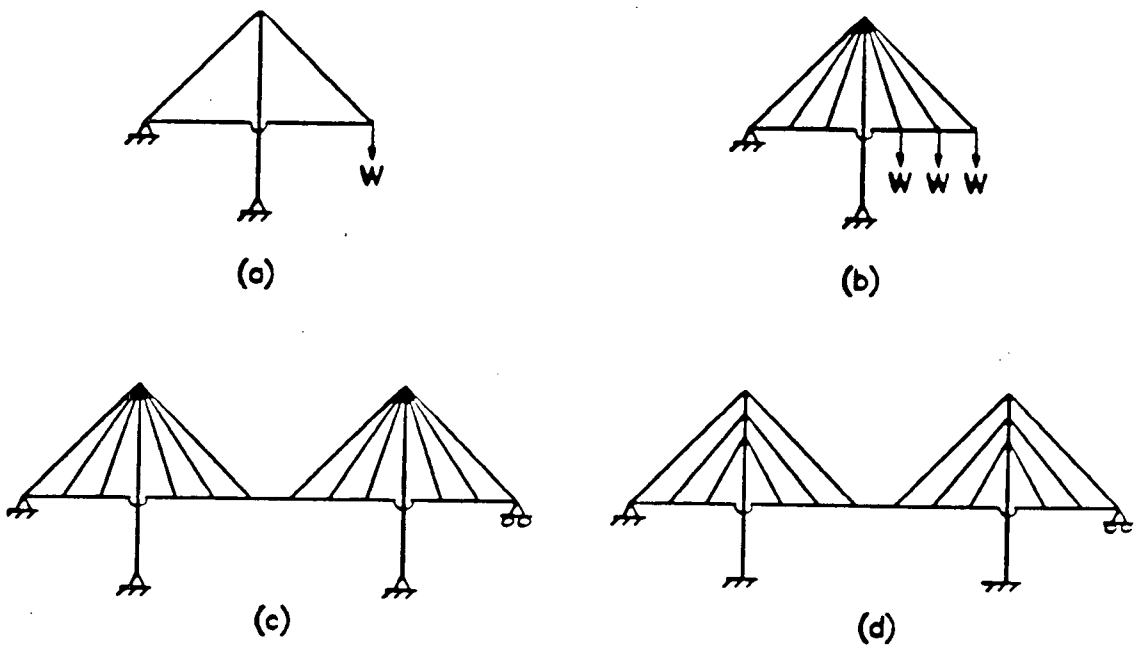


Figure 1.4: Truss model of cable stayed bridge.

1.2 Advantages of Multi-Cable Stayed Bridges

There are many advantages of multi-cable stayed bridges over other types of bridges. The original necessity that brought about cable stayed bridge designs was to have long span bridges that used a minimum of steel. With the cables acting as supports from above the deck, the cost of constructing deep water falsework was eliminated and the passage for navigation was kept open during construction.

Cable stayed bridges share the advantage with suspension and arch bridges that the dead load stresses can be controlled by the erection procedure. With some skill during construction, the dead load of the bridge can be carried moment free. In addition, cable stayed bridges can have smaller live load moments. For suspension and three-hinged arch bridges the maximum live load moment is approximately $w_L l_M^2 / 60$, while for a cable stayed bridge it is about $w_L l_M^2 / 440$. Thus, the deck moments are greatly reduced and a smaller cross section is possible. This results in a lighter bridge that is easier to support and allows even longer spans.

Both suspension and cable stayed bridges can have aerodynamically streamlined decks, but cable stayed bridges have inherent characteristics that make them superior to suspension bridges. In a cable stayed bridge, each of the cables—with the mass of the deck attached to it—has a different natural frequency, and if external forces try to set up resonant flexural oscillations of the deck, the vibrations are effectively dampened by the interference of cables with different frequencies.

A more dramatic aerodynamic advantage is in the resistance to the antisymmetric torsional mode of oscillation—the mode which led to the collapse of the Tacoma-Narrows Bridge. In a suspension bridge the two cables can move against each other, one going up in half of the span and the other going down; thus, allowing torsional movement of the deck. In cable stayed bridges the cables themselves provide a large resistance against this torsional movement. The difference in deflection of the two cable planes is mainly due to the different deflection of the towers in each plane, and with the tower

tops being tied with stiff back stays, the tower movements are much smaller than suspension bridge towers. Further torsional resistance is possible by connecting the towers as shown in Figure 1.1 (top bridge) or by constructing an A-frame as shown by the third bridge of Figure 1.1. Thus, cable stayed bridge decks need not have as large a torsional stiffness as suspension bridge decks.

Further economic advantages are acquired in the ease of erection of cable stayed bridges. The need for heavy suspension cable anchors is gone, and with fixed base towers the cantilever method of construction can be employed, which eliminates the need for falsework. As the number of cables in a span increases, the cables become lighter, the connections are simpler and the construction cantilever length decreases. The construction misalignment at the center of the main span is easily adjusted by slackening and tightening the appropriate cables. Finally, and perhaps paramount to the public who use bridges every day, cable stayed bridges are very aesthetically pleasing.

1.3 Scope of Thesis

The work presented herein was undertaken in order to compare existing cable stayed bridges and to allow preliminary design and analysis without the use of a computer. A large number of cable stayed bridges exist, all of different spans, tower sizes, cable configurations and deck cross sections. In order to compare the wide range of cable stayed bridges, dimensional analysis is used to study the stability, deflections and moments of a cable stayed bridge computer model. Once the behaviour of cable stayed bridges is presented in the form of dimensionless charts, a preliminary design and analysis aid which uses these charts, is developed.

This thesis is applicable to multi-cable stayed bridges with a fan type of cable arrangement (Fig 1.3). Double-tower bridges with fixed bases are modelled with an elastic support—equivalent to one cable—for the deck at each tower. The cables are

attached to the towers rather than allowed to pass through.

The response of the bridge computer model is presented as an analogy to a simple beam on an elastic foundation. Nonlinear elastic computer analysis is done for deck stability as well as for maximum deflection and moment. The response of the deck is determined for distributed live loads. A plane frame analysis is used, thus out of plane loads from wind or earthquake are not considered. Torsion is not considered and axial deformations of the deck and towers are neglected.

Chapter 2

Analysis System

2.1 Current Analysis Procedures

Cable stayed bridges are complicated structures to analyze, just like any other bridge or structure. Analysis procedures for calculating the deflections, moments and buckling behaviour, must be derived based on a model of the actual structure and the materials it is made of. Some assumptions used in the model can be very true to the real situation, such as Young's modulus being constant with increasing strain and plane sections remaining plane upon a change in curvature of a beam. But all models have their limits of validity such as Young's modulus changing when strains become plastic and plane sections not remaining plane for certain cross section shapes.

Some of the modelling assumptions in cable stayed bridges concern the deck stiffness, the axial load in the deck, the cable behaviour and the beam-column on an elastic foundation behaviour of the deck. The deck stiffness of cable stayed bridges can for the majority of the span be constant because of the nature of the moment distribution in the deck. However, because of the increasing axial load induced in the deck by the cables, the cross-sectional area of the deck near the towers might be increased, thus increasing the stiffness as a by-product. The cables are of varying cross-sectional area and tension and hang in the shape of a catenary which results in a varying nonlinear cable behaviour along the span. The combination of the deck stiffness and axial load variations and the cable variation with the cable nonlinearity and deck beam-column nonlinear behaviour makes the beam-column on an elastic foundation model very complex.

The following two sections are overviews of how some researchers have modelled the

cable stayed bridge behaviour at buckling loads and at service loads.

2.1.1 Deck Stability

The most commonly used check for deck buckling is Tang's approximate formula [5] :

$$P_T = 2\sqrt{EI\beta_T}$$

where

P_T = Tang's critical axial load in the deck

E = deck elastic modulus

I = deck moment of inertia

β_T = Tang's elastic foundation constant

$\beta_T = E_C A_C / sS$

E_C = cable elastic modulus

A_C = cable cross-sectional area

S = cable chord length

s = length of deck interval between cables

This is derived from an analogy with a beam-column on an elastic foundation where the axial load is constant throughout the beam-column and the beam stiffness does not vary. This formula is for buckling with no variation of cable stiffness along the beam and with the cables themselves modelled as linear springs. Tang has compared the results from this approximation with that obtained from a computer model based on an energy method that includes the tower interaction with the deck and cables (modelled as linear springs). The computer model accounted for the varying deck axial load and stiffness as well as the varying cable stiffnesses. It was found that the two models give almost identical results for the critical axial load.

Tang's approximation is good for short span bridges only. The deflections of short span bridges are still fairly small near instability, so good analytical results can be

obtained from the linear cable model. With cable stayed bridges being designed with ever longer spans and increasingly slender decks, closer investigation which includes cable nonlinearity, is required.

2.1.2 Bridge Response

Hand calculation procedures to determine several preliminary cable stayed bridge parameters are given in an excellent book by Gimsing [6]. Troitsky [2] also gives approximate hand calculation methods in a chapter of his book. However, because cable stayed bridges are highly statically indeterminate, computer solutions are needed to perform the final detailed analyses of these structures.

Several authors have presented methods of cable stayed bridge analysis suitable for computer application. Smith [7,8] developed a mixed force-displacement method for analysis of single and double plane cable stayed bridges. This was one of the first analytical tools developed for cable stayed bridges and the effects of cable sag and beam-column behaviour were not included. Troitsky and Lazar [9] used a flexibility method to compare with their tests on a physical model. Their physical model included nonlinear effects but their analytical model was still linear. Lazar [10] also used the stiffness method and included nonlinear cables with movable tower-cable connections. Tang [11] employed the transfer matrix method and reproduced the nonlinear cable behaviour with fictitious loads. A three-dimensional linear finite element procedure was presented by Kajita and Cheung [12] for both static and dynamic analysis. Rajaraman, Loganathan and Raman [13] modified a plane frame stiffness program to include beam-column and cable nonlinearity. Como, Grimaldi and Maceri [14] developed a continuous model of cable stayed bridges based on their truss-like behaviour and presented the results in nondimensional form. An energy method of analysis was developed by Hegab [15] in which a small number of Fourier terms for the assumed deflected shape of the deck was sufficient to allow quick convergence.

In all of the above references where cable nonlinearity was modelled, the Ernst [16] or Dischinger equivalent modulus of elasticity was used. For cable stayed bridges with small live to dead load ratios, as was the case for early bridges, the tangent modulus could be used:

$$E_{tan} = \frac{E_C}{1 + \frac{(w_C L)^2 A_C E_C}{12T_s^3}}$$

where

E_{tan} = cable tangent modulus of elasticity

T_s = service (dead plus live) load cable tension

L = horizontal projected length of cable

w_C = weight per unit length of cable

and the other symbols are as defined previously.

For multi-cable stayed bridges the deck is slender, thus lighter than early bridges which results in a higher live to dead load ratio. The initial cable tautness is much less than was the case for early cable stayed bridges, thus the change in cable tension due to the application of live loads is more important and the secant modulus should be used:

$$E_{sec} = \frac{E_C}{1 + \frac{(w_C L)^2 A_C E_C (T + T_s)}{24T^2 T_s}} \quad (2.1)$$

where

E_{sec} = cable secant modulus of elasticity

T = dead load cable tension

The derivation for these formulas assumed a parabolic rather than a true catenary cable shape and the force in the chord direction was taken as the cable tension. Ito and Maeda [17] presented a derivation based on a parabolic cable shape but used the

true cable tension. They noted however, that the difference between using the force in the chord direction and using the true cable tension or the force tangent to the cable was negligible.

2.2 Proposed Analysis Procedure

The model used in developing the analysis procedure used herein incorporates catenaries as the cable shapes with the secant equivalent modulus, $P-\Delta$ effects for beam-columns, and is limited to elastic behaviour.

The analyses conducted for this thesis were done using a plane frame computer program written by this author. The program was designed for ultimate load analysis combining second order effects with plastic hinge formation and is given the acronym ULA. The nonlinear analysis is achieved by incorporating stability functions into member matrices to model the $P-\Delta$ behaviour and by using equivalent areas for cables based on the catenary shape to model the effect of cable sag. Further details of ULA concerning plastic hinge formation, moment axial interaction, strain hardening and the interactive graphics capabilities are given in a thesis by Mill [18]. Details of ULA that are important to this thesis are given in the following paragraphs.

The stability functions used are standard and are presented by many authors including Weaver and Gere [19]. The stability functions depend on the axial forces, and the axial forces depend on the deflected shape. It is therefore necessary to use an iterative procedure to find the solution. This is handled by the interactive graphics format of ULA, where the user can decide upon convergence of the $P-\Delta$ effect by observing the changes in the determinant of the structure matrix.

Most authors use an equivalent Young's modulus to model the stiffness of straight line cable members as actual sagging cables. Herein, an equivalent area is used instead. This choice is a matter of convenience only, in that it is the stiffness of the cable that changes with sag and not the area or elastic modulus. The data input requirements of

ULA are such that each cable can be assigned a unique area easier than an individual modulus.

The equivalent cable area also depends on the axial forces and an iterative procedure is necessary just as for the stability functions. However, this does not mean that separate iterations need to be done because the recalculations for cable sag can be performed during the same iterations that are required for $P-\Delta$ convergence. The convergence of cable area change is monitored by ULA in the same manner and at the same time as that for $P-\Delta$.

Most authors also use what they cite as a parabolic derivation of equivalent cable stiffness (Equation 2.1). The derivation is in fact a hybrid, in that a parabolic shape of the cable is assumed while the weight per unit cable length is used instead of the load per horizontal projection as for a true parabolic deflected shape. Authors were hesitant to use a full catenary derivation because of its complexity, but with series substitution it becomes manageable. The derivation by Hooley [20] is repeated in Appendix A. Note that the equivalent stiffness from this derivation is exactly the same as that from the hybrid derivation. This can be seen by manipulating Equation A.1 appropriately until Equation 2.1 appears with A_C in the place of E_C .

As stated previously, the two derivations produce identical results because of the cable self weight manipulation. In a parabola, the self weight is a constant load per horizontal length; in a catenary, it is a constant load per cable length. The two self weights are related by $\cos \theta$ where θ is the angle between the horizon and the tangent to the cable at any point along the cable. If the cable is tight, then θ is approximately constant and the parabolic and catenary solutions are the same. For a slack cable, θ is not constant and the parabolic solution will not be the same as the catenary.

A comparison between the parabolic method and the catenary method has been made by this author and found that for tight cables ($f = 7$) there is only a 0.1% to 1% difference in deflections. For slack cables ($f = 2$), the parabolic solution is 10% to

15% in error from the catenary solution.

A graphical representation of cable tautness f is given in Appendix B along with an explanation of the implementation of cables into ULA.

2.3 Dimensional Analysis

The response of a cable stayed bridge depends on a multitude of parameters. With the use of dimensional analysis, the parameters can be isolated and the behaviour of a structure can be studied in a more logical manner. The principles of dimensional analysis are well known, with a good explanation of the theory given by Goodier [21]. The procedure in dimensional analysis is to identify all the independent parameters affecting the structure and then construct independent dimensionless ratios using these parameters. A very useful feature of this technique is that the number of dimensionless ratios to be studied is two less than the number of parameters.

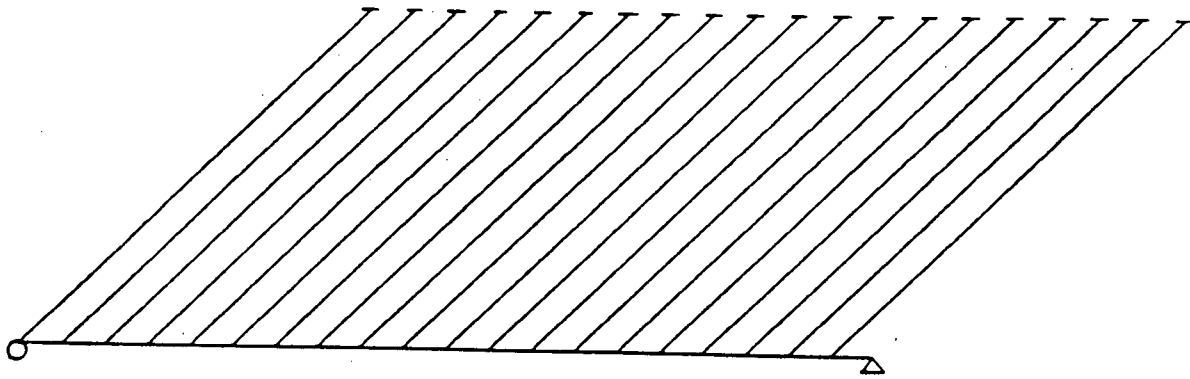
Comparisons can be made between the complex structure at hand and a simpler similar structure. Thus, the complex structure can be thought of as the simple structure with some adjustments. The use of a simple model is also an aid in choosing the parameters that would affect the real structure. The dimensionless ratios are independent, so one ratio can be altered and the response studied without affecting the other ratios. The results from dimensional analysis are applicable to all similar structures, for which the characteristic ratios are the same.

2.4 Computer Models Analyzed

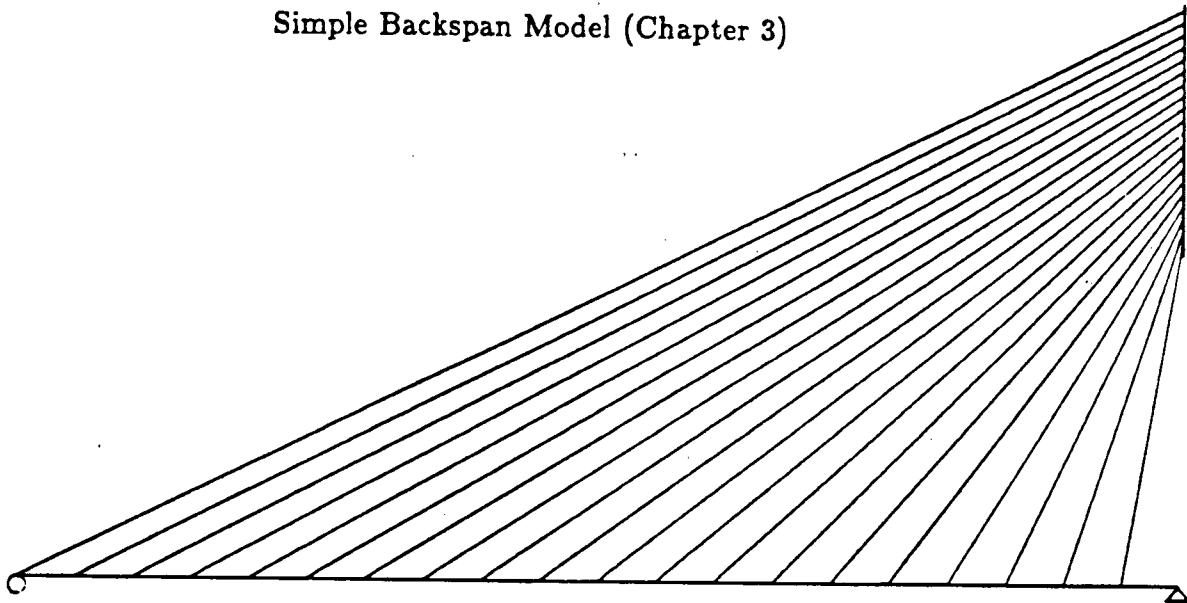
In order to gain an understanding of cable stayed bridge behaviour, the analogy to a beam-column on an elastic foundation will be made. Three computer models of progressive complexity are studied. An extremely simple model is studied first to facilitate the derivations of the dimensionless ratios used to describe the model. The first model

is also designed to display very similar behaviour to that of a beam-column on an elastic foundation. This model is shown in Figure 2.5 and represents the backspan of a cable stayed bridge with the use of uniform cables of constant length. The first model has a constant foundation modulus and is not a good representation of a cable stayed bridge backspan; therefore, the second model is designed to be a truer representation of a cable stayed bridge backspan without adding too many complexities. The second model—also shown in Figure 2.5—has varying cable areas and lengths and the cables are attached to an immovable tower. This model will display the effects of a varying foundation stiffness without the added complexity of a flexible tower. The third model is of an entire cable stayed bridge. The boundary conditions are drawn on Figure 2.5 as well, with the deck vertical support at the tower being equivalent to one vertical cable stay.

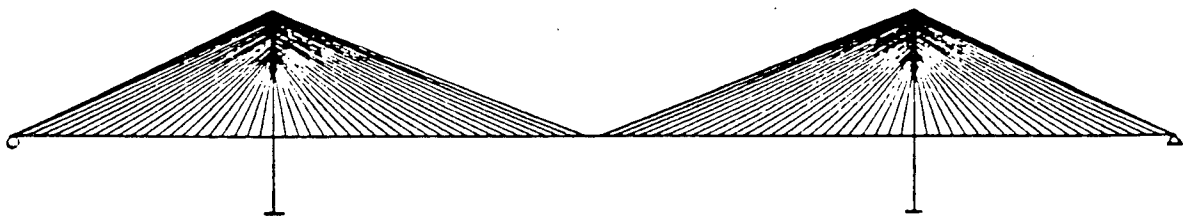
In all three models, dimensional analysis is applied to a standard bridge and then variations from the standard are studied. The standard bridge is defined by setting the dimensionless ratios that describe the bridge to representative values as determined from existing cable stayed bridge designs. With the understanding gained from the simple model and the intermediate model, the full bridge model behaviour can be explained, and the important parameters can be identified. Once the response of the full bridge model is understood, comparisons can be made with existing cable stayed bridges and an analysis procedure can be developed using beam-column on an elastic foundation theory and the results of the dimensional analysis.



Simple Backspan Model (Chapter 3)



Backspan Model (Chapter 4)



Full Bridge Model (Chapter 5)

Figure 2.5: Progressive computer models of cable stayed bridges. (Models drawn to different scales.)

Chapter 3

Simplified Backspan Model

3.1 The Model

A study of a complete cable stayed bridge would be complex, because the relative influence of the towers, the deck—backspan and mainspan—and the cables would be difficult to separate. Therefore, simple models are studied first, and the knowledge gained from these analyses is applied to the more complex model. Simple models are also useful to start with because there are fewer variables to study than in the complete model.

Two models of the backspan—isolated from the tower and mainspan—are chosen as the simple models to study before looking at the full bridge model. The first backspan model—called “simplified backspan model”—is designed to have a uniform elastic foundation; the second model, which is discussed in Chapter 4, has a nonuniform elastic foundation. A sketch of the simplified backspan model, with all the possible parameters defined, is shown in Figure 3.6. In this model all the cables have the same modulus of elasticity, dead weight, area, and length and are attached to the deck at the same angle at equal intervals. The leftmost cable is included to simulate the backstay. The deck is modelled as having constant stiffness EI and the live load is applied as a distributed load.

The definition of all the parameters shown in Figure 3.6 is given in the following:

A_C = cable cross sectional area

E = deck elastic modulus

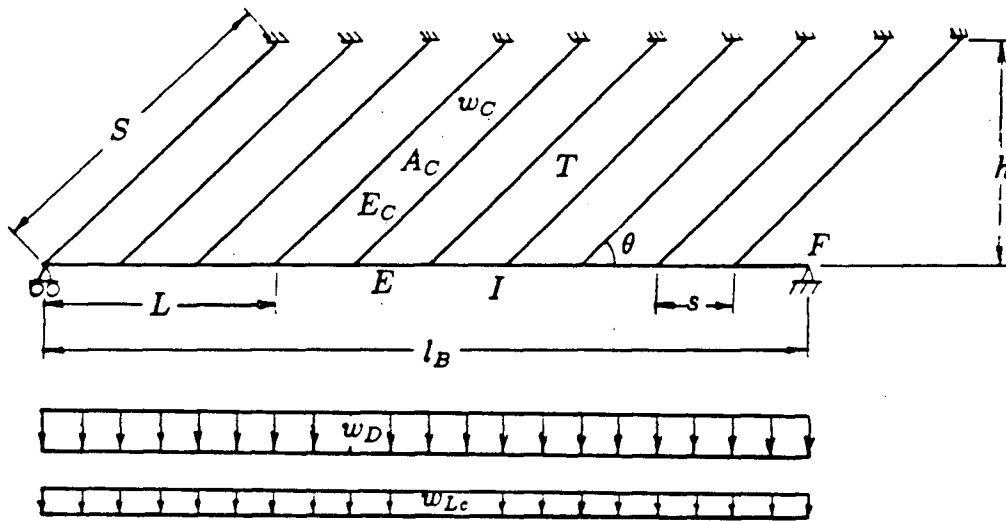
E_C = cable elastic modulus

- F = maximum axial load in deck due to dead load
- h = cable height
- I = deck moment of inertia
- L = horizontal projected length of cable
- l_B = backspan length
- N = number of deck intervals in the backspan
- S = cable chord length
- s = length of deck interval between cables
- T = cable tension in the chord direction due to dead load
- w_C = weight per unit length of cable
- w_D = uniformly distributed dead load
- w_{Lc} = critical uniformly distributed live load
- θ = cable chord angle of inclination to deck

Initially the model is under dead load only and the cable tensions T are set up such that there are no moments or deflections in the deck under the dead load. All the cable tensions are the same, with the cable attached to the roller bearing given the same tension as well.

The parameter F is the maximum axial load in the deck under dead load only. The axial load distribution induced into the deck by the cables is nonuniform and the maximum occurs at the rightmost end.

The computer program ULA has the capability to have axial prestress input as part of a load case. This feature is used to model the dead load cable tensions and dead load deck axial load distribution. The structure dead load is in equilibrium with the prestress; thus, if the prestress is applied as part of a load case, the dead load is not. In other words, the cable tensions represent the dead load, and the distributed



N = Number of deck spaces

$$N = \frac{l_B}{s}$$

Figure 3.6: Simplified backspan model.

dead load is not actually applied as a part of any load case. This also means that the input geometry is the dead load geometry. It should be noted that the $P-\Delta$ effects are calculated from the stability functions using the the initial prestress plus the axial load from a specific load case.

The following sections will deal with the buckling behaviour of the model and the deflections and moments of the deck under application of live load.

3.2 Stability

Modern cable stayed bridges are being built with increasingly slender decks. With the longer spans and smaller deck cross sections of these bridges, the factor of safety against buckling becomes an ever more important consideration. Tang's formula for buckling load is acceptable for short span cable stayed bridges; however, as Tang points out, more detailed analysis is required for long span structures. Herein, a closer investigation of

cable stayed bridge elastic stability is carried out.

3.2.1 Stability Dimensionless Ratios

Not all of the 16 parameters shown in Figure 3.6 can be used as variables in dimensional analysis because they are not all independent of each other. For example, S is a function of L and h , so only two of these three parameters can be used in defining the response of the model, thus reducing the number of parameters that need be considered. A further reduction in the number of parameters is accomplished by combining E and I to get the bending stiffness of the deck EI , and combining A_C and E_C to get the axial stiffness of the cables $A_C E_C$. The 16 parameters reduce to nine independent ones and are given in the following function:

$$w_{Lc} = \mathcal{F}[EI, A_C E_C, l_B, h, \theta, N, w_C, w_D] \quad (3.2)$$

Even though the distributed dead load is not actually applied in the computer analysis, the parameter " w_D " is retained because it is more convenient to use than T and F .

The five parameters not used in Equation 3.2 are related to the nine parameters of Equation 3.2 by:

$$L = \frac{h}{\tan \theta}$$

$$S = \frac{h}{\sin \theta}$$

$$s = \frac{l_B}{N}$$

$$T = \frac{w_D l_B}{N \sin \theta}$$

and

$$F = \sum_{i=1}^N T_i \cos \theta_i = NT \cos \theta = \frac{w_D l_B}{\tan \theta}$$

The next step in dimensional analysis is to construct independent dimensionless ratios from the independent parameters. Buckingham's Π theorem states that the number of dimensionless ratios required is the number of parameters less the number of fundamental units needed to quantify all of the parameters. Since the two units of length and force describe all the variables, seven ratios need to be constructed out of the nine parameters in Equation 3.2. The seven ratios chosen to represent this model are:

$$\begin{aligned}
 & N \\
 & \sin \theta \\
 & \frac{h}{l_B} \\
 & \frac{w_L c}{w_D} \\
 & \frac{w_D l_B}{2 \tan \theta \sqrt{\frac{N A_C E_C E I \sin^3 \theta}{l_B h}}} \\
 & \frac{l_B}{\pi} \sqrt{\frac{N A_C E_C \sin^3 \theta}{l_B h E I}} \\
 & \frac{w_D l_B}{N \sin \theta \sqrt[3]{\frac{A_C E_C}{24} \left(\frac{w_C h}{\tan \theta}\right)^2}}
 \end{aligned}$$

All of these dimensionless ratio have a physical meaning—some more obvious than others—and the remainder of this section is devoted to deriving and explaining the significance of these dimensionless ratios.

Since the stability behaviour of a cable stayed bridge is to be investigated, Hetényi's [22] critical load for an infinitely long beam-column on an elastic foundation is used as part of one ratio.

$$F_H = 2\sqrt{kEI} \quad (3.3)$$

where

F_H = buckling load for a beam-column on an elastic foundation

k = elastic foundation modulus

Note that F_H , k , and EI in Equation 3.3 are all constant along the beam-column.

For the derivation of k , a single cable is isolated along with the tributary length of deck associated with it, as shown in Figure 3.7.

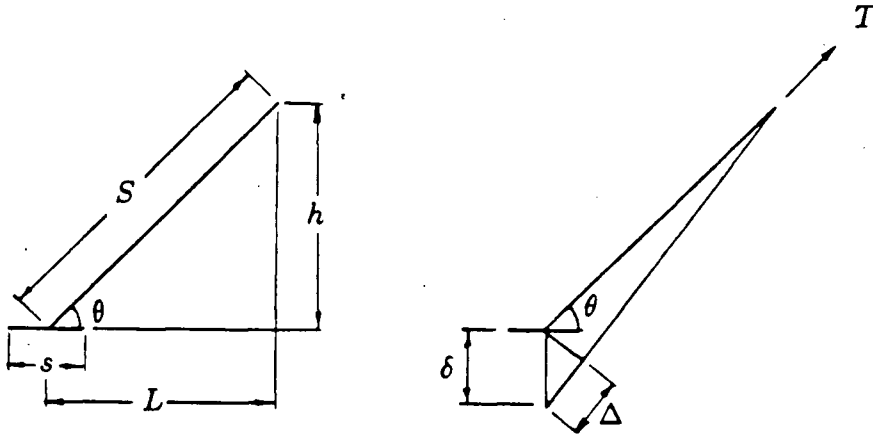


Figure 3.7: Derivation of elastic foundation modulus.

From geometry:

$$\Delta = \delta \sin \theta$$

where

Δ = cable elongation in the chord direction

δ = deck vertical deflection

and from Hooke's law:

$$T = \frac{\Delta A_C E_C}{S}$$

For a unit of deck deflection $\delta = 1$ and span s the foundation modulus k is V/s , where V is the vertical cable force $T \sin \theta$. This results in

$$k = \frac{A_C E_C}{sS} \sin^2 \theta \quad (3.4)$$

Further substitutions using $N = l_B/s$ and $S = h/\sin \theta$ yield

$$k = \frac{N A_C E_C \sin^3 \theta}{l_B h} \quad (3.5)$$

Equation 3.4 can be compared with Tang's

$$\beta_T = \frac{A_C E_C}{sS}$$

Tang omits the $\sin^2 \theta$ term, but the cable properties near the tower—where the deck axial load is greatest—are used in his formula. As long as the cable inclination at the critical deck section is greater than 72° the error in using Tang's approximation is less than 10%.

Substituting Equation 3.5 into Equation 3.3 results in

$$F_H = 2 \sqrt{\frac{N A_C E_C E I \sin^3 \theta}{l_B h}} \quad (3.6)$$

To make a dimensionless ratio from this, the maximum axial load in the deck due to dead load alone $F = w_D l_B / \tan \theta$ is used to compare with F_H to give

$$\frac{F}{F_H} = \frac{w_D l_B}{2 \tan \theta \sqrt{\frac{N A_C E_C E I \sin^3 \theta}{l_B h}}} \quad (3.7)$$

There is no live load in the expression for F/F_H ; therefore, this represents the deck stability under dead load only.

As stated previously, F_H is the buckling load for an infinitely long bar. The true solution for the a finite length bar also involves the number of half-waves n in the buckled shape. Hetényi gives the number of half-waves as

$$n = \frac{l_B}{\pi} \sqrt{\frac{k}{EI}}$$

which in terms of the independent parameters is

$$n = \frac{l_B}{\pi} \sqrt{\frac{N A_C E_C \sin^3 \theta}{l_B h E I}} \quad (3.8)$$

Thus, two dimensionless ratios— F/F_H and n —are defined as a measure of deck stability.

In order to explore the effect of cable nonlinearity on the response, the nondimensional cable tautness f as derived in Appendix A is used as one of the dimensionless ratios.

$$f = \frac{H}{\beta}$$

where

$$H = T \cos \theta = \frac{w_D l_B}{N \tan \theta}$$

and

$$\beta = \sqrt[3]{\frac{w_C^2 L^5 A_C E_C}{24 S^3}}$$

as is explained in Appendix A. The expression for f in terms of the independent parameters becomes

$$f = \frac{w_D l_B}{N \sin \theta \sqrt[3]{\frac{A_C E_C}{24} \left(\frac{w_C h}{\tan \theta}\right)^2}} \quad (3.9)$$

There is no live load in the expression for f ; therefore, this represents the cable tautness under dead load only. A physically intuitive description of f is that at high values of f the cable is very taut and has nearly the same stiffness as a straight bar. In fact, at $f = 2$ the cable stiffness would still be 85% of the straight bar stiffness. The cable stiffness then decreases rapidly as f decreases to the limit of zero.

The critical live load is an obviously important parameter and this will be represented by the dimensionless ratio w_{Lc}/w_D .

N , $\sin \theta$ and h/l_B , which describe the geometric characteristics of the model, are used as the last three ratios required.

A complete set of dimensionless ratios has been found and can be proven to be independent of each other. The reader can convince himself of this by noting that all nine parameters are used in forming the seven ratios, and by going through a process of elimination to prove independence. The ratio f is obviously independent of the other ratios because it is the only one containing w_C . Of the six remaining ratios, w_{Lc} appears only in w_{Lc}/w_D . With w_{Lc}/w_D eliminated, F/F_H is the only ratio containing w_D ; therefore, is independent of the others. The three geometric ratios are obviously independent of each other, which leaves n as the only ratio left; thus, independent of all the others.

The critical live load causing instability of the simple backspan model is described by the function:

$$\frac{w_{Lc}}{w_D} = \mathcal{F} \left[N, \sin \theta, \frac{h}{l_B}, f, n, \frac{F}{F_H} \right]$$

This function is based on beam-column on an elastic foundation stability theory with both the cable slackness and the $P-\Delta$ nonlinearities modelled.

3.2.2 Parameters and Ratios from Existing Bridge Designs

In order to construct the standard¹ simple backspan model to reflect actual bridges as closely as possible, data was aquired from four steel deck and five concrete deck cable stayed bridges. Appendix C.1 shows the numerical values for the parameters, and the resulting dimensionless ratios are given in Appendix C.2. Typical values for concrete and steel E are chosen and the value for cable E is that for modern parallel strand cables. The density of the cables γ_C is taken to be 77 kN/m^3 . The moment of inertia of a deck varies in a real bridge but in this study I is kept constant. I is calculated from a representative section of the backspan which is usually a long central section of

¹Defined in the last paragraph of Chapter 2.

constant cross section.

For this model, constant values of cable area, height and angle are needed. To obtain values for these parameters the “centroid cable” is defined as the cable nearest the centroid of the triangle formed by the backspan, tower and backstay cable. The area, height and angle of this centroid cable are used as the representative values for the bridge and as the constant values for the model.

The uniformly distributed live load w_L for the standard model is assumed to be the AASHTO HS20 lane load for highway bridges. For railway bridges, the actual design specifications for live load are used. The dead loads are estimated from both the cable prestresses and the deck cross sectional area. N is the number of cables in the backspan with all the backstay cables counted as one cable. F is calculated from $w_D l_B / \tan \theta_{cen}$.

The dimensionless ratios could be calculated for every cable in each bridge to get the average values for each bridge; however, to reduce the need for tedious calculations on the part of future users of this thesis, the centroid cable values of the dimensionless ratios are taken as the average values. The dimensionless ratio values actually used for the standard simple backspan model are given in Appendix C.2. These values are averages of the 9 cable stayed bridge values, and are repeated here:

$$\begin{aligned} N &= 20 \\ \sin \theta &= 0.70 \\ h/l_B &= 0.40 \\ f &= 7 \\ n &= 3 \\ F/F_H &= 0.10 \\ w_L/w_D &= 0.20 \end{aligned}$$

where, for the purpose of calculating f : $w_C = A_{Ccen} \gamma_C$.

3.2.3 Results of Stability Analysis

The standard simplified backspan model of Figure 3.6 is constructed using the preceding values for the dimensionless ratios. In order to find the buckling load for this standard model, the structure is analyzed with the computer program ULA. The live load starts out at 20% of the dead load ($w_L/w_D = 0.20$) and is increased until the critical live load that causes elastic instability is reached. (Structure instability is recognized when the determinant of the stiffness matrix becomes zero.) The standard live load is increased by multiplying it by the factor λ , called the “load level.” With this nomenclature the critical load ratio becomes

$$\frac{w_{Lc}}{w_D} = \frac{\lambda w_L}{w_D}$$

The structure buckles under the combination of 50 original live loads ($\lambda = 50$) and one dead load—which is to say $w_{Lc}/w_D = 10$. In other words, the buckling load is

$$w_D + \lambda w_L$$

where λ is taken as the factor of safety against failure. Thus, the factor of safety on the live load against elastic buckling of the standard model is 50. This is a very high factor of safety and cannot be related to cable stayed bridges because the model is too simplistic. The simple model is necessary, however, to be able to verify the computer program results against the theoretical beam-column on an elastic foundation before analyzing more complex models.

To this end, the deflected shape of the deck just before stability failure is shown in Figure 3.8 along with the axial load (dead load plus live load) and moment distributions. Note that the deflection and moment shapes exhibit half-waves close to l_B/n or, in this case $l_B/3$. The nonlinear distribution of deck axial load occurs because of the large deck deflections which cause cable tensions to increase beyond the linear live load tensions.

As an aside, the possibility of a more severe loading condition for instability can be seen in Figure 3.8. If an uplift pressure (from wind and/or inertia) is applied in

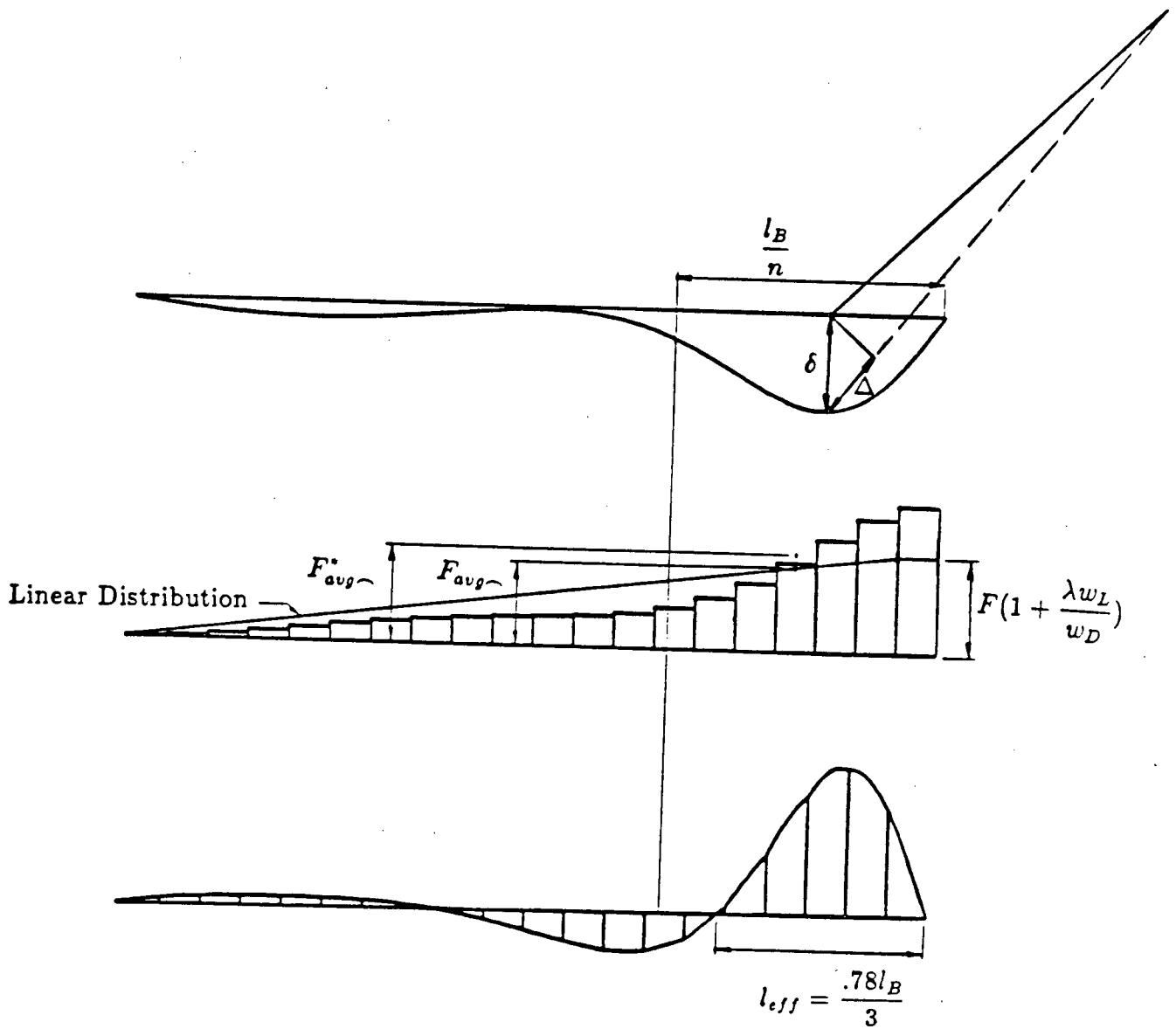


Figure 3.8: Stability failure of simplified backspan model.

the region of deck negative moment (the center section), a more severe deflected shape would result. This uplift pressure would also reduce the deck axial load which stabilizes the structure. To determine the overall effect of the uplift pressure, the factor of safety is calculated from computer analyses for a range of uplift pressure magnitudes over the region of negative moment. The result is shown in Figure 3.9 where the abscissa is the uplift pressure expressed as a percentage of the live load magnitude. It can be seen that for this backspan model the reduction in deck axial load overrides the more severe deflected shape and the factor of safety increases with increasing uplift pressure.

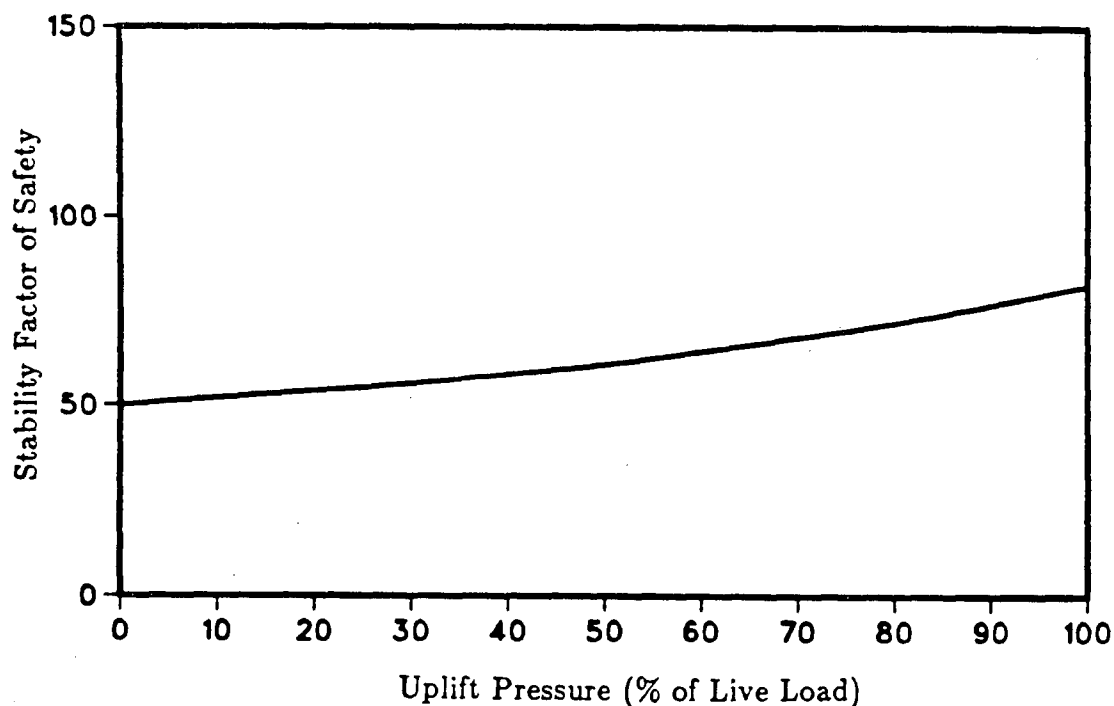


Figure 3.9: Stability factor of safety with uplift pressure.

The backspan model buckled with $F/F_H = 0.10$. However, the theoretical beam-column on an elastic foundation will only buckle when the constant axial load in the beam-column is exactly as calculated by $F_H = 2\sqrt{kEI}$. For this reason it might be expected that F/F_H should equal 1.0 in order for the model to buckle. This discrepancy of a factor of ten exists because

1. F does not include the live load,
2. the actual axial load distribution is nonuniform and nonlinear,
3. F_H is for an infinitely long bar, not for the case at hand.

Most of the discrepancy is due to the live load not being in F . To analytically account for the live load, F is multiplied by $(w_D + \lambda w_L)/w_D$; which for this case ($\lambda w_L/w_D = 10$) gives

$$\frac{F}{F_H} \frac{w_D + \lambda w_L}{w_D} = 1.10$$

instead of 0.10. Thus, the discrepancy is brought down from a factor of 10 to an error of 10%. It still remains to explain why there is still this 10% deviation.

Since the axial load varies along the deck it is more reasonable to use an average axial load over a half-wave F_{avg} as shown in Figure 3.8. An approximation to F_{avg} is $F(1 + \lambda w_L/w_D)(2n - 1)/(2n)$. This is approximate because it does not include the axial load induced by the backstay cable. For large values of N this approximation is fairly good. The exact formula is

$$F_{avg} = F \left(1 + \frac{\lambda w_L}{w_D} \right) \left(\frac{2n - 1}{2n} + \frac{1}{2N} \right)$$

Due to the $P-\Delta$ effect the real average is larger. Computer runs near critical show that the real average F_{avg}^* is $1.156F_{avg}$ for the particular case shown in Figure 3.8.

The dimensionless ratio now becomes

$$\frac{F_{avg}^*}{F_H} = 1.156 \frac{F}{F_H} \left(1 + \frac{\lambda w_L}{w_D} \right) \left(\frac{2n - 1}{2n} + \frac{1}{2N} \right) = 1.091$$

A final refinement can be included by considering the boundary conditions of the model. Hetényi's formula $F_H = 2\sqrt{kEI}$ is for an infinitely long bar, and needs to be changed to reflect the true case. The formula for the buckling load of a finite length pin-pin bar is given by Hetényi as

$$\frac{\pi^2 EI}{l_B^2/n^2} + \frac{l_B^2 k}{n^2 \pi^2}$$

where all the parameters are as defined previously. To make this applicable to the situation in Figure 3.8, l_B/n is substituted by the measured effective length of the half-wave, $0.78l_B/n$, to give

$$F_{H\sim} = \left(\frac{3}{0.78l_B}\right)^2 \pi^2 EI + \left(\frac{0.78l_B}{3}\right)^2 \frac{N_{AC} E_C \sin^3 \theta}{\pi^2 l_B h}$$

The ratio $F_H/F_{H\sim}$ is calculated to be 0.886 and the final ratio

$$\frac{F_{avg\sim}^*}{F_{H\sim}} = 0.97$$

Thus, the simplified backspan model is equivalent to a beam-column on an elastic foundation within 3%. In future stability plots the only adjustment made will be to multiply F/F_H by $(1 + \lambda w_L/w_D)$. The deviation from Hetényi's solution due to nonuniform axial load distribution and finite length will not be corrected, but will be left as a visual indication on the plots.

The standard model is next varied by altering only F/F_H and then determining the live load necessary to cause the deck to buckle. The result of this exercise is shown in Figure 3.10.

The theoretical result for a beam-column on an elastic foundation is also plotted in Figure 3.10 and labelled as "Hetényi." The discrepancy between the two results is due to the same three reasons as explained for the standard model. If the live load is included in F the resulting plot is shown in Figure 3.11. If the rest of the refinements are made, the ratio $F_{avg\sim}^*/F_{H\sim}$ at the ordinate intercept, for example, is 1.05 as compared to $F/F_H = 1.32$. Which differs from the the 0.97 obtained for $w_L/w_D = 0.2$ because of errors in measuring the half-wave effective lengths and obtaining $F_{avg\sim}^*$.

The dimensionless ratio n is now varied to determine how n affects the model. The range of n in existing cable stayed bridge designs is from 2 to 4 and the stability curves for $n = 2$ and $n = 4$ are plotted in Figure 3.12 along with the curve for $n = 3$.

There is a variation with n in that the three curves differ from each other. This variation is not expected with Hetényi's theoretical result, and if all of the adjustments

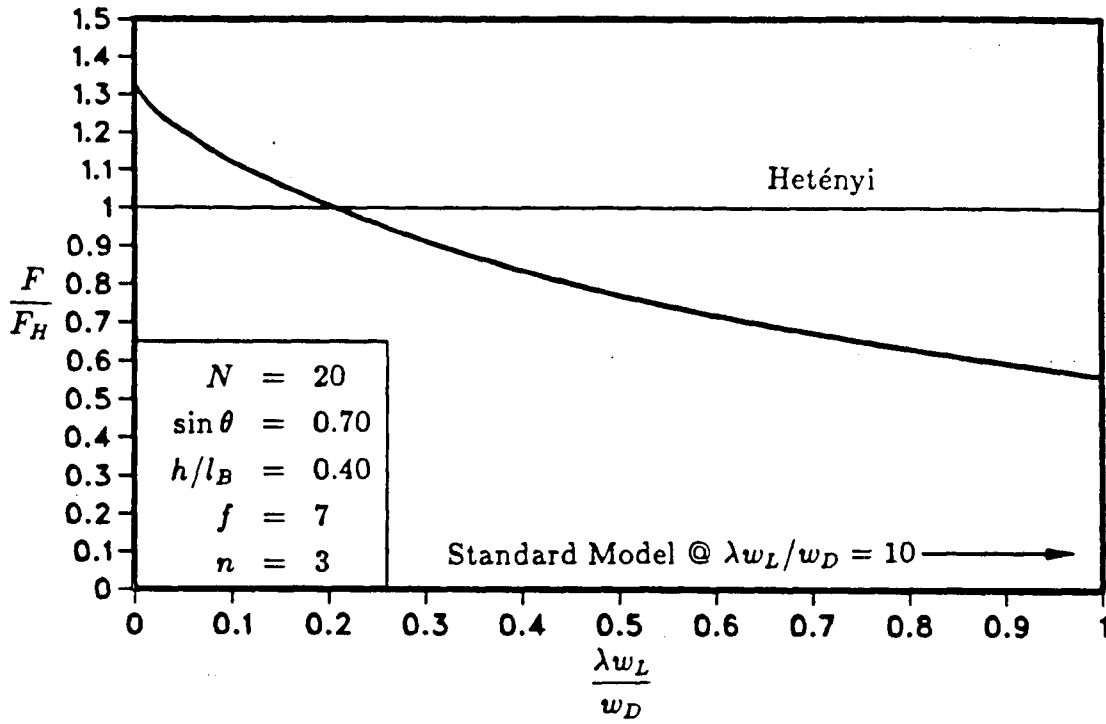


Figure 3.10: Stability of simplified backspan model (F/F_H).

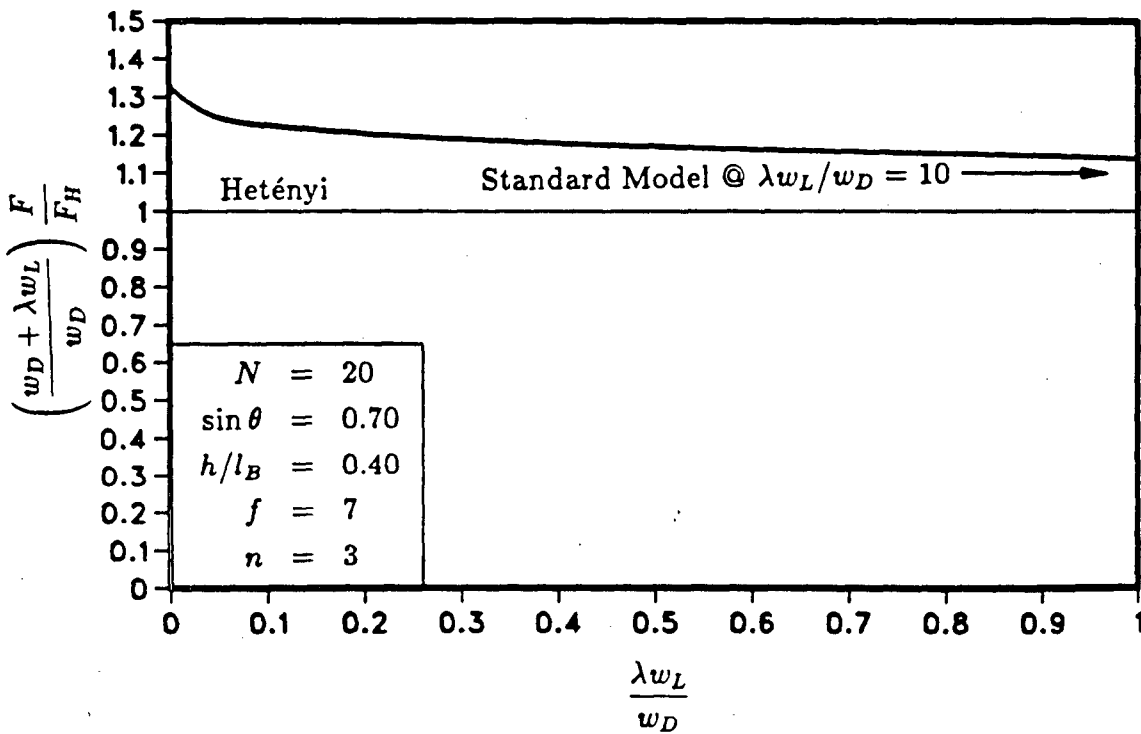


Figure 3.11: Stability of simplified backspan model.

to F/F_H are made to the curves as was done for the standard model, all three curves would plot as nearly the same. (They will not be exactly the same due to the errors mentioned previously.) The following table summarizes the result of these adjustments for the ordinate intercepts:

n	$\frac{F}{F_H}$	$\frac{F_{avg}^*}{F_H}$
4	1.25	1.06
3	1.32	1.05
2	1.48	1.03

Thus, it can be seen that the stability of the simplified backspan model can be compared to a beam-column on an elastic foundation with reasonable accuracy.

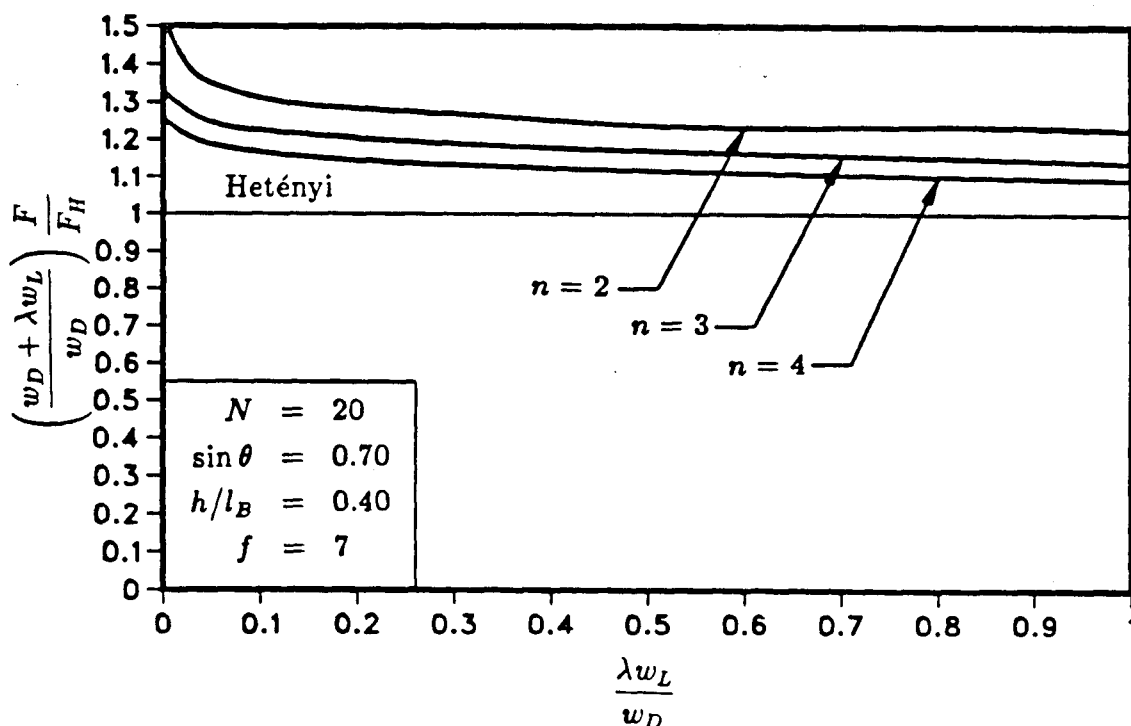


Figure 3.12: Stability of simplified backspan model— n varied.

As mentioned previously, a nonlinear response is expected due to the changes in cable sag when the cables experience a load change. To investigate this, the standard

model is varied by altering the initial cable tautness f . In the normal range of 5 to 9, the cable tautness ratio does not affect the model behaviour. Only when the cables are slack ($f < 2$) is an effect seen, and then only for low live loads because higher loads tighten the cables. The curves for $f = 5$ and $f = 9$ are precisely the same as the curve for $f = 7$.

The remaining dimensionless ratios, which are all based on the model geometry, are not investigated for this model.

3.3 Deflection and Moment

It is important to check the deck for instability to assess the factor of safety against buckling failure, but this will usually not govern the design. In preliminary design analyses, the maximum deflection and maximum moment are the governing parameters for the deck. Herein, dimensional analysis is applied to the response of the deck and compared to the response of a simple beam on an elastic foundation.

3.3.1 Deflection Dimensionless Ratios

For the dimensional analysis of cable stayed bridge deflection only one extra parameter is needed and that is the maximum backspan deflection δ_B . All the other parameters are exactly those used in the stability analysis with the exception of using w_L instead of w_{Lc} . The definition of the backspan model deflection in terms of independent parameters is

$$\delta_B = \mathcal{F}[EI, A_C E_C, l_B, h, \theta, N, w_C, w_D, w_L]$$

Buckingham's II theorem requires that one more dimensionless ratio be constructed. In order to compare the deflection of the backspan model to a simple beam-column on an elastic foundation, the dimensionless ratio δ_B/δ_H is used. The symbol δ_H refers to the maximum deflection of a simply supported beam on an elastic foundation under a uniformly distributed load, without an axial load. The deflection as a function of x is

given by Hetényi as

$$\delta_H(x) = \frac{wL}{k} \left[1 - \frac{\cosh \gamma x \cos \gamma(l_B - x) + \cos \gamma x \cosh \gamma(l_B - x)}{\cosh \gamma l_B + \cos \gamma l_B} \right] \quad (3.10)$$

where

$$\gamma = \sqrt{\frac{k}{4EI}}$$

and k is given by Eq. 3.5. The deflection for a beam on an elastic foundation rather than a beam-column on an elastic foundation is used so that the amplification of deflections due to the axial load will become apparent. Also, Hetényi assumes a constant axial load in his derivation of beam-column on an elastic foundation deflections, while for cable stayed bridges the axial load varies along the deck. Complications due to the different axial distributions are thus avoided by comparing cable stayed bridge deflections to the beam on an elastic foundation deflections without axial load.

In Eq. 3.10 the variable γ is related to n , the number of half-waves in the buckled shape. For response analysis it is advantageous to change this equation to reflect the decay length of the beam rather than the buckled shape. The decay length l_D is the length over which a local deflection or moment in a beam dies out. Two examples are shown in Figure 3.13.

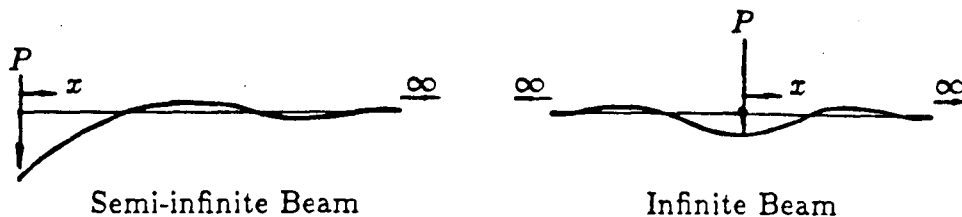


Figure 3.13: Examples of deflection decay in a beam on an elastic foundation.

The equations for deflection are composed of two parts, an exponential decaying part and a sinusoidally varying part. For example, the deflection of the semi-infinite

beam on an elastic foundation in Figure 3.13 is

$$\delta(x) = \frac{2P\gamma}{k} e^{-\gamma x} \cos \gamma x$$

and for the infinite beam on an elastic foundation the deflection is

$$\delta(x) = \frac{P\gamma}{2k} e^{-\gamma x} (\cos \gamma x + \sin \gamma x)$$

The decay length could be defined as the distance from the maximum deflection to the point at which the deflection first becomes zero. This is governed by the sinusoidal part, but the location of this point depends on the boundary conditions and whether it is deflection or moment that is of interest. Therefore, this method of defining decay length is not good.

The best way to define decay length is to say it is the distance to the point where at least 95% of the maximum deflection or moment is dissipated. This occurs for all instances when $e^{-\gamma x} < 0.05$. For $\gamma x = 3$, $e^{-\gamma x} = .049$, thus we get $\gamma l_D = 3$ or $l_D = 3/\gamma$.

This definition of decay length is arbitrary and Hetényi uses π instead of 3, which results in a longer decay length. For this historical reason and for convenience in relating l_D to n , π is used herein.

The new dimensionless ratio to replace n will be l_D/l_B where

$$\frac{l_D}{l_B} = \frac{\pi}{\gamma l_B}$$

Substituting for γ and using Eq. 3.5 gives

$$\frac{l_D}{l_B} = \frac{\pi\sqrt{2}}{l_B} \sqrt{\frac{l_B h EI}{N A_C E_C \sin^3 \theta}} \quad (3.11)$$

This equation can be simplified by use of Eq. 3.8 to give

$$\frac{l_D}{l_B} = \frac{\sqrt{2}}{n}$$

A more meaningful expression for $\delta_H(x)$ can now be derived using l_D instead of γ . Specifically, using

$$\gamma = \frac{\pi}{l_D}$$

then

$$\delta_H(x) = \frac{w_L}{k} \left[1 - \frac{\cosh \pi \frac{x}{l_D} \cos \frac{\pi}{l_D} (l_B - x) + \cos \pi \frac{x}{l_D} \cosh \frac{\pi}{l_D} (l_B - x)}{\cosh \pi \frac{l_B}{l_D} + \cos \pi \frac{l_B}{l_D}} \right]$$

In the dimensional analysis of the backspan model, the maximum deflection of Hetényi's model is compared to the maximum deflection of the computer model. Hetényi's maximum deflection δ_H occurs when the derivative of $\delta_H(x)$ is equal to zero. This derivative (the slope) is equal to zero when $x = \frac{3}{4}l_D$ and because of the symmetry of the simply supported beam on an elastic foundation, the maximum value of x is $l_B/2$ or

$$\frac{l_B}{2} = \frac{3}{4}l_D$$

or

$$\frac{l_D}{l_B} = \frac{2}{3}$$

Thus, when $l_D/l_B \leq 2/3$, $x = \frac{3}{4}l_D$ should be used and when $l_D/l_B \geq 2/3$, $x = l_B/2$ should be used. This results in two equations for the maximum deflection δ_H of a beam on an elastic foundation:

$$\delta_H = \begin{cases} \frac{w_L}{k} \left[1 - \frac{\cosh \frac{3}{4}\pi \cos\left(\frac{\pi}{l_D/l_B} - \frac{3}{4}\pi\right) + \cos \frac{3}{4}\pi \cosh\left(\frac{\pi}{l_D/l_B} - \frac{3}{4}\pi\right)}{\cosh \frac{\pi}{l_D/l_B} + \cos \frac{\pi}{l_D/l_B}} \right] & \text{for } \frac{l_D}{l_B} \leq \frac{2}{3} \\ \frac{w_L}{k} \left[1 - \frac{2 \cosh \frac{\pi}{2l_D/l_B} \cos \frac{\pi}{2l_D/l_B}}{\cosh \frac{\pi}{l_D/l_B} + \cos \frac{\pi}{l_D/l_B}} \right] & \text{for } \frac{l_D}{l_B} \geq \frac{2}{3} \end{cases} \quad (3.12)$$

For convenience and reference a dimensionless plot of $\delta_H k/w_L$ versus l_D/l_B is given in Figure 3.14 as a graphical representation of Eq. 3.12.

The dimensionless ratios used in describing the maximum deflection of the simple backspan model are listed by the function:

$$\frac{\delta_B}{\delta_H} = \mathcal{F} \left[N, \sin \theta, \frac{h}{l_B}, f, \frac{l_D}{l_B}, \frac{w_L}{w_D}, \frac{F}{F_H} \right]$$

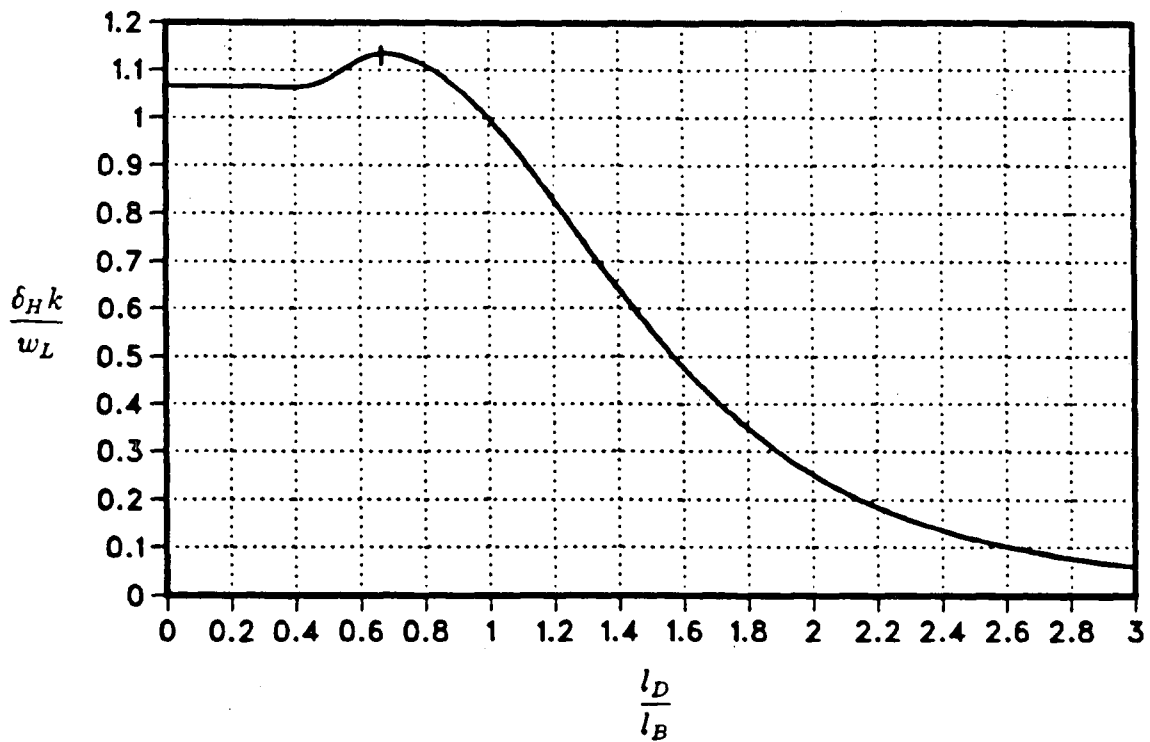


Figure 3.14: Dimensionless plot of Hetényi's deflection.

With δ_H defined by Eq. 3.12 this function will show the magnification of the maximum deck deflection due to the deck axial load.

3.3.2 Results of Deflection Analysis

The same standard simplified backspan model is used for maximum deflection analysis as that for the stability analysis ($l_D/l_B = 0.47$ for $n = 3$). The deflection of the standard model under a uniformly distributed live load w_L ($w_L/w_D = 0.20$), is shown in Figure 3.15 along with the beam on an elastic foundation deflection. This deflection is due to live load only, since the dead load deflection is zero. The live load deflection is magnified due to $P-\Delta$ effects from the combination of the dead and live load deck axial forces. The δ_B/δ_H ratio is equal to 1.024 which indicates that there is very little magnification due to the deck axial load in the standard model. The maximum live load deflection versus span ratio is 1/2000 (calculations are shown in Appendix D)

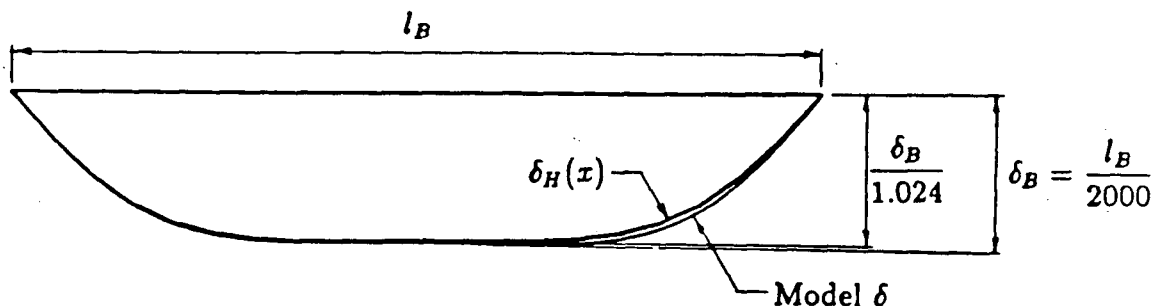


Figure 3.15: Deflection of standard simple backspan model.

which is well within the recommendation of $1/500$.²

The standard model is now varied by altering the F/F_H ratio while keeping all other ratios constant. The maximum deflection is then determined from a computer analysis and the δ_B/δ_H ratio is plotted against F/F_H . The result is given as the solid curve in Figure 3.16 for a range of F/F_H values.

In the δ_B/δ_H ratio, the “ δ_B ” is the magnified maximum deflection of the deck due to the presence of axial load in the deck. The “ δ_H ” is Hetényi’s maximum deflection of a beam on an elastic foundation without axial load. Thus, the δ_B/δ_H ratio is equal to 1.0 for F/F_H equal to zero, and increases as F/F_H increases, showing the magnification behaviour.

A comparison can be made with Hetényi’s maximum deflection for a beam-column on an elastic foundation with constant axial load $\delta_{H_{axial}}$ where:

$$\delta_{H_{axial}} = \frac{w_L}{k} \left[1 - \frac{\cosh \beta x \cos \alpha(l_B - x) + \cos \alpha x \cosh \beta(l_B - x)}{\cosh \beta l_B + \cos \alpha l_B} - (\beta^2 - \alpha^2) \frac{\sinh \beta x \sin \alpha(l_B - x) + \sin \alpha x \sinh \beta(l_B - x)}{2\alpha\beta(\cosh \beta l_B + \cos \alpha l_B)} \right]$$

²Recommended by the Task Committee on Cable-Suspended Structures of the Committee on Special Structures of the Committee on Metals of the Structural Division. [23]

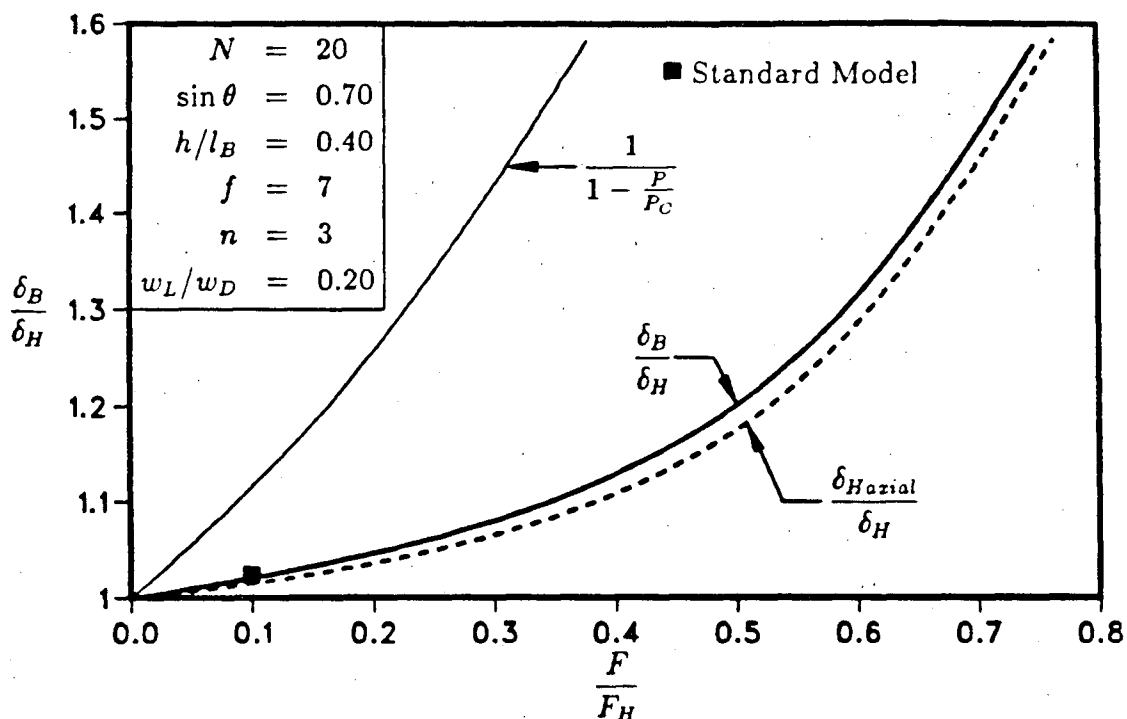


Figure 3.16: Magnification of maximum deflection.

where

$$\alpha = \sqrt{\sqrt{\frac{k}{4EI} - \frac{F}{4EI}}}$$

$$\beta = \sqrt{\sqrt{\frac{k}{4EI} + \frac{F}{4EI}}}$$

and

$$F = \frac{w_D l_B}{\tan \theta}$$

is constant and equal to the maximum value in the deck. A new ratio δ_{Haxial}/δ_H is formed and plotted as the dashed curve on Figure 3.16. It can be seen that the computer model behaves very similarly to the Hetényi model, with the small difference being due to the different axial distributions in the beam. It is interesting to note that the triangular axial load distribution in the computer model produces a more severe magnification of the maximum deflection than the constant axial load of Hetényi's

model. For interest sake, the standard amplification formula for a simply supported beam-column is applied to this model and is also plotted on Figure 3.16. It can be seen that the elastic foundation significantly suppresses the deflection of the beam-column.

To assess the cable tautness effect on the maximum deflection, the f ratio is varied while all the other ratios are kept at their standard values and the maximum deflection is determined from the computer analysis. The result of this is shown in Figure 3.17. The cable tautness does not affect the deflection of the backspan for normal values of f (> 5). The importance of having tight cables is demonstrated however, by the magnification of the deflection for low values of f .

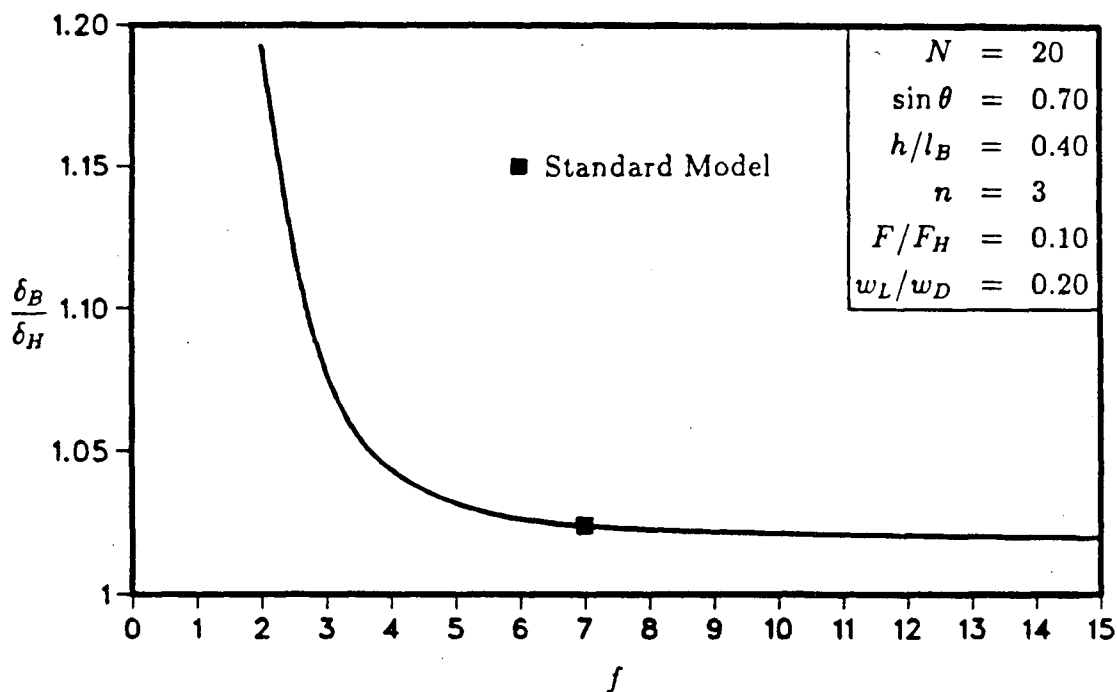


Figure 3.17: Dimensionless deflection versus dimensionless cable tautness.

The deflection plot as a function of dimensionless decay length l_D/l_B is shown in Figure 3.18. δ_B/δ_H depends very little on l_D/l_B with there being only a slight increase in magnification due to the axial load as the decay length reaches the backspan length and beyond. As the decay length becomes very long, the effect of the initial axial load

diminishes and the δ_B/δ_H ratio reduces asymptotically to 1. At the other end of the scale, the increase in δ_B/δ_H is not due to the short decay length per se; rather, due to a deviation of structural behaviour from a beam on an elastic foundation. To maintain accuracy in modelling a beam with a continuous elastic foundation by a beam with discrete springs, there should be at least 4 or 5 springs over the decay length. In other words, l_D/l_B should be greater than $4/N$. Thus, for the standard backspan of $N = 20$ and l_D/l_B less than 0.20, the response is no longer similar to a beam on an elastic foundation response. To demonstrate this graphically, the curve for $N = 80$ is plotted as the dotted line.

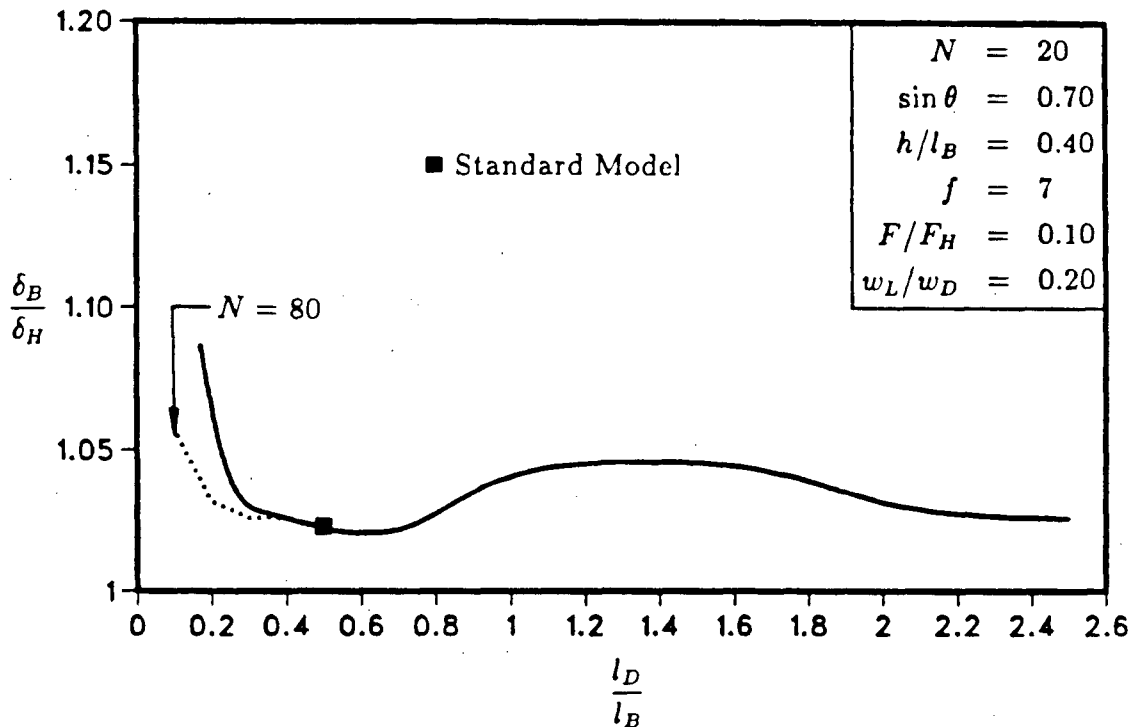


Figure 3.18: Dimensionless deflection versus dimensionless decay length.

Figure 3.19 shows the relationship between δ_B/δ_H and the live load to dead load ratio w_L/w_D . It can be seen that the maximum deflection of the standard simple backspan model is closely represented by Hetényi's equation (Eq. 3.12) for any value of live load. The small slope shown in Figure 3.19 is due to the nonlinear $P-\Delta$ effects

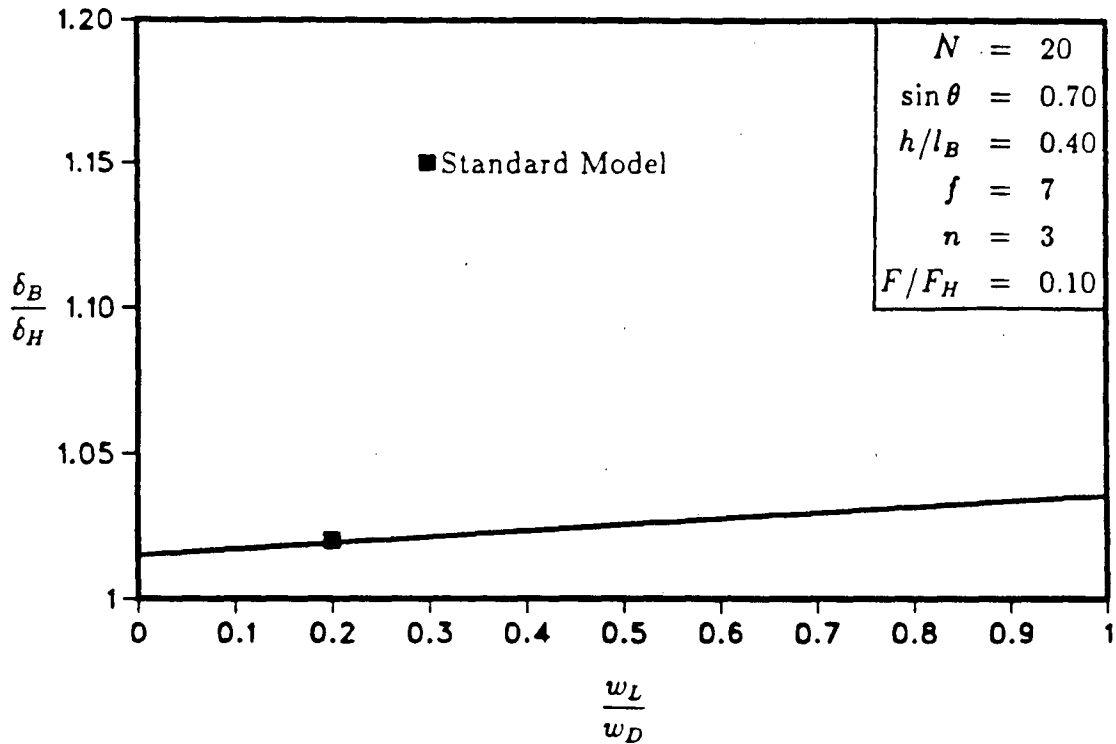


Figure 3.19: Dimensionless deflection versus dimensionless load.

induced by the extra live load axial force in the deck.

3.3.3 Moment Dimensionless Ratios

The dimensional analysis of cable stayed bridge moment is carried out exactly the same as that for the deflection analysis, with the substitution of the maximum backspan moment M_B for the maximum backspan deflection δ_B . The definition of the backspan model moment in terms of independent parameters is

$$M_B = \mathcal{F}[EI, A_C E_C, l_B, h, \theta, N, w_C, w_D, w_L]$$

In order to compare the moment of the backspan model to a simple beam-column on an elastic foundation, the dimensionless ratio M_B/M_H is used. The symbol M_H refers to the maximum moment of a simply supported beam on an elastic foundation under a uniformly distributed load, without an axial load. The moment as a function

of x is given by Hetényi as

$$M_H(x) = \frac{w_L}{2\gamma^2} \frac{\sinh \gamma x \sin \gamma(l_B - x) + \sin \gamma x \sinh \gamma(l_B - x)}{\cosh \gamma l_B + \cos \gamma l_B}$$

where

$$\gamma = \sqrt{\frac{k}{4EI}}$$

and k is given by Eq. 3.5. Using this formula, the amplification of moments due to the axial load will become apparent, just as in the deflection analysis.

A more meaningful expression for $M_H(x)$ using l_D instead of γ , is

$$M_H(x) = \frac{w_L l_D^2}{2\pi^2} \left[\frac{\sinh \pi \frac{x}{l_D} \sin \frac{\pi}{l_D} (l_B - x) + \sin \pi \frac{x}{l_D} \sinh \frac{\pi}{l_D} (l_B - x)}{\cosh \pi \frac{l_B}{l_D} + \cos \pi \frac{l_B}{l_D}} \right]$$

The maximum moment M_H occurs when the derivative of $M_H(x)$ is equal to zero. This derivative (the shear) is equal to zero when $x = l_D/4$ and because of the symmetry of the simply supported beam on an elastic foundation, the maximum value of x is $l_B/2$ or

$$\frac{l_B}{2} = \frac{l_D}{4}$$

or

$$\frac{l_D}{l_B} = 2$$

Thus, when $l_D/l_B \leq 2$, $x = l_D/4$ should be used and when $l_D/l_B \geq 2$, $x = l_B/2$ should be used. This results in two equations for the maximum moment M_H of a beam on an elastic foundation:

$$M_H = \begin{cases} \frac{w_L l_B^2}{2\pi^2} \left(\frac{l_D}{l_B} \right)^2 \left[\frac{\sinh \frac{\pi}{4} \sin \left(\frac{\pi}{l_D/l_B} - \frac{\pi}{4} \right) + \sin \frac{\pi}{4} \sinh \left(\frac{\pi}{l_D/l_B} - \frac{\pi}{4} \right)}{\cosh \frac{\pi}{l_D/l_B} + \cos \frac{\pi}{l_D/l_B}} \right] & \text{for } \frac{l_D}{l_B} \leq 2 \\ \frac{w_L l_B^2}{\pi^2} \left(\frac{l_D}{l_B} \right)^2 \left[\frac{\sinh \frac{\pi}{2l_D/l_B} \sin \frac{\pi}{2l_D/l_B}}{\cosh \frac{\pi}{l_D/l_B} + \cos \frac{\pi}{l_D/l_B}} \right] & \text{for } \frac{l_D}{l_B} \geq 2 \end{cases} \quad (3.13)$$

For convenience and reference a dimensionless plot of $M_H/(w_L l_B^2)$ versus l_D/l_B is given in Figure 3.20 as a graphical representation of Eq. 3.13.

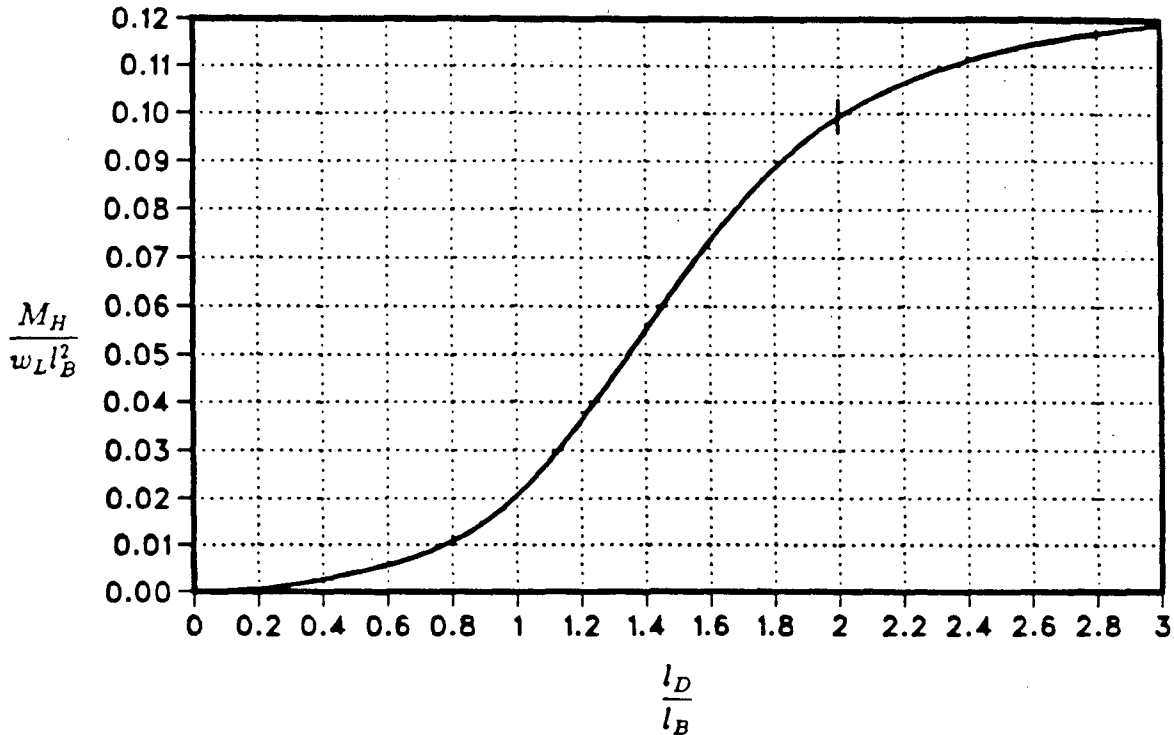


Figure 3.20: Dimensionless plot of Hetényi's moment.

The dimensionless ratios used in describing the maximum moment of the simple backspan model are listed by the function:

$$\frac{M_B}{M_H} = \mathcal{F} \left[N, \sin \theta, \frac{h}{l_B}, f, \frac{l_D}{l_B}, \frac{w_L}{w_D}, \frac{F}{F_H} \right]$$

With M_H defined by Eq. 3.13 this function will show the magnification of the maximum deck moment due to the deck axial load.

3.3.4 Results of Moment Analysis

The same standard simplified backspan model is used for maximum moment analysis as that for the deflection analysis. The moment of the standard model with $w_L/w_D = 0.20$, is shown in Figure 3.21 along with the beam on an elastic foundation moment. The

M_B/M_H ratio is equal to 1.057 which indicates that there is very little magnification due to the deck axial load in the standard model. The maximum moment is $w_L l_B^2/262$ (calculations shown in Appendix D) which is a tremendous reduction from the simple span maximum moment of $w_L l_B^2/8$.

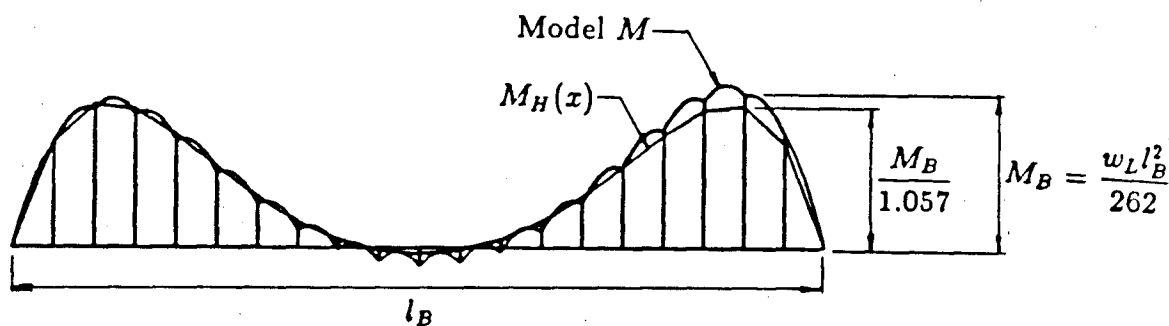


Figure 3.21: Moment of standard simple backspan model.

In Figure 3.21 it can be seen that local fixed ended moments of the deck between stays are superposed on the overall structure moment diagram. These local bending moments are caused by the application of the live load as a continuous distributed load. The effect of the local moments is to add small negative moments at the cable-deck connections and to produce a nonlinear moment distribution along the deck between any two connections. These effects are small—and decrease with increasing N —and will not be explicitly regarded in the analysis. The maximum backspan moment M_B is taken as the maximum moment at a cable connection, with the nonlinear effect included. Note, however, that the dead load moments are not included in the model, which is to say the dead load is applied as point loads at the cable-deck connections. This method of applying the dead load is used to achieve a moment and deflection free model as a starting point.

The live load being uniformly distributed over the deck implies that the construction method of having floor beams attached directly to the main longitudinal girders is used

between cable-deck connections, as shown in Figure 3.22. However, the local dead load deflections and moments are not accounted for in this study but can be superimposed on the results of this study if required by the reader. The other construction method shown in Figure 3.22 makes use of stringers that span between floor beams placed at cable-deck connections. This layout transfers most of the live and dead load to the floor beams, thus the distributed loads act as concentrated loads on the main longitudinal girders at the cable-deck connections. Realizing that the dead loads are applied at the panel points and that the local effects of live load are relatively small, the results of this study can be applied to both types of deck construction.

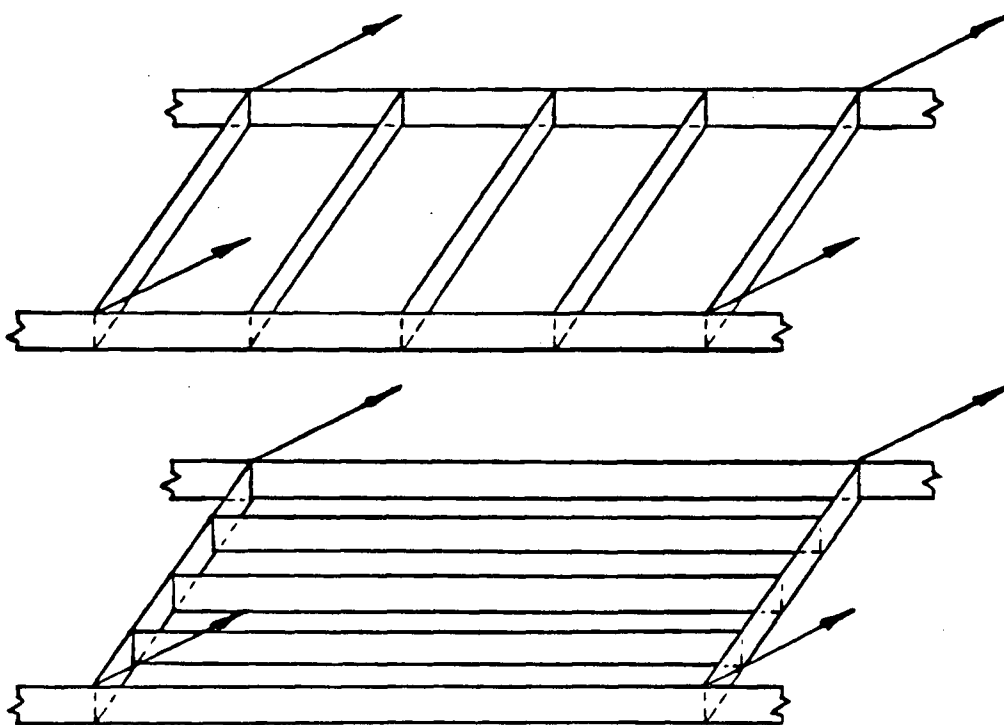


Figure 3.22: Bridge deck construction methods.

The standard model is now varied by altering the F/F_H ratio while keeping all other ratios in the function constant. The maximum moment is then determined from a computer analysis and the M_B/M_H ratio is plotted against F/F_H . The result is given as the thick solid curve in Figure 3.23 for a range of F/F_H values.

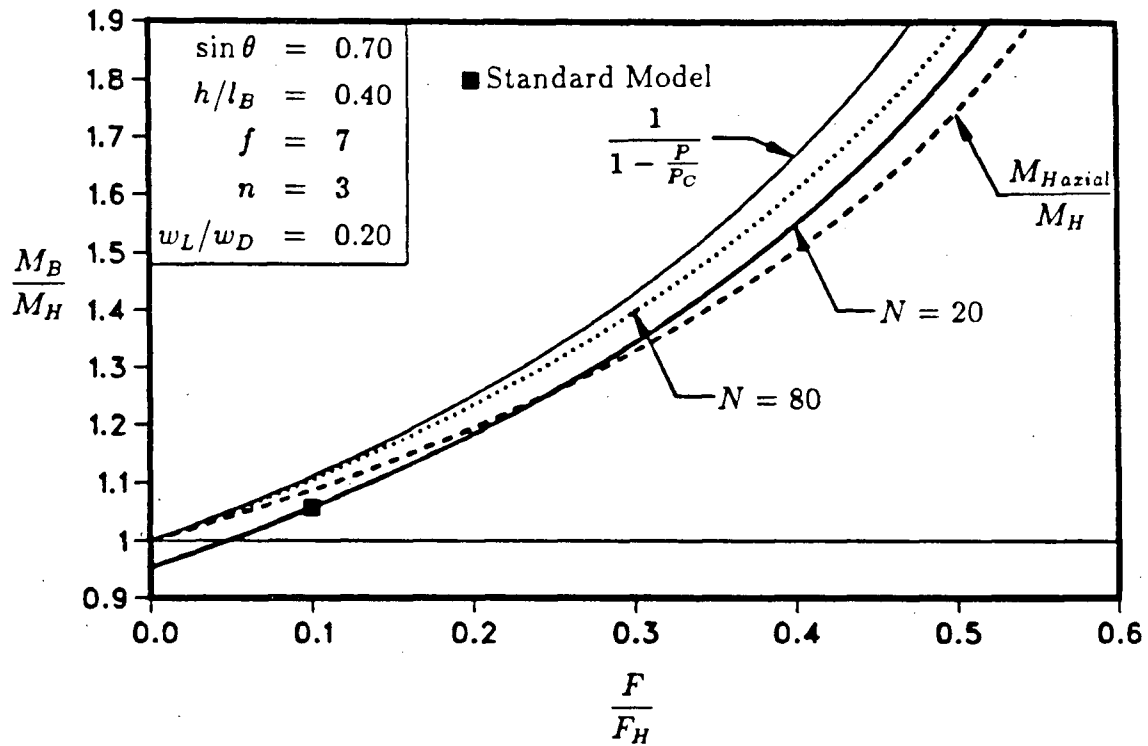


Figure 3.23: Magnification of maximum moment.

In the M_B/M_H ratio, the “ M_B ” is the magnified maximum moment of the deck due to the presence of axial load in the deck. The “ M_H ” is Hetényi’s maximum moment of a beam on an elastic foundation without axial load. Thus, the M_B/M_H ratio should be equal to 1.0 for F/F_H equal to zero, and increase as F/F_H increases, showing the magnification behaviour.

Note that the ordinate intercept is actually less than 1.0. This is due to the fact that the deck moments are dependent on the locations of the cable connections to the deck. If a different layout of cable spacing is used such that a connection occurs at the point on the deck corresponding to the maximum moment location for a continuous elastic foundation, then the deck would be subjected to the maximum possible moment. Thus, it can be seen that the curve obtained for $N = 20$ is really a happenchance result (within a narrow range) and for design purposes should be replaced with the curve that represents the maximum possible moment. The cable layout in the simplified

backspan model could be adjusted to achieve this, but a more convenient way to get the maximum possible moment is to increase the number of cables to 80. Increasing the number of cables also has the effect of reducing the local negative bending moments, which increases the maximum positive moment as well. The result for $N = 80$ is plotted on Figure 3.23 as the dotted curve. This curve behaves as expected and should now be the one to refer to in future discussions.

A comparison can be made with Hetényi's maximum moment for a beam-column on an elastic foundation with constant axial load $M_{H_{axial}}$ where:

$$M_{H_{axial}} = \frac{EIw_L}{k} \frac{(\beta^2 + \alpha^2)^2}{2\alpha\beta(\cosh \beta l_B + \cos \alpha l_B)} [\sinh \beta x \sin \alpha(l_B - x) + \sin \alpha x \sinh \beta(l_B - x)]$$

where α and β are the same as defined for deflections. The ratio $M_{H_{axial}}/M_H$ is formed and plotted as the dashed curve on Figure 3.23. The standard amplification formula for a simply supported beam-column is applied to this model and is also plotted on the figure. The model moment amplification is much higher than the deflection amplification, which may be because the suppressed deflection causes severe curvatures. It is again noted that the triangular axial load distribution in the computer model produces a more severe magnification of the maximum moment than the constant axial load of Hetényi's model.

Figures 3.24 to 3.26 show the model moment magnification for varying cable tautness, deck decay length and live load. Looking at the curves for $N = 80$ it can be seen that the moment magnification is slightly more severe than the deflection magnification, but the general behaviour with varying dimensionless ratios is similar to the deflection behaviour.

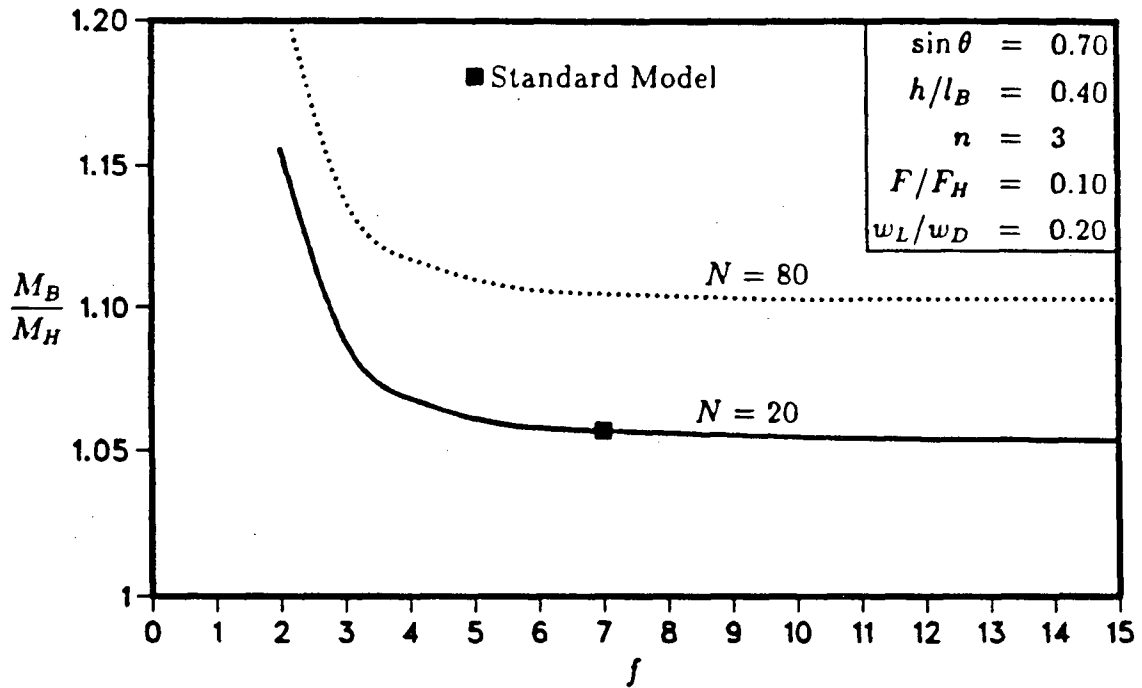


Figure 3.24: Dimensionless moment versus dimensionless cable tautness.

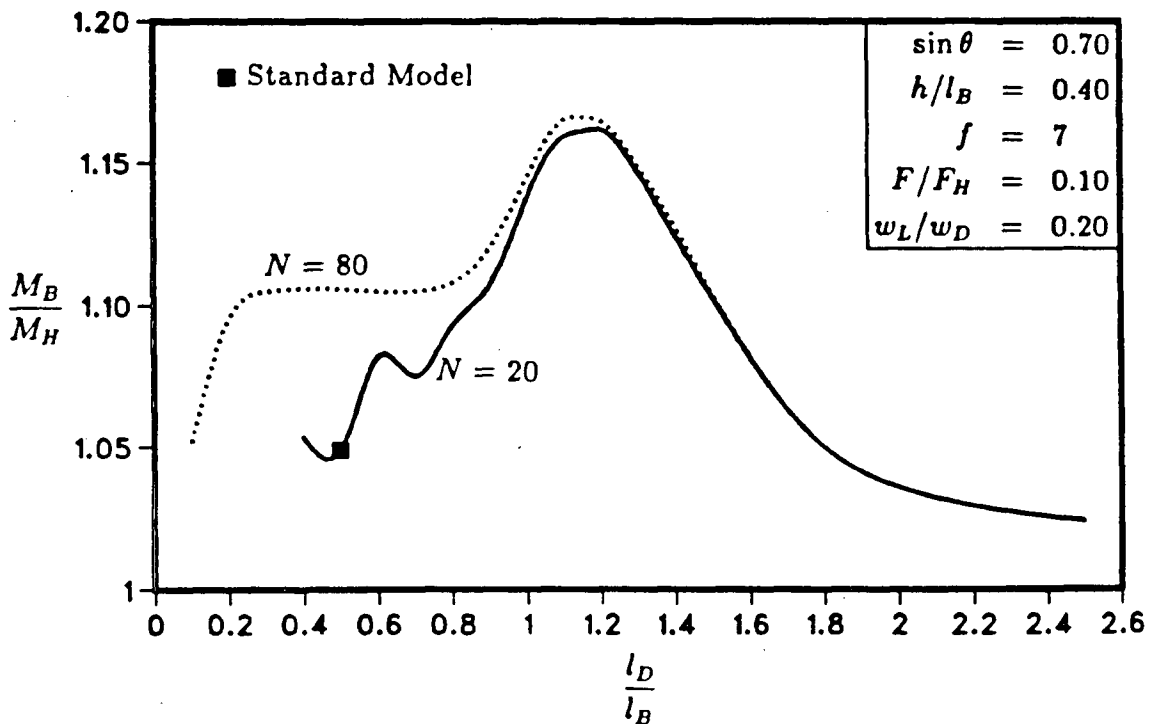


Figure 3.25: Dimensionless moment versus dimensionless decay length.

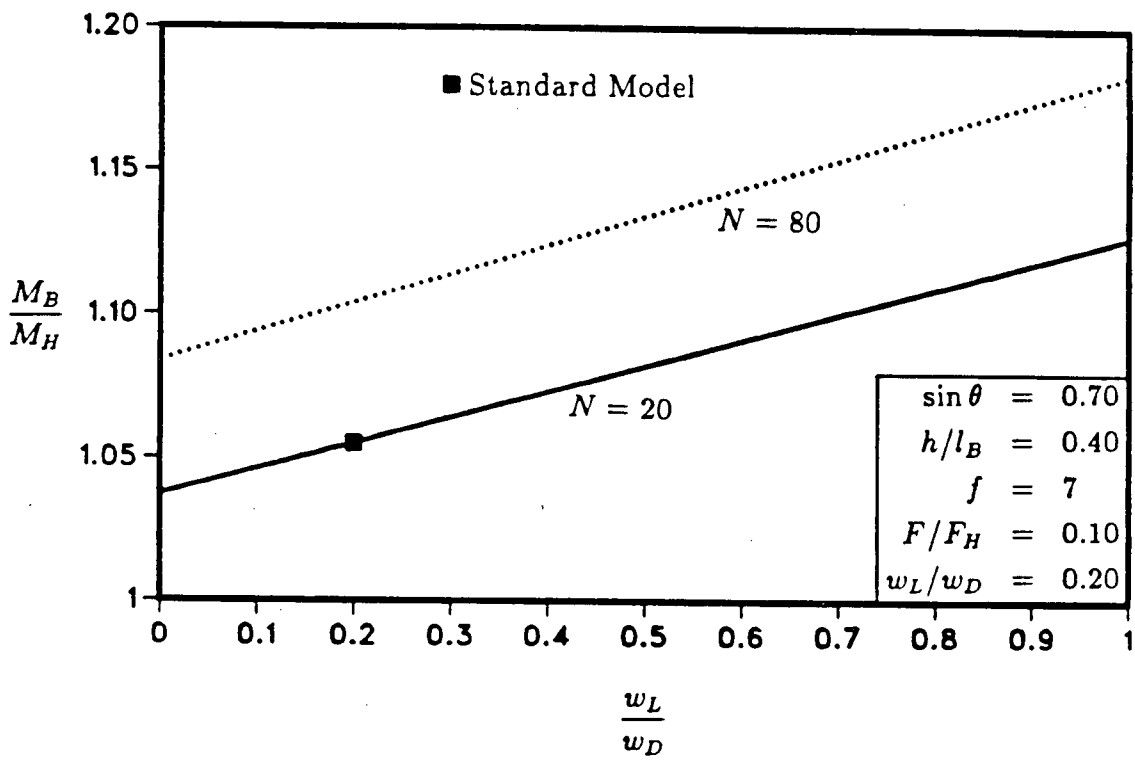


Figure 3.26: Dimensionless moment versus dimensionless load.

Chapter 4

Backspan Model

4.1 The Model

The second model is a more faithful representation of a cable stayed bridge backspan as shown in Figure 4.27. This model has varying cable lengths, inclinations and areas, and all the cables are attached to an imaginary immovable tower. It may seem that the model has changed drastically from the first model, but in fact the result of all the individual changes is only to produce a nonuniform elastic foundation and a slightly different distribution of deck axial load. The deck has a constant stiffness and the live load is applied as a distributed load, just as in the first model.

All of the model properties shown in Figure 4.27 have been identified in Chapter 3 except for s' , which is the cable spacing at the tower. However, most of the properties now have a subscript. The general subscript is " i " where $i = 1$ signifies the cable or deck section closest to the tower and $i = N$ is the backstay and corresponding deck section. The subscripts are necessary to describe the model, but in the dimensional analysis of this model, representative values will be used when referring to the backspan parameters and dimensionless ratios. This representative value shall be indicated by the subscript " $N/2$ " where $N/2$ is as calculated for even values of N , and for odd values of N , $N/2$ signifies the average value of two cables. For example, if $N = 11$ then $A_{C_{N/2}}$ would be the average of A_{C_5} and A_{C_6} .

The major geometric change from the first model is the varying cable height h_i . The parameters (h_N) and (h_1) will define the top and bottom cable locations. The

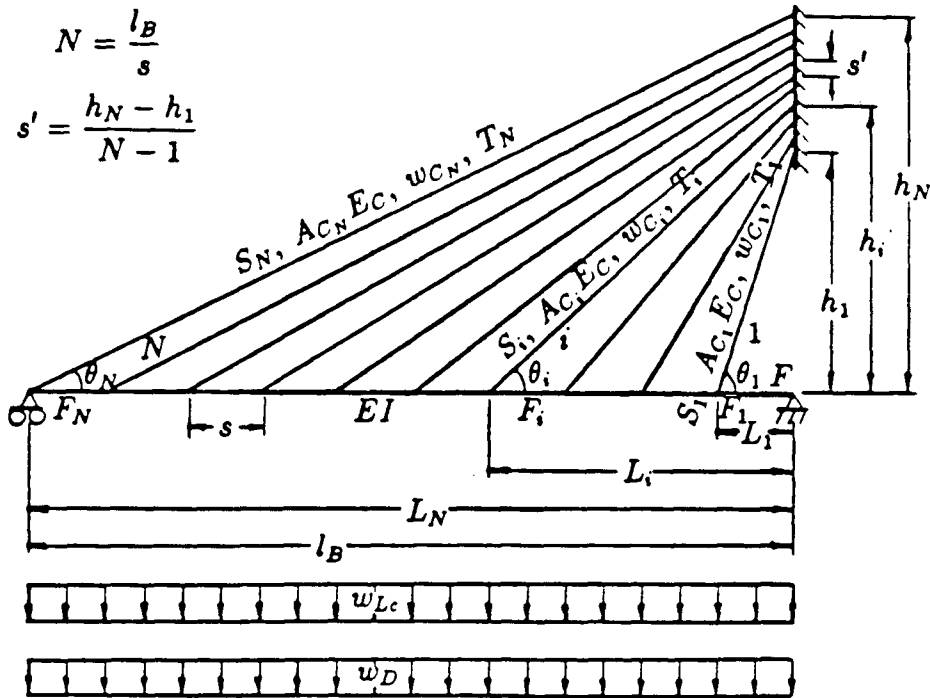


Figure 4.27: Backspan model.

remainder are at a constant spacing of s' , where

$$s' = \frac{h_N - h_1}{N - 1}$$

This nomenclature allows the entire range of cable layouts to be defined, from the radiating shape to the harp arrangement. The relationship of the first model cable height h to this model is $h = h_N/2$.

Initially the model is under dead load only and the cable tensions T_i are set up such that there are no moments in the deck at input geometry. The cable tensions represent the dead load, and the distributed dead load is not actually applied, just as in the first model. A common desire in cable stayed bridge design is to have all the cable dead load stresses the same. Since the cable inclinations vary, it is also necessary to vary the cable areas in order to maintain constant cable stresses. The free-body diagram of a cable-deck connection in Figure 4.28 helps to explain this requirement. The symbol " σ_C " represents the cable stress which is to be the same for all cables. By equilibrium

of forces:

$$w_D s = \sigma_C A_{C_i} \sin \theta_i$$

or

$$A_{C_i} = \frac{w_D l_B}{N \sigma_C \sin \theta_i}$$

The constant σ_C can be determined from the representative cable as

$$\sigma_C = \frac{w_D l_B}{N A_{C_{N/2}} \sin \theta_{N/2}}$$

so that

$$A_{C_i} = \frac{A_{C_{N/2}} \sin \theta_{N/2}}{\sin \theta_i}$$

which clearly shows that the cable areas vary.

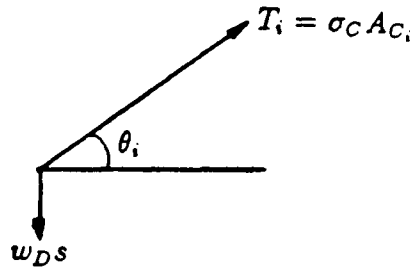


Figure 4.28: Free-body diagram of a cable-deck connection.

The parameter F is the maximum axial load in the deck induced by the cables in the initial state, i.e., for dead load only. The F_i represent the axial load in the i 'th deck section due to T_i , i.e., $F_i = T_i \cos \theta_i$ and $F = \sum_{i=1}^N F_i$.

4.2 Stability

4.2.1 Stability Dimensionless Ratios

The critical live load of the system is defined by the function

$$w_{Lc} = \mathcal{F}[EI, A_{C_{N/2}} E_C, l_B, h_1, h_N, N, w_{C_{N/2}}, w_D] \quad (4.14)$$

All nine of the parameters in Equation 4.14 are independent of each other. The parameters that do not appear in the equation are functions of the ones given in Equation 4.14, i.e.,

$$L_{N/2} = \frac{h_{N/2}}{\tan \theta_{N/2}} = \frac{l_B}{2}$$

$$S_{N/2} = \frac{h_{N/2}}{\sin \theta_{N/2}}$$

$$s = \frac{l_B}{N}$$

$$s' = \frac{h_N - h_1}{N - 1}$$

$$T_{N/2} = \frac{w_D l_B}{N \sin \theta_{N/2}}$$

$$F = \sum_{i=1}^N T_i \cos \theta_i = \frac{w_D l_B}{N} \sum_{i=1}^N \cot \theta_i$$

where

$$\sum_{i=1}^N \cot \theta_i = \sum_{i=1}^N \frac{i l (N - 1)}{N [h_1 (N - i) + h_N (i - 1)]}$$

$$\tan \theta_{N/2} = \frac{h_1 + h_N (1 - \frac{2}{N})}{l_B - \frac{l_B}{N}}$$

and

$$h_{N/2} = \frac{h_1 + h_N (1 - \frac{2}{N})}{2 - \frac{2}{N}}$$

for both even and odd values of N . Note that because h_1 and h_N are used as independent parameters, $\theta_{N/2}$ and $h_{N/2}$ —which were used in the previous model as θ and h —cannot be used for this model.

Seven dimensionless ratios need to be constructed out of the nine parameters in Equation 4.14. The seven ratios chosen to represent this model are:

$$\begin{aligned}
 & N \\
 & \frac{h_1}{l_B} \\
 & \frac{h_N}{l_B} \\
 & \frac{w_{Lc}}{w_D} \\
 & \frac{F}{F_H} = \frac{\frac{w_D l_B}{N} \sum_{i=1}^N \cot \theta_i}{2 \sqrt{\frac{N A_{C_{N/2}} E_C E I \sin^3 \theta_{N/2}}{l_B h_{N/2}}}} \\
 & \frac{l_D}{l_B} = \frac{\pi \sqrt{2}}{l_B} \sqrt{\frac{l_B h_{N/2} E I}{N A_{C_{N/2}} E_C \sin^3 \theta_{N/2}}} \\
 & f = \frac{w_D l_B}{N \sin \theta_{N/2} \sqrt{\frac{A_{C_{N/2}} E_C}{24} \left(\frac{w_{C_{N/2}} h_{N/2}}{\tan \theta_{N/2}} \right)^2}}
 \end{aligned}$$

The last three dimensionless ratios above are the same as the ones used for the first model, the only difference being in the use of the subscript “ $N/2$ ” and $F = \sum_{i=1}^N F_i$. The ratios N and w_{Lc}/w_D are exactly the same as those used in Chapter 3. The only new ratios are the ones that define the cable layout, h_1/l_B and h_N/l_B .

In summary, the stability of the backspan model is described by the function:

$$\frac{w_{Lc}}{w_D} = \mathcal{F} \left[N, \frac{h_1}{l_B}, \frac{h_N}{l_B}, f, \frac{l_D}{l_B}, \frac{F}{F_H} \right]$$

This function is based on beam-column on an elastic foundation stability theory with both the cable slackness and the $P-\Delta$ nonlinearities modelled.

4.2.2 Parameters and Ratios from Existing Bridge Designs

The same nine cable stayed bridges that were used for the first model are used to acquire data for the construction of this model. However, the subscripting system introduced for this model suggests a choice of representative values for cable area, height and angle different from the “centroid cable” of Chapter 3. The new representative cable is the one (or average of two, as explained previously) corresponding to $i = N/2$. The area, height and angle of this cable are used as the representative values for the bridge and as the “ $i = N/2$ ” values for the model. Appendix C.3 shows the numerical values obtained for this backspan model.

All the other parameters are determined from the design drawings in exactly the same manner as described in Chapter 3, except for F . In the dimensional analysis of this model F is calculated as $F = \frac{w_D l_B}{N} \sum_{i=1}^N \cot \theta_i$ but this is too unwieldy to use in acquiring data from design drawings. A simple method is to use $F = NF_{N/2}$ or $F = w_D l_B / \tan \theta_{N/2}$. This is based on a linear distribution of F_i ; however, since the actual distribution for this model is concave in shape, $F_{N/2}$ is larger than that for a linear distribution and $NF_{N/2}$ is a conservative value for F .

The representative dimensionless ratios for each of the nine bridges are calculated using the data in Appendix C.3. The averages of these nine ratios are used to construct the new standard backspan model. These values are given in Appendix C.4 and are repeated here:

$$N = 20$$

$$h_1/l_B = 0.30$$

$$h_N/l_B = 0.50$$

$$f = 7$$

$$l_D/l_B = 0.50$$

$$F/F_H = 0.10$$

$$w_L/w_D = 0.20$$

where, for the purpose of calculating f : $w_{CN/2} = A_{CN/2} \gamma_C$.

4.2.3 Results of Stability Analysis

The standard backspan model of Figure 4.27 is constructed using the preceding values for the dimensionless ratios. Using the computer program ULA, the critical load ratio for this standard model is found to be $w_{Lc}/w_D = \lambda w_L/w_D = 18.2$, which is to say, since $w_L/w_D = 0.20$, that the factor of safety on the live load against elastic buckling of the standard model is 91. Just as in Chapter 3, the factor of safety for this model does not apply to cable stayed bridges because only the backspan is modelled. However, the very much higher factor of safety over the 50 obtained for the simplified backspan model should be explained. The reason for the increase is the nonuniform elastic foundation. Due to the increasing cable angle, a much stiffer foundation exists at the high axial load area of the deck than in the previous model; which means that higher axial loads are needed to cause instability.

The deflected shape of the deck just before stability failure is shown in Figure 4.29 along with the axial load (dead load plus live load) and moment distributions. The nonlinear distribution of deck axial load is mostly due to the varying cable inclinations and to a smaller degree due to the deck deflections.

The possibility of an uplift pressure causing a more critical loading condition is investigated for this model in the same manner as for the previous model. The resulting factor of safety plot is given in Figure 4.30. In this case, the forced deflected shape is more influential than the reduction in deck axial load and the factor of safety decreases with increasing uplift pressure. This decrease, however, is not severe—there is only a 8.2% drop in the factor of safety when the uplift pressure is 50% of the live load magnitude. There is a further drop of 20.1% for an uplift pressure of 100% of the live load magnitude. High uplift pressures are possible, [24] but the occurrence of a full live

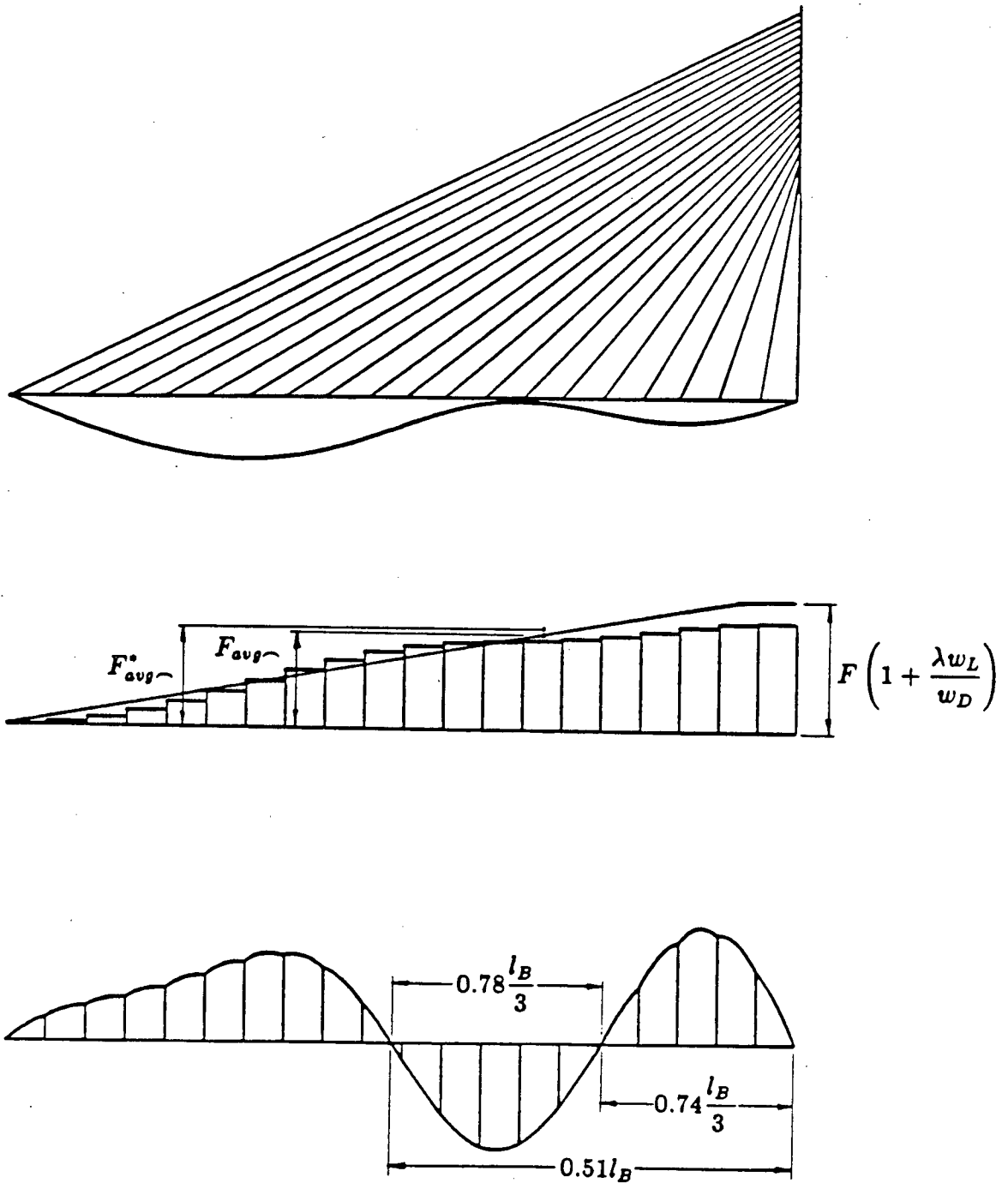


Figure 4.29: Stability failure of backspan model.

load at very high wind velocities is improbable, therefore, the high uplift pressure range of Figure 4.30 is not truly applicable. Wind and dynamic loads are beyond the scope of this thesis and the uplift pressure load case will not be used in further analyses for this model, but it should be kept in mind that a slightly more severe result is possible.

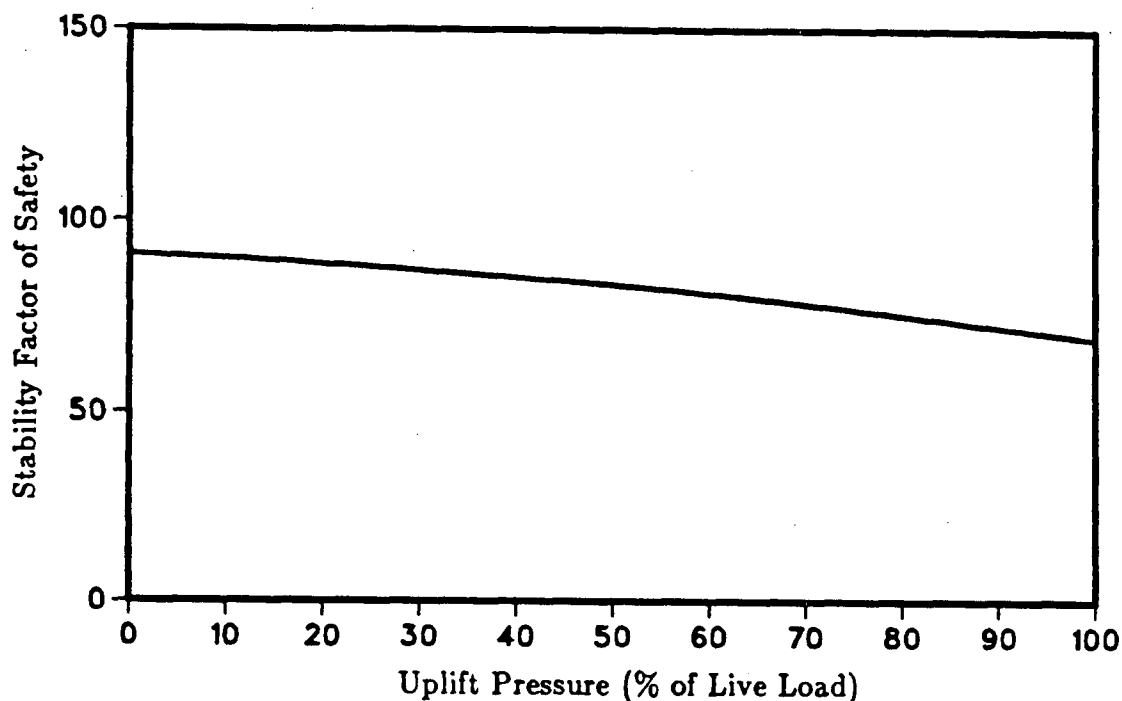


Figure 4.30: Stability factor of safety of backspan model.

The fact that the backspan buckled at $F/F_H = 0.10$ and not at $F/F_H = 1.0$ is accounted for by the same three reasons given for the simplified backspan model. However, the critical deck section is not as easy to determine as for the simplified backspan model. For the previous model it was obvious that the deck section with the highest axial load was critical because the elastic foundation was uniform. In this case, with the varying foundation stiffness and the fairly uniform axial distribution over two half-waves, a closer investigation is needed to identify the critical section.

A plot of F_{avg}^*/F_H vs x/l_B is shown in Figure 4.31 for the simplified backspan model of the previous chapter. The curve is calculated by taking the average of l_B/n

(in this case $l_B/n = 20/3$) deck axial forces nearest a cable and dividing by $F_{H\sim}$ as given in Chapter 3. Figure 4.31 clearly shows that the critical deck section is defined by the half-wave nearest to the tower.

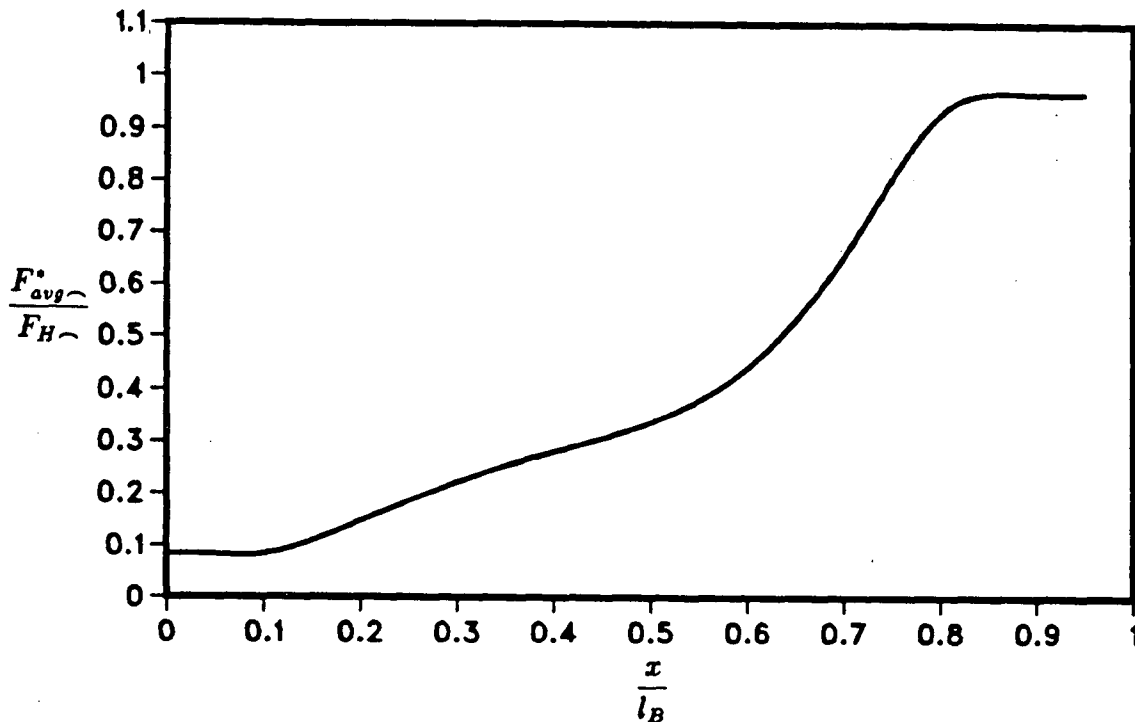


Figure 4.31: Critical simplified backspan section.

The corresponding plot for the current backspan model is shown in Figure 4.32. Three curves are plotted, each based on the assumption that only one of the three half-waves is critical. The curves are calculated using average deck axial loads as was done for the simplified backspan, with the variation of foundation stiffness of this model averaged out in the same manner. From this figure it can be seen that the middle half-wave is the critical section.

It is academically interesting to identify the critical deck section, but this knowledge is of little practical use. Therefore, for simplicity in future calculations and with only a small loss in accuracy, the deck section with the highest average axial load—whether it spans over one or more half-waves—shall be assumed to be the critical section. With

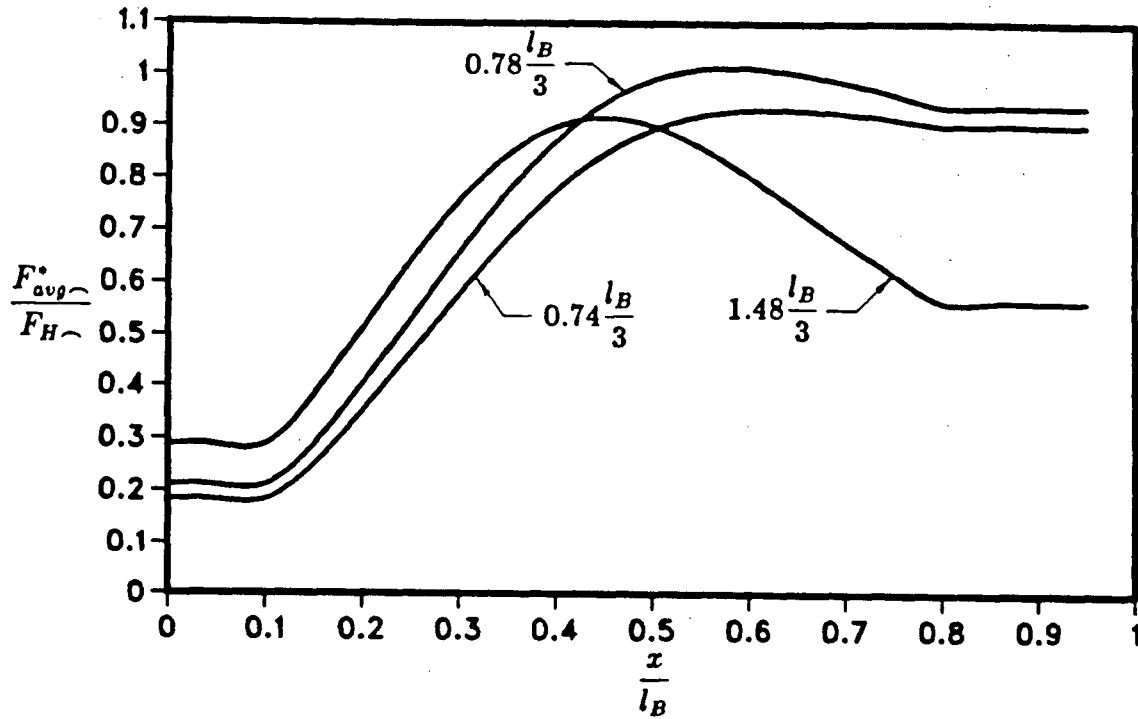


Figure 4.32: Critical backspan section.

this in mind, the three adjustments to F/F_H will be made for the standard backspan model.

The first adjustment gives

$$\frac{F}{F_H} \frac{w_D + \lambda w_L}{w_D} = 0.1(18.2 + 1.0) = 1.92$$

The second adjustment is to use the average axial load over the critical deck section. In this case, that will be over the two half-waves nearest to the tower. The " F_{avg} " nomenclature is retained to represent this, with the " \sim " subscript symbolizing one or more half-waves. The linear formula for this average is

$$F_{avg\sim} = F \left(1 + \frac{\lambda w_L}{w_D} \right) \left(\frac{2n - 2}{2n} + \frac{1}{2N} \right)$$

Due to the nonlinear axial distribution this is not the real average. Computer runs near critical show that the real average $F^*_{avg\sim}$ is $1.006F_{avg\sim}$ for the particular case shown in Figure 4.29.

The dimensionless ratio now becomes

$$\frac{F_{avg\sim}^*}{F_H} = 1.006 \frac{F}{F_H} \left(1 + \frac{\lambda w_L}{w_D} \right) \left(\frac{2n-2}{2n} + \frac{1}{2N} \right) = 1.336$$

The final refinement is to replace F_H with $F_{H\sim}$ which reflects the boundary conditions and average foundation stiffness of the critical region. The effective length of the critical half-wave is $0.51l_B/2$ as is shown in Figure 4.29, and the properties of cable 5 are used to calculate the average foundation stiffness, i.e.,

$$F_{H\sim} = \left(\frac{2}{0.51l_B} \right)^2 \pi^2 EI + \left(\frac{0.51l_B}{2} \right)^2 \frac{N A_{C_5} E_C \sin^3 \theta_5}{\pi^2 l_B h_5}$$

The ratio $F_H/F_{H\sim}$ is calculated to be 0.680 and the final ratio is

$$\frac{F_{avg\sim}^*}{F_{H\sim}} = \frac{F_{avg\sim}^*}{F_H} \frac{F_H}{F_{H\sim}} = 1.336 \times 0.680 = 0.91$$

Thus, the backspan model stability mechanism can be understood in terms of a beam-column on an elastic foundation if the effect of the nonuniform elastic foundation is taken into consideration.

The standard model is next varied by altering only F/F_H and then determining the live load necessary to cause the deck to buckle. The result of this exercise is shown in Figure 4.33, where the F/F_H ratio is adjusted to include the live load.

The theoretical result for a beam-column on an elastic foundation is also plotted in Figure 4.33 and labelled as "Hetényi." The discrepancy between the two results can be eliminated if all the adjustments as explained for the standard model, are made. For example, if the calculation for the ordinate intercept were carried out, the ratio $F_{avg\sim}^*/F_{H\sim}$ would be 1.01 as compared to $F/F_H = 1.64$.

The dimensionless ratio l_D/l_B is now varied in the same manner that n was varied for the simplified backspan model. The range of l_D/l_B in existing cable stayed bridge designs is from 0.40 to 0.65 and the stability curves for $l_D/l_B = 0.40$ and $l_D/l_B = 0.65$ are plotted in Figure 4.34 along with the curve for $l_D/l_B = 0.50$.

There is a variation with l_D/l_B in that the three curves differ from each other. Just as in the simplified backspan model, this variation is not expected with Hetényi's

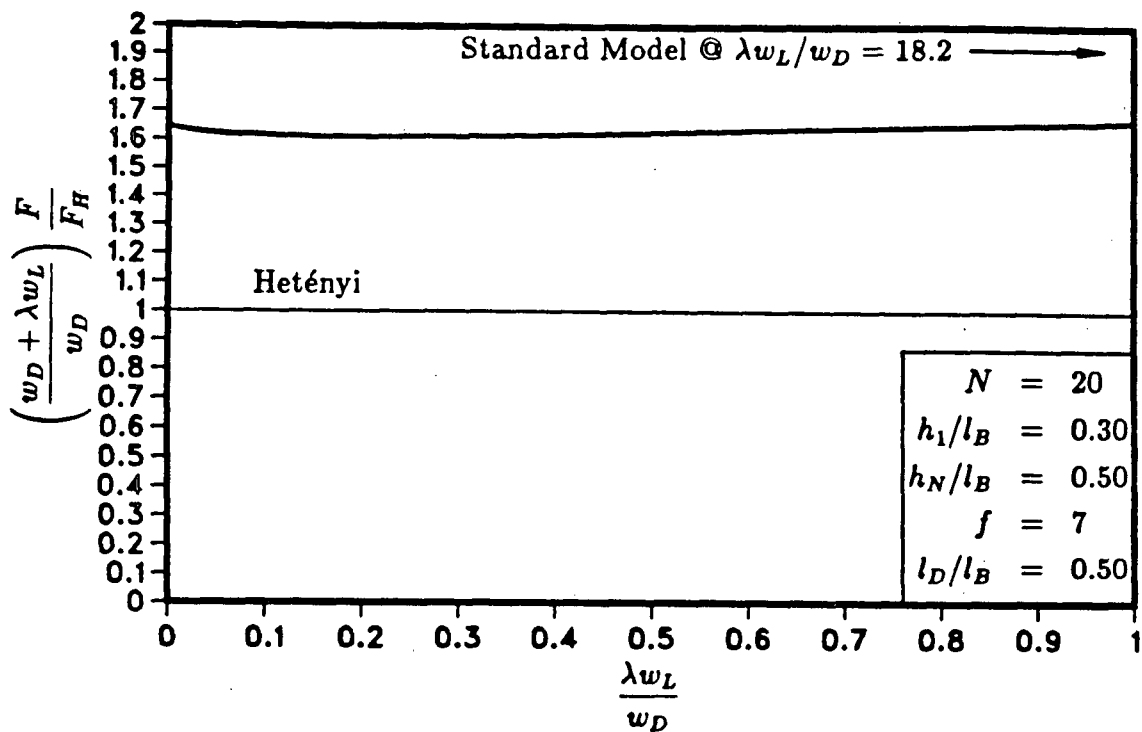


Figure 4.33: Stability of backspan model.

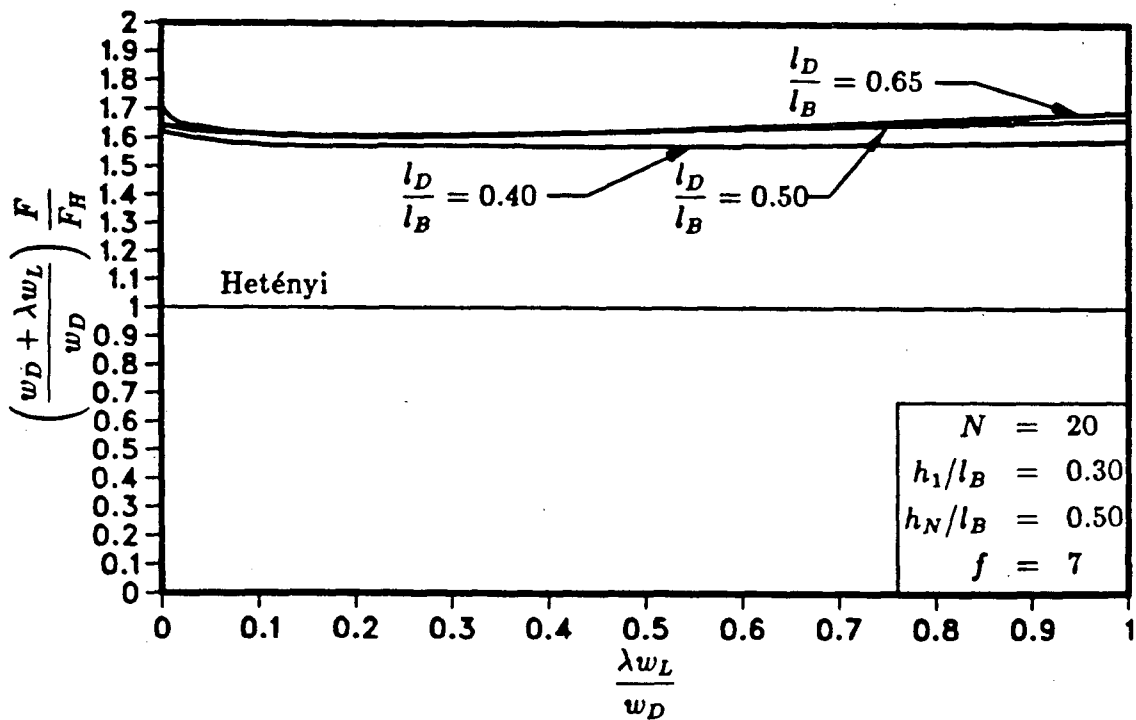


Figure 4.34: Stability of backspan model— l_D/l_B varied.

theoretical result, and if all of the adjustments to F/F_H are made to the curves as was done for the standard model, all three curves would plot nearly the same. The following table summarizes the result of these adjustments for the ordinate intercepts:

$\frac{l_D}{l_B}$	$\frac{F}{F_H}$	$\frac{F_{avg}^*}{F_H}$
0.40	1.62	1.01
0.50	1.64	1.04
0.65	1.71	0.99

Thus, it can be seen that the stability of the backspan model can be compared to a beam-column on an elastic foundation.

Just as in the previous model, altering the initial cable tautness f in the normal range of 5 to 10, did not affect the model behaviour. Only when the cables are slack ($f < 2$) is an effect seen, and then only for low live loads because higher loads tighten the cables.

The remaining dimensionless ratios, which are all based on the model geometry, are not investigated for this model.

4.3 Deflection and Moment

The choice of deflection and moment functions to represent this backspan model is based on the same rationale presented in Chapter 3.

The definition of the backspan model deflection in terms of independent parameters is

$$\delta_B = \mathcal{F}[EI, A_{C_{N/2}} E_C, l_B, h_1, h_N, N, w_{C_{N/2}}, w_D, w_L]$$

and the maximum nondimensional deflection of the backspan model is described by the function:

$$\frac{\delta_B}{\delta_H} = \mathcal{F}\left[N, \frac{h_1}{l_B}, \frac{h_N}{l_B}, f, \frac{l_D}{l_B}, \frac{w_L}{w_D}, \frac{F}{F_H}\right]$$

With δ_H defined by Eq. 3.12 and

$$k = \frac{N A_{C_{N/2}} E_C \sin^3 \theta_{N/2}}{l_B h_{N/2}}$$

this function will show the magnification of the maximum deck deflection due to the deck axial load. All other ratios in this function are the same as the ones defined for the stability analysis of this model.

The definition of the backspan model moment in terms of independent parameters is

$$M_B = \mathcal{F}[EI, A_{C_{N/2}} E_C, l_B, h_1, h_N, N, w_{C_{N/2}}, w_D, w_L]$$

and the maximum nondimensional moment of the backspan model is described by the function:

$$\frac{M_B}{M_H} = \mathcal{F} \left[N, \frac{h_1}{l_B}, \frac{h_N}{l_B}, f, \frac{l_D}{l_B}, \frac{w_L}{w_D}, \frac{F}{F_H} \right]$$

With M_H defined by Eq. 3.13 this function will show the magnification of the maximum deck moment due to the deck axial load.

4.3.1 Results of Deflection Analysis

The same standard backspan model is used for maximum deflection analysis as that for the stability analysis. The deflection of the standard model under a uniformly distributed live load ($w_L/w_D = 0.20$), is shown in Figure 4.35 along with the beam on an elastic foundation deflection. The δ_B/δ_H ratio is equal to 1.420 which is a significant deviation from the Hetényi deflection. This is mostly due to the fact that this backspan model has a varying foundation stiffness, which makes it a significantly different structure from the Hetényi model and the backspan of Chapter 3. The effect of the varying foundation in this model is readily seen in that the right side or "stiff foundation" deck deflection is much less than the left side deck deflection. Also, the slight deflection magnification in the previous model was at the high axial load deck section, as expected; whereas, in this model the large deflection occurs in the low axial

load deck section, which indicates that the flexible foundation in this region is the cause of the large deflections. The maximum live load deflection versus span ratio is $1/1500$ which is well within the recommended value of $1/500$.

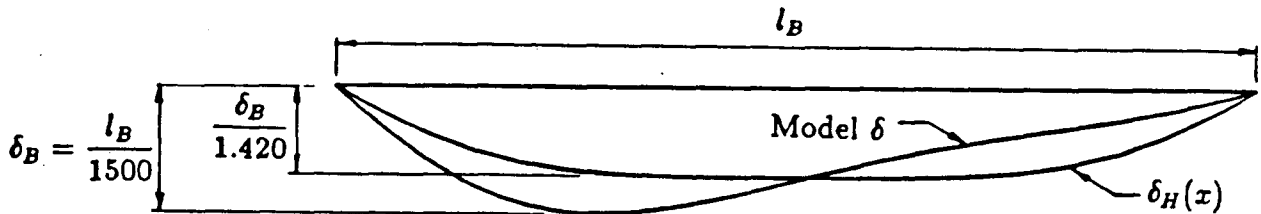


Figure 4.35: Deflection of standard backspan model.

The standard model is now varied by altering the F/F_H ratio while keeping all other ratios constant. The maximum deflection is then determined from a computer analysis and the δ_B/δ_H ratio is plotted against F/F_H . The result is given in Figure 4.36 for a range of F/F_H values.

The deflection magnification is apparent in that the δ_B/δ_H ratio increases from 1.4 to 2.05 as F/F_H increases from 0.0 to 1.2. This is a less rapid rate of increase in δ_B/δ_H than the simplified backspan model amplification (Figure 3.16) but the actual deviation from the Hetényi model is greater in this model for $F/F_H > 0.8$. The high initial deflection is due to the low foundation stiffness at the left deck section and the low rate of magnification is due to δ_B being at the low axial load deck section.

The deflection plot as a function of dimensionless decay length l_D/l_B is shown in Figure 4.37. It can be seen that δ_B/δ_H is highly dependent on l_D/l_B in the normal range (l_D/l_B from 0.40 to 0.65) for cable stayed bridges. This dependency is not present in the simplified backspan model, in fact at the standard value of $l_D/l_B = 0.50$, the δ_B/δ_H ratio is almost 1.0 for the previous model. The varying foundation stiffness of the

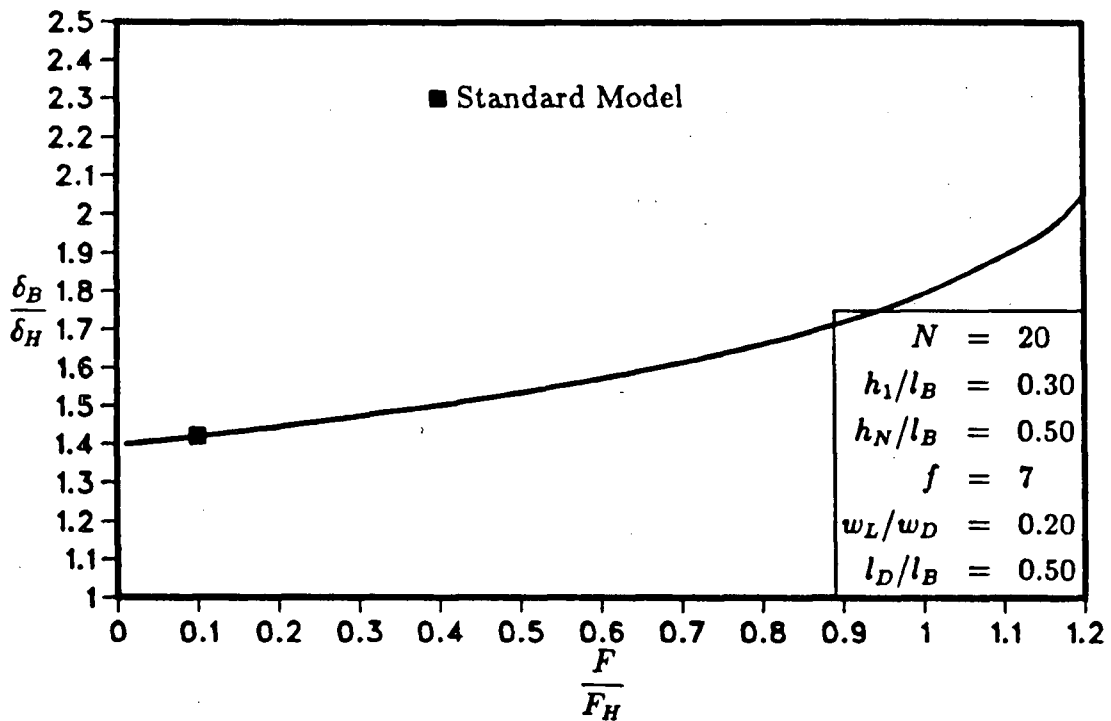


Figure 4.36: Magnification of maximum deflection.

current model produces a value of 1.42 for δ_B/δ_H at $l_D/l_B = 0.50$ (and $F/F_H = 0.10$) instead of $\delta_B/\delta_H \approx 1.0$, and $\delta_B/\delta_H = 1.40$ for $F/F_H = 0.0$. If Figure 4.36 were to be used for design purposes it would be necessary to plot a series of curves, each with a different value of l_D/l_B . From Figure 4.37 it is apparent that the curves for $l_D/l_B > 2.0$ would all be the same and δ_B/δ_H would be equal to 1.0 for $F/F_H = 0.0$. Note, that for $l_D/l_B > 2.0$ the foundation stiffness would be essentially constant over the backspan length and the behaviour would closely follow that of the simplified backspan model.

The cable tautness graph is shown in Figure 4.38. The cable tautness effect is the same as for the simplified model except for the asymptote being at 1.42 instead of 1.02. The importance of having tight cables is again demonstrated by the magnification of the deflection for low values of f .

Figure 4.39 shows the relationship between δ_B/δ_H and the live load to dead load ratio w_L/w_D . It can be seen that w_L/w_D has very little influence on δ_B/δ_H , even less

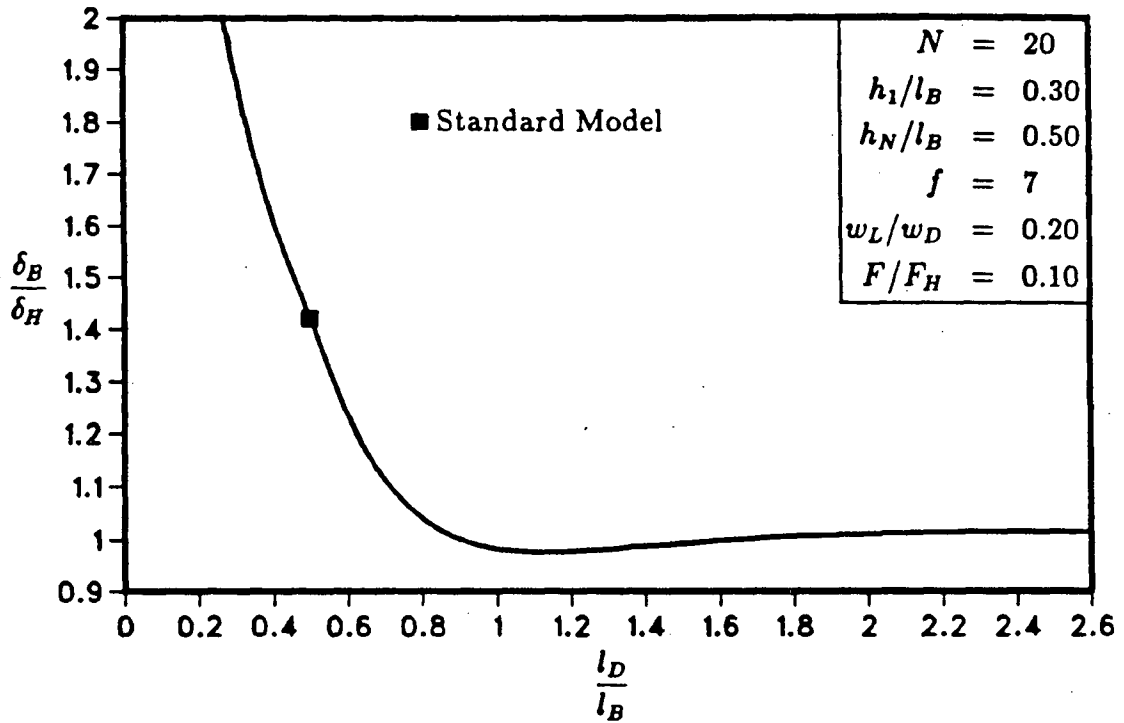


Figure 4.37: Dimensionless deflection versus dimensionless decay length.

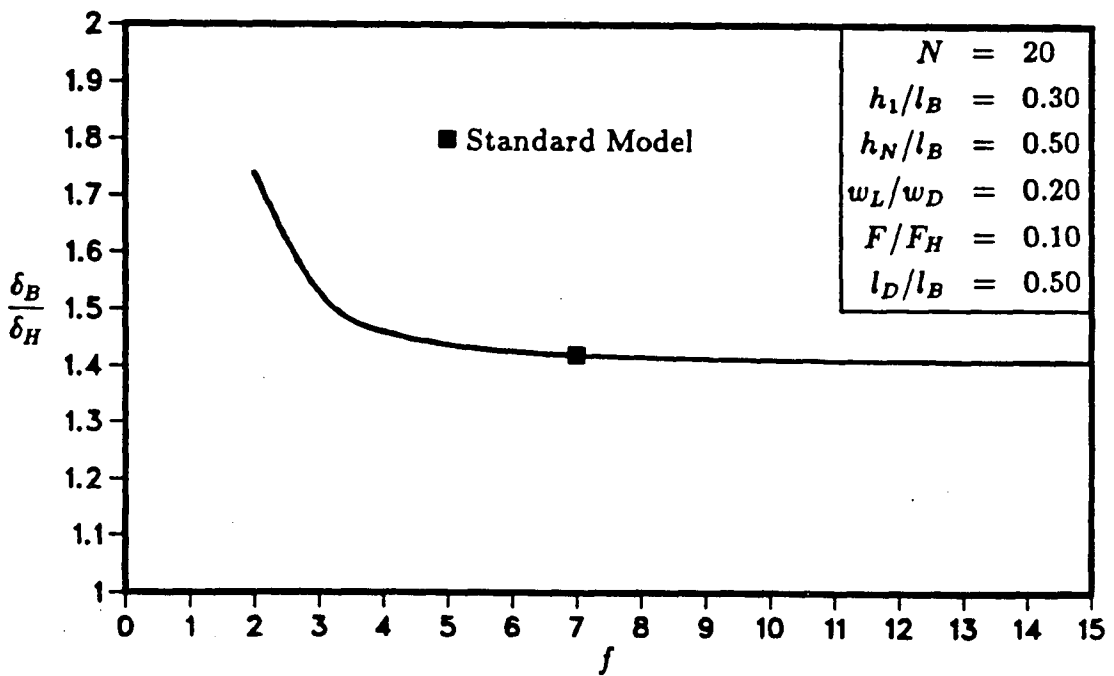


Figure 4.38: Dimensionless deflection versus dimensionless cable tautness.

than was exhibited for the simplified model. Again, this is because δ_B is at the low axial load deck section where the nonlinear $P-\Delta$ effect is not as pronounced as at the high deck axial load section.

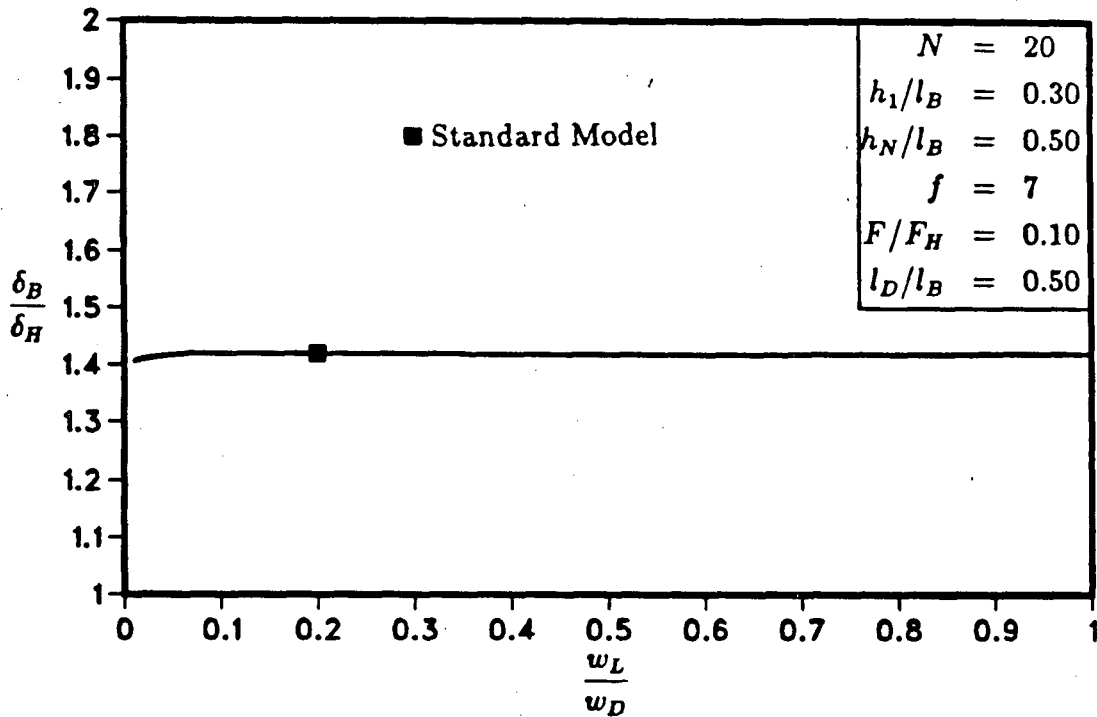


Figure 4.39: Dimensionless deflection versus dimensionless load.

4.3.2 Results of Moment Analysis

The same standard backspan model is used for maximum moment analysis as that for the deflection analysis. The moment distribution of the standard model with $w_L/w_D = 0.20$, is shown in Figure 4.40 along with the beam on an elastic foundation moment. The M_B/M_H ratio is equal to 1.685. This large deviation from the Hetényi moment is due to the relatively flexible foundation of the model in the leftmost region, which allows more severe curvatures than the Hetényi and Chapter 3 models. The maximum moment is $w_L l_B^2 / 140$ which is an 85% increase over the simplified backspan model moment.

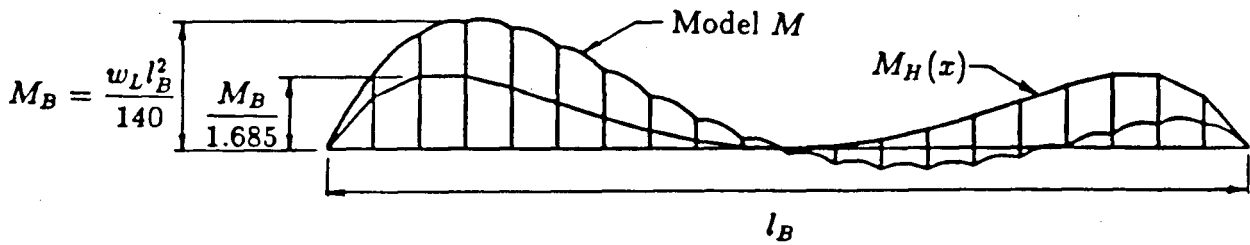


Figure 4.40: Moment of standard backspan model.

The standard model is now varied by altering the F/F_H ratio and the M_B/M_H ratio is plotted against F/F_H in Figure 4.41. It can be seen that this plot is quite different from the corresponding plot (Figure 3.23) for the simplified backspan model. The moment magnification follows a different path, the ordinate intercept is not zero, and the curve for $N = 80$ is not as significant as it is for the previous model.

The analysis for $N = 80$ is done in order to increase the chance of having a cable connected to the deck at the theoretical maximum moment location. In this case, the flatter curve of the moment diagram (compare Figure 4.40 with Figure 3.21) improves the chances of the twenty cable layout to produce the maximum possible moment. In fact, the two curves of Figure 4.40 cross each other which indicates that the local bending moment influence is greater than the cable location dependency at high F/F_H ratios.

It is interesting to note that there is very little moment magnification due to F/F_H until F/F_H is greater than 0.7. The magnification increases when F/F_H increases beyond 0.7, but this is well beyond the existing cable stayed bridge maximum F/F_H ratio of 0.3. Thus, there is very little moment magnification of the standard model and the models within normal ranges, but there is a high initial deviation from the Hetényi moment. This is due to the same reasons given for the deflection magnification plot, i.e., the low foundation stiffness at the left deck section and M_B is at the low deck axial

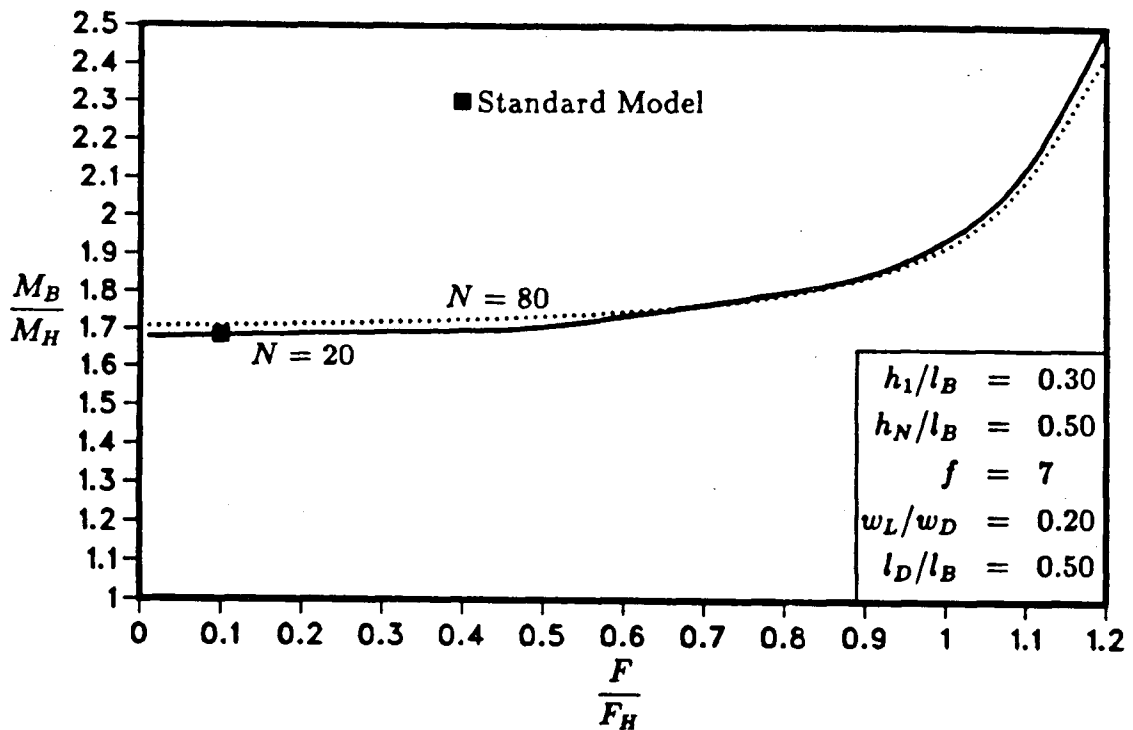


Figure 4.41: Magnification of maximum moment.

load region.

The moment plot as a function of dimensionless decay length l_D/l_B is shown in Figure 4.42. It can be seen that M_B/M_H is highly dependent on l_D/l_B in the normal range (l_D/l_B from 0.40 to 0.65) for cable stayed bridges. For $l_D/l_B < 0.5$ the model with twenty cables loses accuracy and the model with $N = 80$ should be used for analysis purposes. Just as for deflection, if Figure 4.41 were to be used for design purposes it would be necessary to plot a series of curves, each with a different value of l_D/l_B , with the curves for $l_D/l_B > 2.0$ all being the same and going through $M_B/M_H = 1.0$ at $F/F_H = 0.0$.

Figures 4.43 and 4.44 show the model moment deviation for varying cable tautness and live load, respectively. It can be seen that the moment deviation is more severe than the deflection deviation, but the general behaviour with varying dimensionless ratios is similar to the deflection behaviour.

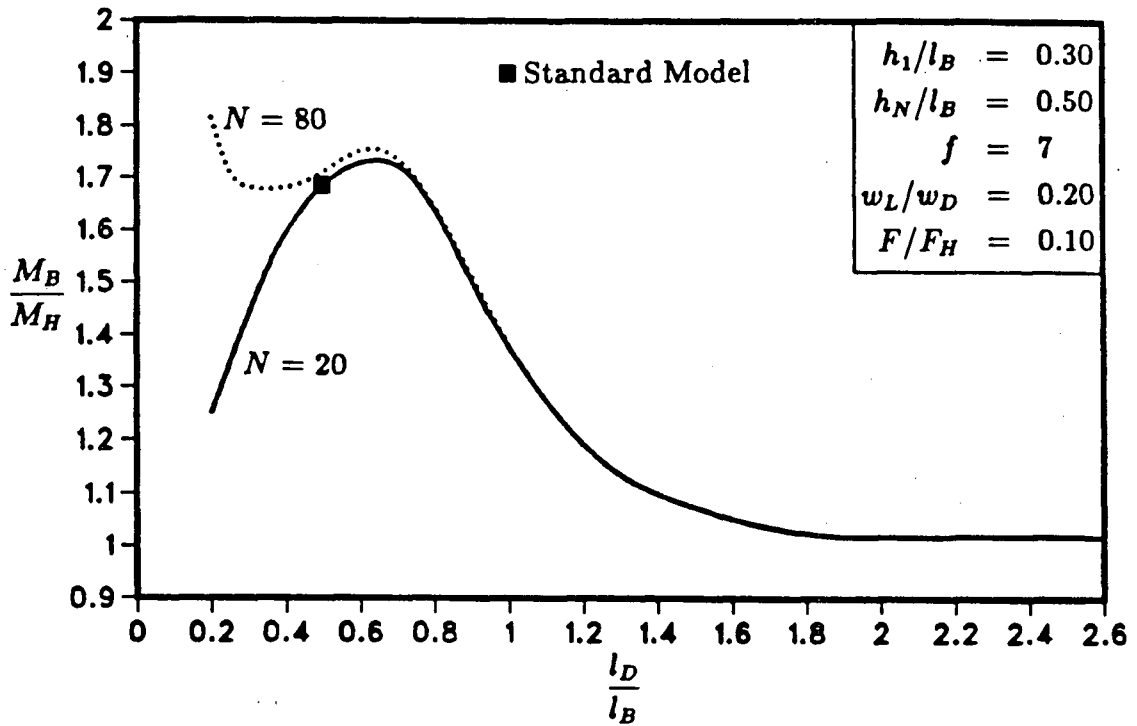


Figure 4.42: Dimensionless moment versus dimensionless decay length.

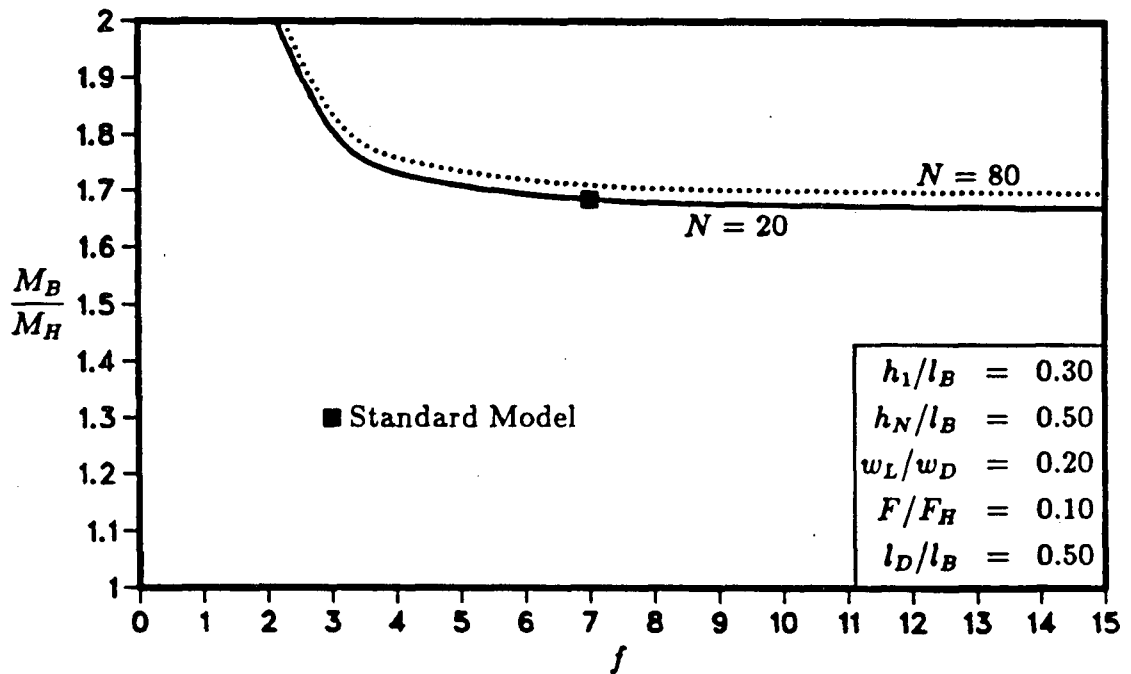


Figure 4.43: Dimensionless moment versus dimensionless cable tautness.

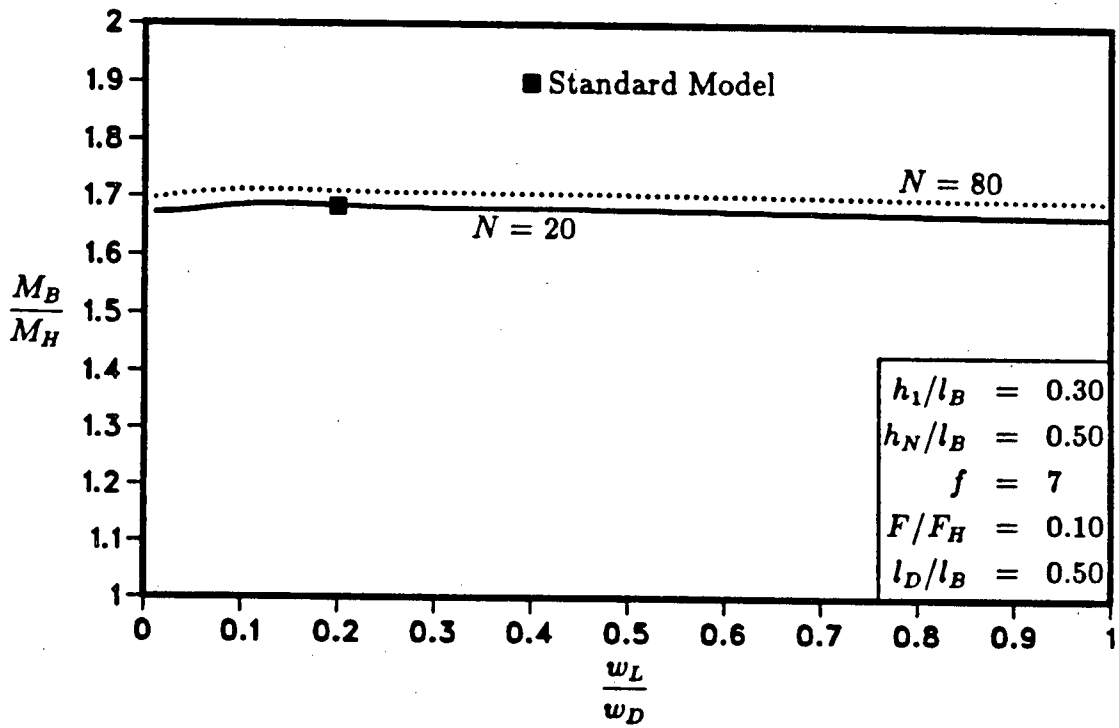


Figure 4.44: Dimensionless moment versus dimensionless load.

Chapter 5

Full Bridge Model

5.1 The Model

The final model is a representation of an entire cable stayed bridge, half of which is shown in Figure 5.45. The cables are attached to the back and main spans at constant spacing s and to the towers at constant spacing s' . The towers are fixed to the ground but not directly connected to the deck. A spring, equivalent to a single vertical cable, is connected to the deck at the deck-tower intersections to keep the deck spans between cable stays constant at the towers. The cables are arranged in a fan shape with the anchor stay cables attached to a single point on the deck. The mainspan stays are arranged such that a deck section of length s is at the center of the bridge. The deck stiffness is constant along the entire bridge and the live load is applied as a distributed load.

The definition of all the parameters used in this model is given in the following:

A_{C_i} = i 'th cable cross-sectional area

A_{C_a} = total anchor cable cross-sectional area

E = deck elastic modulus

E_C = cable elastic modulus

E_T = tower elastic modulus

F = maximum axial load in deck due to dead load

F_i = i 'th axial load in deck due to i 'th cable

h_i = i 'th cable height

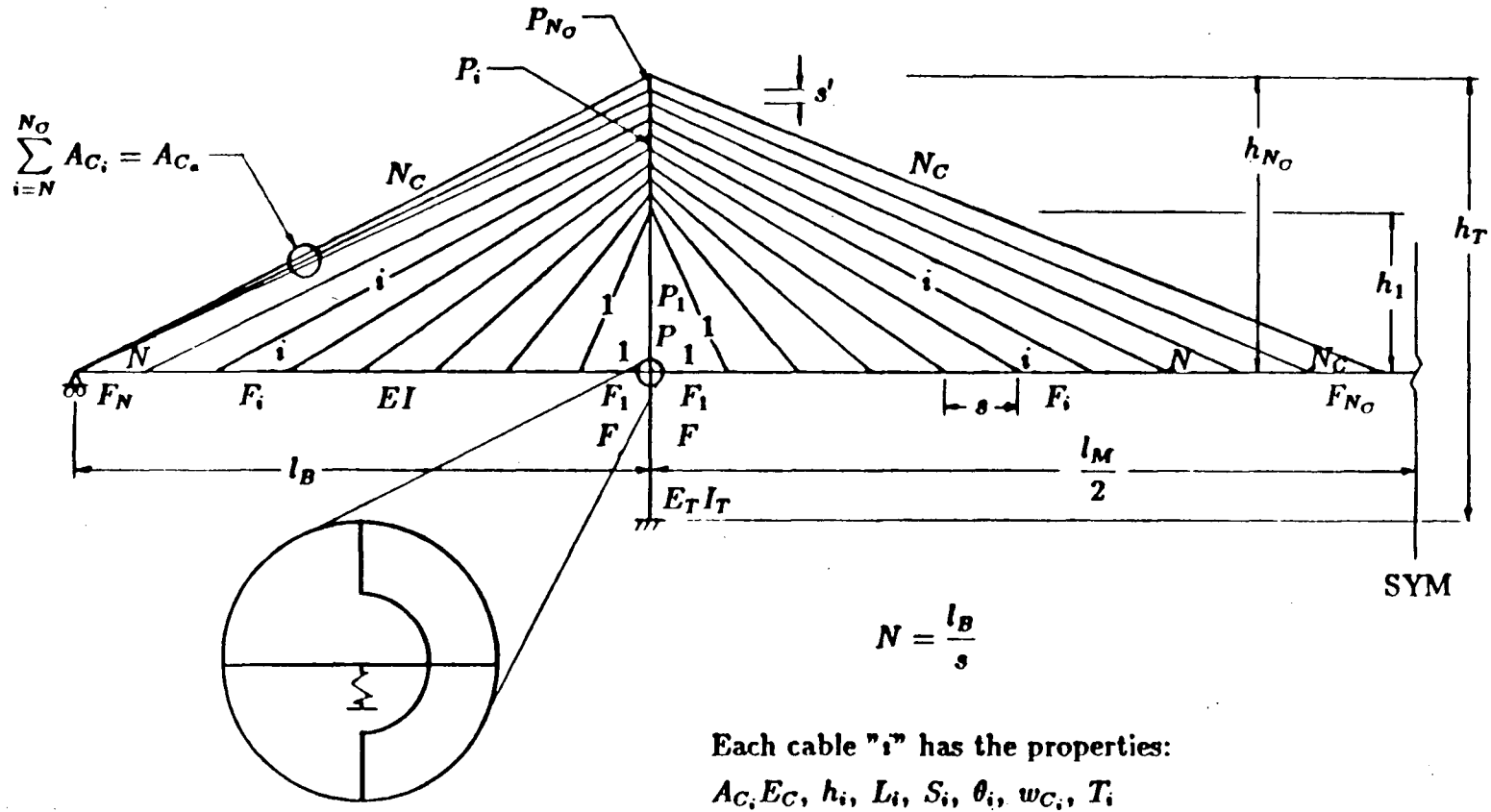


Figure 5.45: Bridge model (half shown—symmetric, except right bearing is a fixed pin).

- h_T = tower height
 I = deck moment of inertia
 I_T = tower moment of inertia
 L_i = horizontal projected length of i 'th cable
 l_B = backspan length
 l_M = mainspan length
 N = number of deck intervals in the backspan
 N_C = number of cables in the backspan or half the mainspan
 P = maximum axial load in tower due to dead load
 P_i = i 'th axial load in tower due to i 'th pair of cables
 S_i = i 'th cable chord length
 s = length of deck interval between cables
 s' = length of tower interval between cables
 T_i = i 'th cable tension in the chord direction due to dead load
 w_{C_i} = weight per unit length of i 'th cable
 w_D = uniformly distributed dead load
 w_{L_c} = critical uniformly distributed live load
 θ_i = i 'th cable chord angle of inclination to deck

There are four new parameters introduced in Figure 5.45: $E_T I_T$, h_T , l_M and A_{C_a} . The tower stiffness $E_T I_T$ is modelled as being constant along the entire length h_T . (The tower height is measured from the tower foundation; whereas, the cable heights are measured from the deck.) The anchor cable in the previous models was a single cable that was modelled in the same manner as the rest of the backspan cables. That single cable is present in this model with the addition of several more cables acting as anchors. This group of cables is referred to as the anchor cable and the total area A_{C_a} .

of this anchor cable is independent of the rest of the backspan cables. The number of cables that comprise the anchor cable is determined by the number of extra cables required to keep the cable spacing constant over the mainspan length l_M . Thus, each tower has the same number of cables attached to the mainspan side as to the backspan side.

In this model the maximum value of the subscript "i" is N_C where N_C is the number of cables attached on one side of a tower. This is different from the previous model which has a maximum value of N —the number of deck spaces in the backspan. The representative values for cable properties is still taken as the " $N/2$ " value. The maximum cable height, however, is now h_{N_C} with the bottom cable location at h_1 . The remainder are at a constant spacing of s' , where

$$s' = \frac{h_{N_C} - h_1}{N_C - 1}$$

This nomenclature allows the entire range of cable layouts to be defined, from the radiating shape to the harp arrangement. The relationship of the previous model cable height h_N to this model is $h_N = h_{N_C}$.

Initially the the input geometry is the dead load geometry and the cable tensions T_i are calculated such that there are no moments or deflections in the deck or towers. This is shown in Figure 5.46 which is an exploded view of Figure 5.45. The horizontal and vertical components of the cable tensions are drawn at the cable ends and the reactions of these forces are drawn at the corresponding tower and deck locations. The dead loads are also shown, but they are not actually applied in the computer model. That is, the cable, tower and deck axial forces at input geometry are in equilibrium with the deck dead load.

For a moment free tower at input geometry, the horizontal components of the anchor cable tensions and the corresponding mainspan cables must be equal. This means that the anchor cable vertical forces are not equal to the corresponding mainspan cable vertical forces, as is shown in Figure 5.46. The effect of this is a slight eccentricity of

the tower axial load if the cable to tower connections are not on the tower centerline. The effect of this horizontal eccentricity of the cable connections is neglected in this analysis.

The parameter P is the maximum axial load in the tower induced by the cables under dead load only. The P_i represent the axial load in the i 'th tower section due to the pair of cables attached above that section. For non-anchor cables, $P_i = 2w_D s$. For the anchor cables, $P_i = T_i \sin \theta_i + w_D s$ where T_i and θ_i are the anchor cable tensions and angles. The axial load in the tower at any location is the sum of the P_i above that point, and $P = \sum_{i=1}^{N_C} P_i$. The prestress due to the tower self-weight is small compared to the cable induced prestress and is not considered in this model.

The parameter F is the maximum axial load in the deck induced by the cables under dead load only. The F_i represent the axial load in the i 'th deck section due to T_i , i.e., $F_i = T_i \cos \theta_i$ and $F = \sum_{i=1}^{N_C} F_i$ for the mainspan. The backspan deck i only goes to N , but the sum of the mainspan F_i and backspan F_i are equal which means that the backspan F_N is equal to the mainspan $\sum_{i=N}^{N_C} F_i$.

To fulfill the desire to have all the cable dead load stresses the same, the stay cable areas are again determined by

$$A_{C_i} = \frac{A_{C_{N/2}} \sin \theta_{N/2}}{\sin \theta_i}$$

The anchor cable area A_{C_a} is independent of the stay cable areas, but the proportioning of the individual anchor cables is determined by the constraints of constant dead load cable stress and the sum of the individual anchor cable areas being equal to the aggregate anchor cable area. This involves solving a system of linear equations; i.e., the requirement of constant cable stress

$$\frac{A_{C_N}}{T_N} = \frac{A_{C_{N+1}}}{T_{N+1}} = \dots = \frac{A_{C_{N_C}}}{T_{N_C}}$$

produces $N_C - N$ equations while there are $N_C - N + 1$ unknowns (the individual cable areas of the anchor cable, i.e., $A_{C_i}, i = N, N_C$ —the cable tensions are known). The

final equation comes from the anchor cable area relationship:

$$\sum_{i=N}^{N_C} A_{C_i} = A_{C_a}$$

where A_{C_a} is acquired from existing cable stayed bridge designs.

An approximate analytical method of determining the anchor cable area is derived from the assumption of dead load stress in the anchor cable being equal to the other cables. That is,

$$\frac{\left(\frac{l_M}{2} - l_B\right) w_D}{A_{C_a} \sin \theta_{N_C}} = \sigma_C = \frac{w_D l_B}{N A_{C_{N/2}} \sin \theta_{N/2}}$$

Rearranging terms and using $l_B/l_M = 0.4$ (from the standard model) gives

$$A_{C_a} = \frac{N A_{C_{N/2}} \sin \theta_{N/2}}{4 \sin \theta_{N_C}}$$

where for the standard model again,

$$\frac{\sin \theta_{N/2}}{\sin \theta_{N_C}} \approx 1.3$$

which results in

$$A_{C_a} \approx \frac{N A_{C_{N/2}}}{3}$$

This formula could be used in preliminary design values for the anchor cables, but in this study the actual bridge anchor cable areas are used.

5.2 Stability

5.2.1 Stability Dimensionless Ratios

The critical live load of the system is defined by the function

$$w_{L_c} = \mathcal{F}[EI, E_T I_T, A_{C_{N/2}} E_C, A_{C_a}, l_B, l_M, h_1, h_{N_C}, h_T, N, w_{C_{N/2}}, w_D] \quad (5.15)$$

All thirteen of the parameters in Equation 5.15 are independent of each other. The parameters that do not appear in the equation are functions of the ones used in Equation 5.15, i.e.,

$$L_{N/2} = \frac{h_{N/2}}{\tan \theta_{N/2}} = \frac{l_B}{2}$$

$$S_{N/2} = \frac{h_{N/2}}{\sin \theta_{N/2}}$$

$$s = \frac{l_B}{N}$$

$$N_C = \frac{l_M - s}{2s}$$

$$s' = \frac{h_{N_C} - h_1}{N_C - 1}$$

$$T_{N/2} = \frac{w_D l_B}{N \sin \theta_{N/2}}$$

$$P \approx w_D l_M$$

$$F = \sum_{i=1}^{N_C} T_i \cos \theta_i = \frac{w_D l_B}{N} \sum_{i=1}^{N_C} \cot \theta_i$$

where i is the counter along the mainspan from the tower to midspan and

$$\sum_{i=1}^{N_C} \cot \theta_i = \sum_{i=1}^{N_C} \frac{i l_B (N - 1)}{N [h_1 (N - i) + h_N (i - 1)]}$$

$$\tan \theta_{N/2} = \frac{h_1 + h_N (1 - \frac{2}{N})}{l_B - \frac{l_B}{N}}$$

$$h_{N/2} = \frac{h_1 + h_N (1 - \frac{2}{N})}{2 - \frac{2}{N}}$$

and

$$h_N = h_{N_C} - (N_C - n) s'$$

for both even and odd values of N .

Eleven dimensionless ratios need to be constructed out of the thirteen parameters in Equation 5.15. The eleven ratios chosen to represent this model are:

$$N$$

$$\frac{h_1}{l_B}$$

$$\frac{h_{N_C}}{l_B}$$

$$\frac{h_T}{l_B}$$

$$\frac{l_B}{l_M}$$

$$\frac{E_T I_T}{EI}$$

$$\frac{A_{C_a}}{\sum A_C} = \frac{\sum_{i=N}^{N_C} A_{C_i}}{\sum_{i=1}^{N-1} A_{C_i}}$$

$$\frac{w_{Lc}}{w_D}$$

$$\frac{F}{F_H} = \frac{\frac{w_D l_B}{N} \sum_{i=1}^{N_C} \cot \theta_i}{2 \sqrt{\frac{N A_{C_{N/2}} E_C EI \sin^3 \theta_{N/2}}{l_B h_{N/2}}}}$$

$$\frac{l_D}{l_B} = \frac{\pi \sqrt{2}}{l_B} \sqrt{\frac{l_B h_{N/2} EI}{N A_{C_{N/2}} E_C \sin^3 \theta_{N/2}}}$$

$$f = \frac{w_D l_B}{N \sin \theta_{N/2} \sqrt[3]{\frac{A_{C_{N/2}} E_C}{24} \left(\frac{w_{C_{N/2}} h_{N/2}}{\tan \theta_{N/2}} \right)^2}}$$

The dimensionless ratios N , h_1/l_B , w_{LC}/w_D , l_D/l_B , and f are the exactly the same as the ones used for the previous model. The ratios h_{NC}/l_B and F/F_H are respectively equivalent to h_N/l_B and F/F_H of the previous model. That is to say F is the same in both models but the individual F_i are different in the two models, and as stated previously, h_{NC} is the same as h_N of the backspan model.

The new ratios are the ones that define the tower, mainspan and anchor cable properties. The ratios h_T/l_B , l_B/l_M and $E_T I_T/EI$ have obvious physical meanings and $A_{C_a}/\sum A_C$ is simply the ratio of anchor cable area to backspan cable area.

In summary, the stability of the full bridge model is described by the function:

$$\frac{w_{Lc}}{w_D} = \mathcal{F} \left[N, \frac{h_1}{l_B}, \frac{h_{NC}}{l_B}, \frac{h_T}{l_B}, \frac{l_B}{l_M}, \frac{E_T I_T}{EI}, \frac{A_{C_a}}{\sum A_C}, f, \frac{l_D}{l_B}, \frac{F}{F_H} \right]$$

This function is based on beam-column on an elastic foundation stability theory with both the cable slackness and the $P-\Delta$ nonlinearities modelled.

5.2.2 Parameters and Ratios from Existing Bridge Designs

The same nine cable stayed bridges that were used for the first two models are used to acquire data for the construction of the full bridge model. The representative cable is the one corresponding to $i = N/2$ as explained previously. The other parameters that are applicable to both the backspan model and the full bridge model are determined from the design drawings in exactly the same manner as described in Chapter 4. Indeed, the parameters and dimensionless ratios given in Appendices C.3 and C.4 are used for the full bridge model.

The fact that F/F_H is made the same as the previous model is of no consequence in the dimensional analysis, but it does require some explanation in regards to the actual

values for the existing designs. The full bridge model F is the sum of N_C deck forces, whereas the previous model F is the sum of N deck forces. In the cases where N_C is greater than N , F is obviously greater for the full bridge model than the backspan model, which is also true for $F/F_H - F_H$ being the same for both models. The new values for F and F/F_H along with N_C are given in Appendices C.5 and C.6 along with all the other parameters and ratios. F is calculated using the approximation of $F = N_C F_{N_C/2}$, or

$$F = \frac{w_D l_M}{2 \tan \theta_{N_C/2}}$$

which is—as explained in Chapter 4—a conservative calculation of F . The average value of F/F_H for the full bridge model is now greater than 0.1, but 0.1 is chosen as the representative value for the sake of continuity with the previous models.

The additional parameters necessary to model the towers, mainspan and anchor cables are acquired from the bridge designs and listed in Appendix C.5. (Unfortunately, the tower and anchor cable information was not available to this author for three of the nine bridges.) As stated previously, the tower height h_T is measured from the tower foundation and the anchor cable area A_C is the sum of the cross sectional areas of the cables acting as anchors. The tower moment of inertia I is modelled as being constant throughout its length. In the real cable stayed bridge designs this is rarely the case, and for the varying I towers a substitute tower with a constant I is used. The substitute tower I is calculated to make the free standing tower deflections of both the real and substitute towers the same for a unit lateral point load at the top. The tower moment of inertia for the Alex Fraser concrete design is so much larger than the other bridges—most probably because of architectural considerations—that it is not included in finding the representative ratios.

The representative dimensionless ratios of the standard full bridge model are

$$N = 20$$

$$h_1/l_B = 0.30$$

$$h_{NC}/l_B = 0.50$$

$$h_T/l_B = 0.80$$

$$l_B/l_M = 0.40$$

$$E_T I_T / EI = 50$$

$$A_{C_s} / \sum A_C = 0.50$$

$$f = 7$$

$$l_D/l_B = 0.50$$

$$F/F_H = 0.10$$

$$w_L/w_D = 0.20$$

where, for the purpose of calculating f : $w_{C_{N/2}} = A_{C_{N/2}} \gamma_C$.

5.2.3 Results of Stability Analysis

The standard bridge model of Figure 5.45 is constructed using the preceding values for the dimensionless ratios. In order to find the minimum live load at which the model buckles, the most severe load distribution must be determined. To this end, influence lines for maximum axial load in the deck are calculated using the computer program ULA. Four load cases, which result from the influence lines for maximum axial load at the towers and at the backspan anchor connections, are indicated from this study as shown in Figure 5.47. The load cases are numbered one to four, indicating maximum deck axial load from left to right.

The bridge deflected shape, deck axial load (dead load plus live load) and deck moment just before stability failure are shown in Figures 5.48 and 5.49 for all four load cases on the standard model. The four axial distributions are drawn to the same scale and the four moment diagrams are drawn to the same scale as well, but different from the axial scale.

Using the computer program ULA, the critical load ratio for the standard model

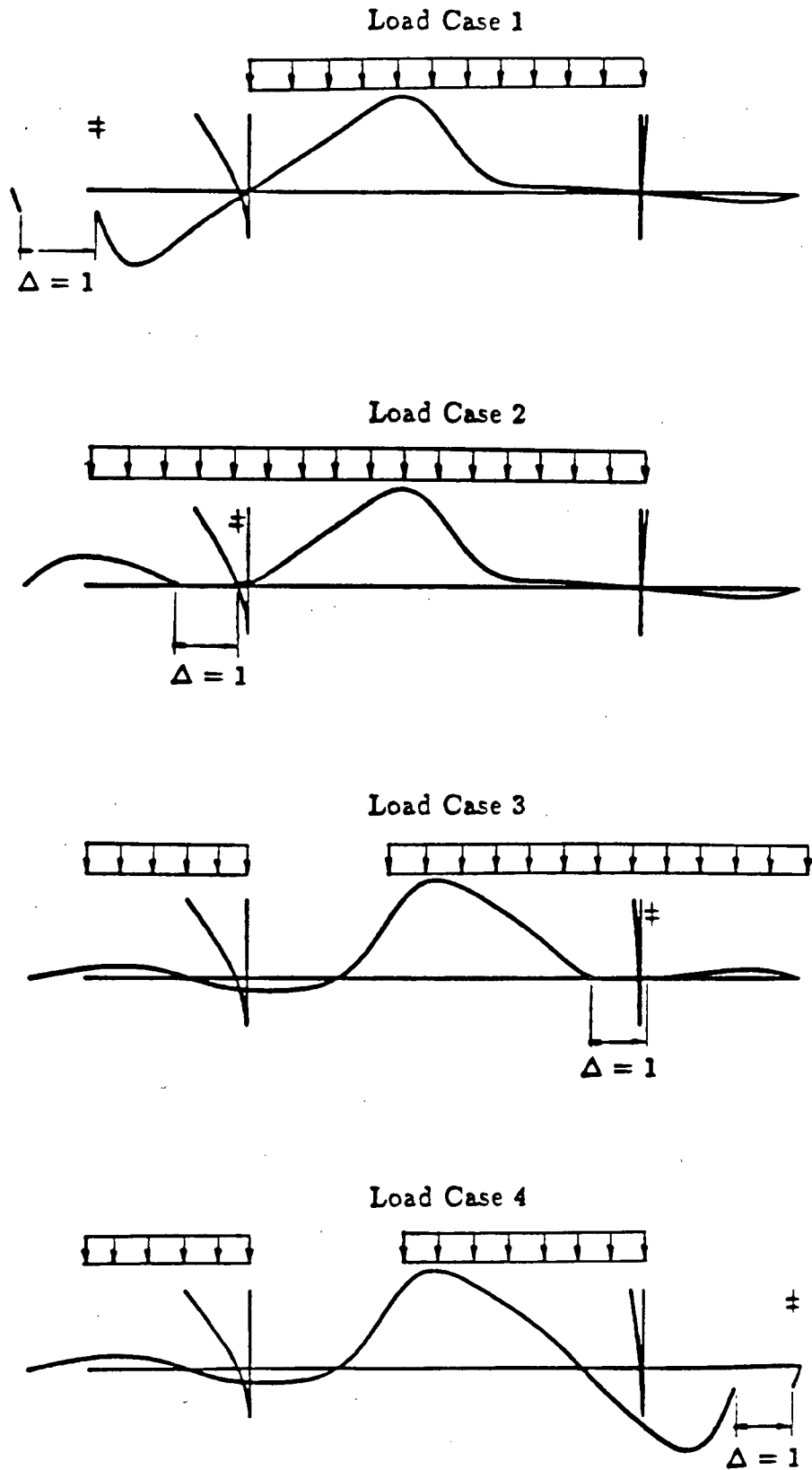


Figure 5.47: Axial influence lines and load cases for instability.

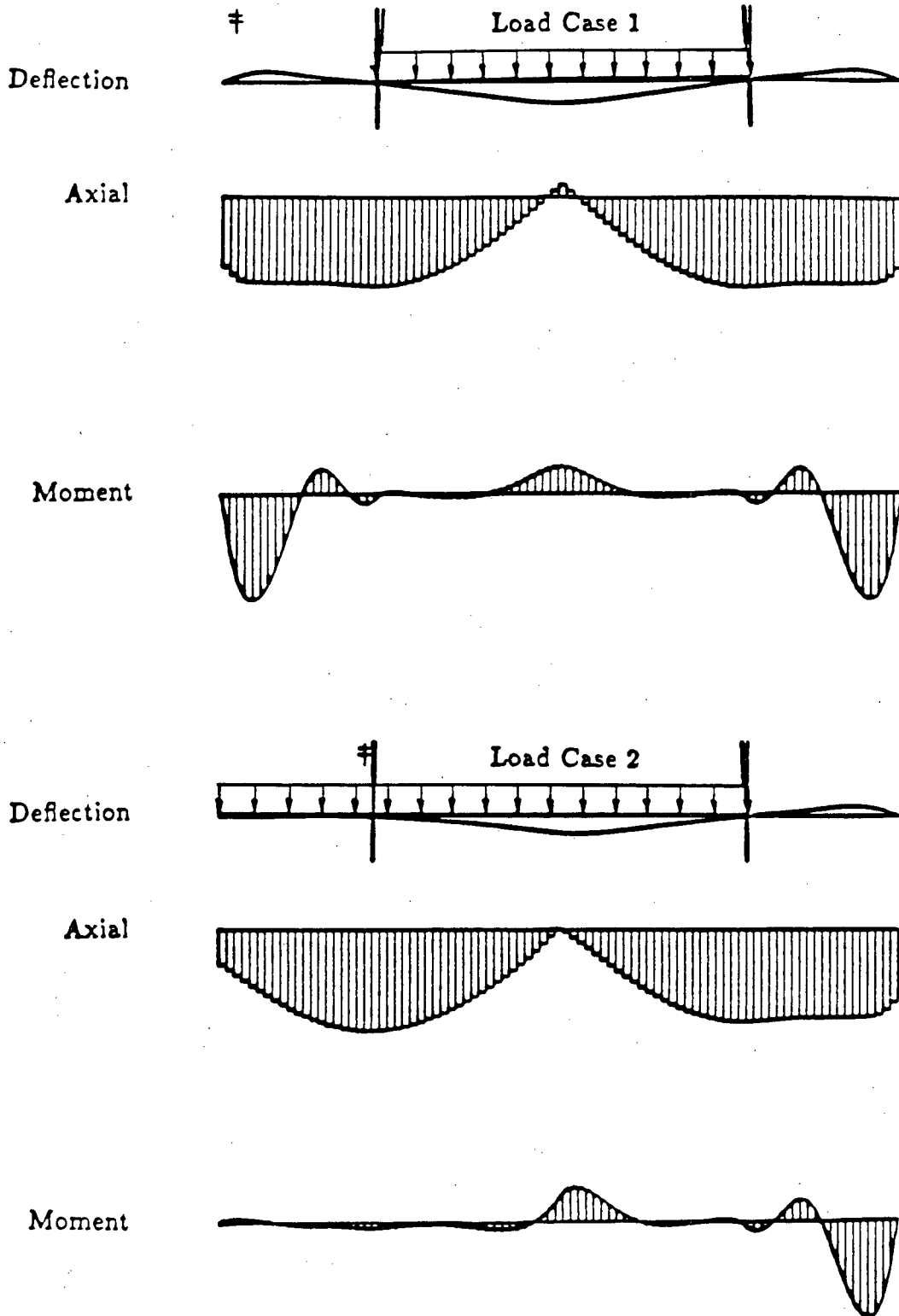


Figure 5.48: Stability failure of standard bridge model—load cases 1 and 2.

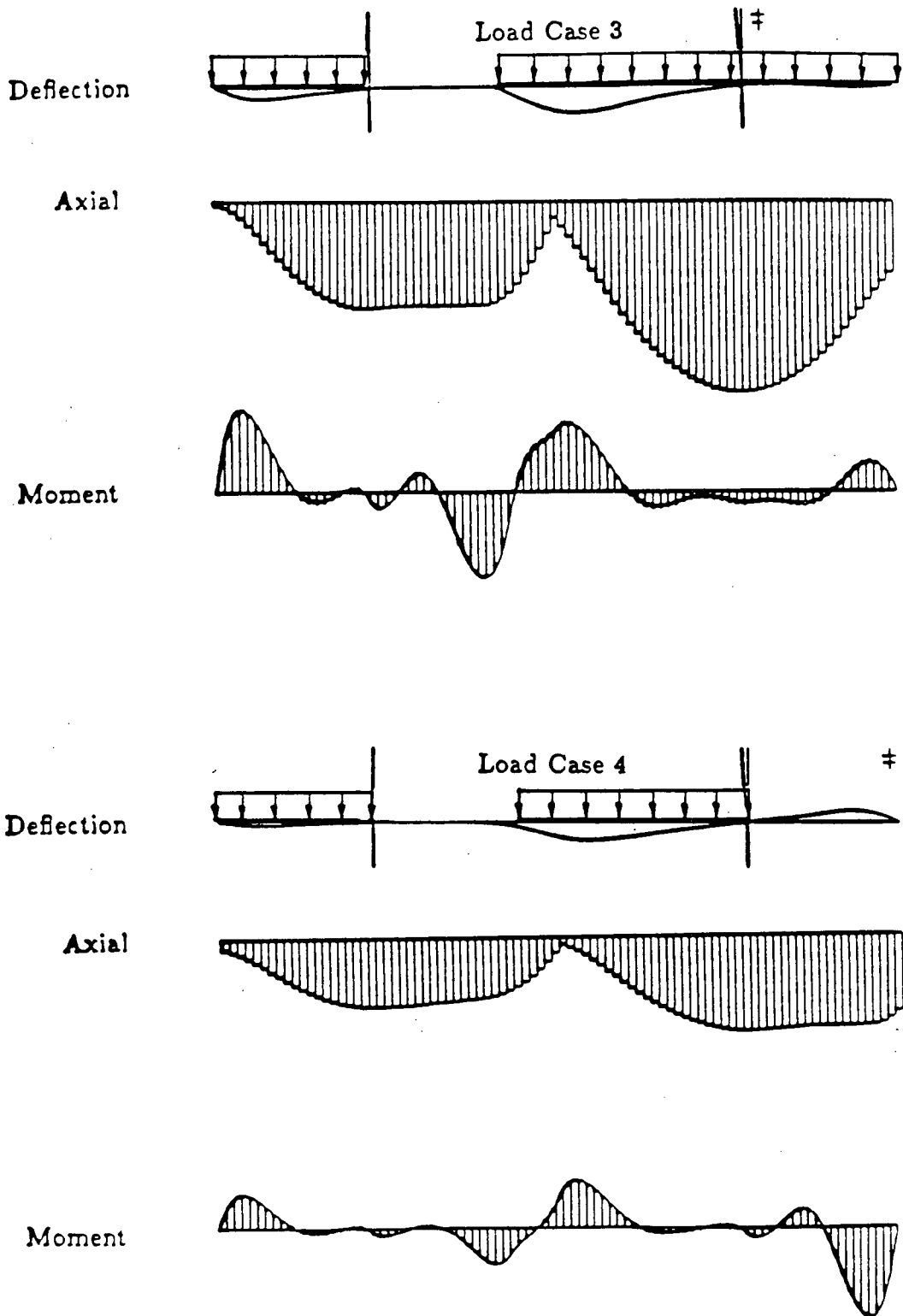


Figure 5.49: Stability failure of standard bridge model—load cases 3 and 4.

under each load case is found, and the factor of safety against elastic stability failure is calculated. For example, the critical load ratio for load case 4 is found to be $w_{Lc}/w_D = \lambda w_L/w_D = 2.37$, which is to say, since $w_L/w_D = 0.2$, that the factor of safety on the live load against elastic buckling of the standard model is 11.9. This is far less than the factor of 91 obtained for the backspan model. This is mostly due to the extra backspan cable tensions from the live load in the mainspan and—as will be explained shortly—due to a less stiff deck section causing instability. The critical load ratios for the four load cases and the corresponding factors of safety against elastic stability failure are:

Load Case	$\frac{w_{Lc}}{w_D}$	Factor of Safety
1	2.63	13.2
2	2.50	12.5
3	5.24	26.2
4	2.37	11.9

The influence of an uplift pressure on the factor of safety is investigated by placing uplift pressures on the deck regions that are not loaded (as indicated by the axial influence lines). The resulting factor of safety plot for a range of uplift pressures on all four load cases is given in Figure 5.50. The uplift pressure has a pronounced effect on the factor of safety, with a near linear decline of 37% to 30% uplift pressure. The rate of decline decreases for higher uplift pressure with a further drop of 52% for uplift pressures of 100% of the live load. Wind and dynamic loads, and the probabilities of load combinations are beyond the scope of this thesis and the uplift pressure load case will not be used in further analyses, but it should be kept in mind that a more severe result is possible.

The previous discussions were concerned about the effect of various loading patterns on the elastic stability of the standard model with $F/F_H = 0.10$. The fact that the bridge buckled at all (one might expect that instability would occur only if $F/F_H = 1.0$)

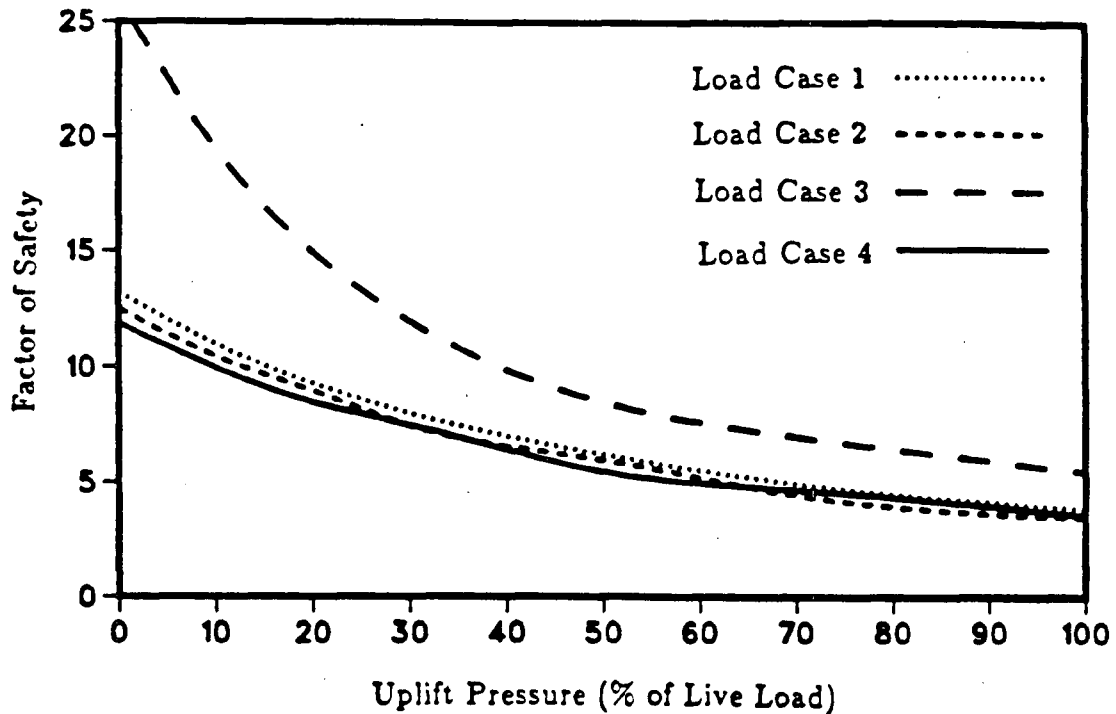


Figure 5.50: Stability factor of safety of bridge model.

is accounted for by the same three reasons given for the previous models; that is, the live load axial force must be accounted for, along with the nonuniformity of the axial distribution, and F_H must be calculated for the critical deck section. Analytical adjustments cannot be made for the axial load in this model as was done for the previous two models. Instead, numerical values of average deck axial loads over a half-wave are taken as the values for F_{avg}^* .

The corresponding values of $F_{H\sim}$ also cannot be calculated in the same manner as previously because the critical deck section is not a pin-pin beam-column on an elastic foundation. The deflected shapes and moment diagrams in Figures 5.48 and 5.49 suggest that semi-infinite boundary conditions are appropriate. The deck section in the mainspan near the right tower—for load cases 1, 2 and 4—with the near zero moment and smooth deflection, behaves like the end of a semi-infinite beam-column on an elastic foundation. In load case 3, the deck section just to the left of the left tower can be

thought of as the end of a semi-infinite beam-column on an elastic foundation. Hetényi gives the critical axial load for a semi-infinite beam-column on an elastic foundation as \sqrt{kEI} and $F_{H\sim}$ is calculated as the average value of this formula over a half-wave. That is,

$$F_{H\sim} = \sqrt{\frac{A_C E_C EI \sin^3 \theta}{sh}}$$

where A_C is the final cable area after the changes are made for the catenary calculations.

Plots of $F_{avg\sim}^*/F_{H\sim}$ along the deck for each of the four load cases are given in Figure 5.51. It can be seen that the rightmost deck section is critical ($F_{avg\sim}^*/F_{H\sim} = 1$) except for load case 3 where the critical deck section is between the center of the mainspan and the left tower. However, load case 3 does not govern in stability considerations and in general the worst case bridge stability failure is caused by the combination of low cable stiffness near the end of the bridge and the high deck axial loads induced by the backspan cables which are acting as tiebacks for the mainspan cables which in turn, support the mainspan loads. Thus, the full bridge model stability mechanism can be understood in terms of a beam-column on an elastic foundation if the effects of the nonuniform elastic foundation, varying axial loads, and applicable boundary conditions are taken into consideration.

The standard model is next varied by altering only F/F_H and then determining the live load necessary to cause the deck to buckle. The results of this exercise for each load case are shown in Figure 5.52. The F/F_H ratio is not adjusted to include the live load as was done in the previous chapters because of the noncontinuous load distributions of the four load cases.

The standard model is represented by the solid square in Figure 5.52 and load case 4 produces the lowest factor of safety for this model. Load case 4 is also the governing load case for all values of F/F_H , and this load case will be used for the rest of the stability analyses. It is interesting to note that load cases 1, 2 and 4 exhibit nearly identical behaviour in Figure 5.52 yet load case 3 is unique. This is because load case

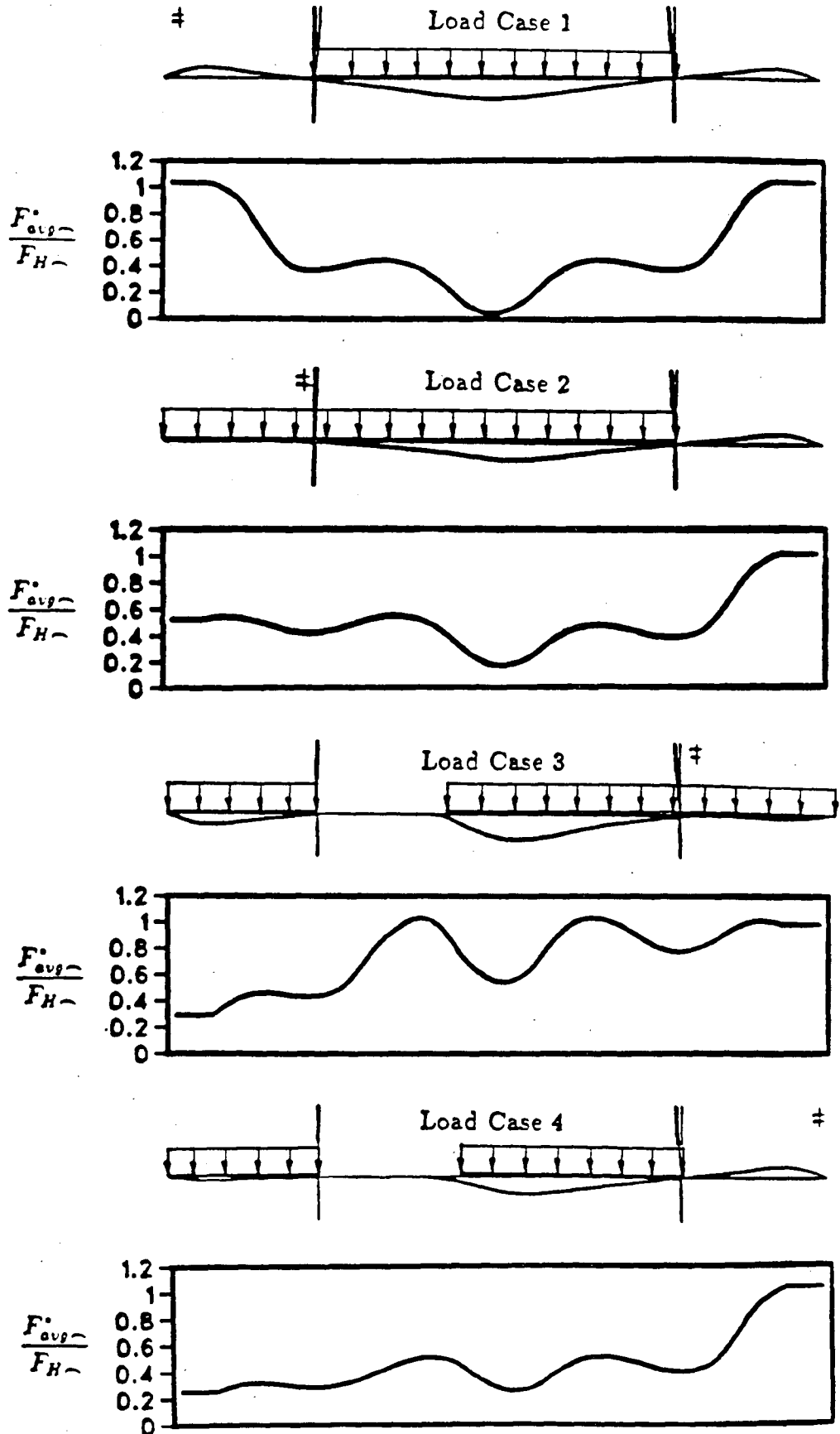


Figure 5.51: Critical deck section for each load case.

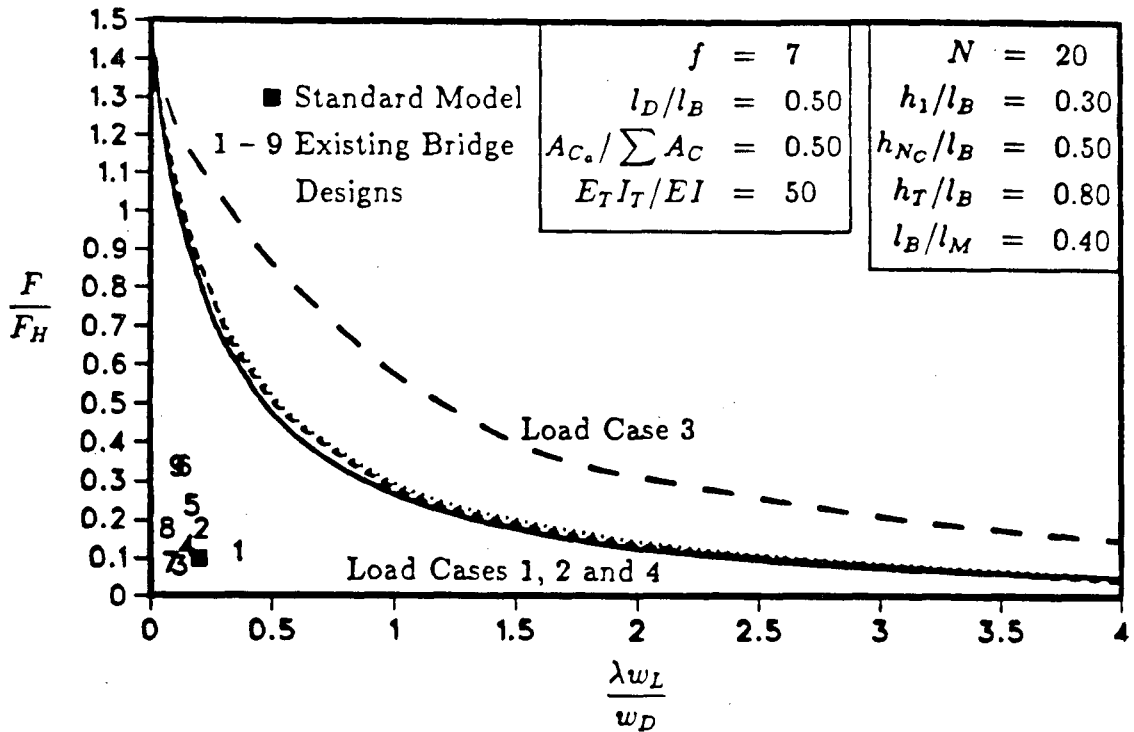


Figure 5.52: Stability of full bridge model.

3 causes the bridge instability to occur at a different deck section, as demonstrated in Figure 5.51. The nine existing bridge designs from Appendix C are plotted on Figure 5.52 as the numerals 1 to 9. The scatter of the numerals qualitatively shows how the existing bridge designs compare with each other.

The theoretical result for a beam-column on an elastic foundation would plot on Figure 5.52 as a horizontal line at $F/F_H = 1.0$. This apparent discrepancy between the Hetényi and computer results can be eliminated if F_{avg}^*/F_H is used instead of F/F_H . This is illustrated by Figure 5.53 where plots of F_{avg}^*/F_H along the deck for load case 4 are shown for different values of F/F_H . It can be seen that as F/F_H increases, the boundary conditions of the critical deck section change from a semi-infinite to a pin-pin beam-column on an elastic foundation. In order to get the expected Hetényi result the apparent boundary conditions must be used to calculate F_H along with the appropriate deck section F_{avg}^* .

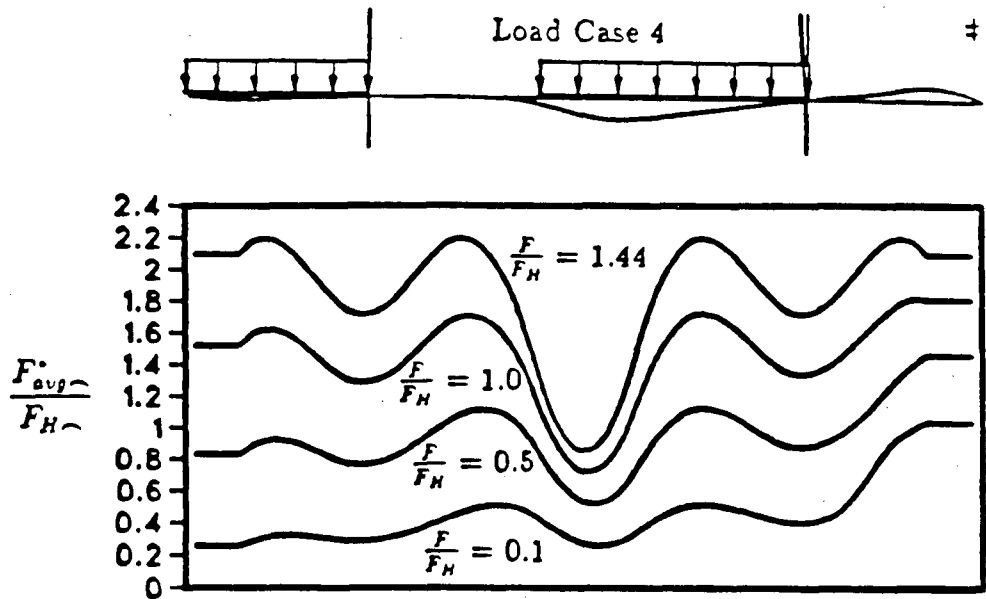


Figure 5.53: Critical deck section for varying F/F_H .

Looking again at Figure 5.52 it can be seen that the factor of safety against buckling decreases with increasing F/F_H . The rate of this decrease is shown in Figure 5.54 for the standard model with $w_L/w_D = 0.20$ and load case 4. The possibility of F/F_H being 0.20 for a bridge with $w_L/w_D = 0.20$ is quite likely—as indicated by the distribution of actual bridges on Figure 5.52—and the factor of safety for this bridge is 6.5, which is a drop of 45% from the standard model factor of safety of 11.9. This is comparable to a 40% uplift pressure on the standard model.

Figure 5.54 can be used to determine the factor of safety on the live load if a load factor is applied to the dead load. This is calculated by using the fact that F is directly proportional to w_D . Thus, if w_D is multiplied by 1.5, for example, then F/F_H is multiplied by 1.5 and the corresponding factor of safety for the new F/F_H ratio is read off of Figure 5.54. This procedure yields 8.7 as the factor of safety against elastic stability failure. In other words, instead of $w_D + 11.9w_L$ causing instability,

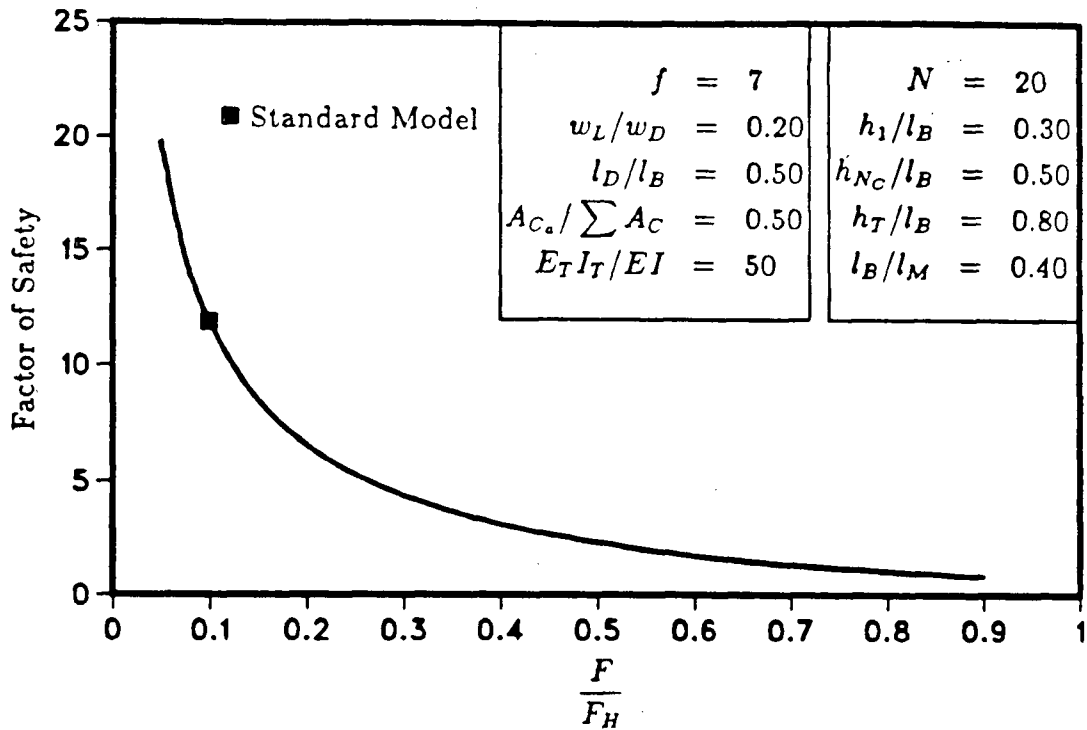


Figure 5.54: Factor of safety vs F/F_H .

$1.5w_D + 8.7w_L$ causes instability. As another example, the factor of safety on the live load is 6.7 when the dead load factor is 2; i.e., $2.0w_D + 6.7w_L$ also causes instability.

The decay length to backspan length dimensionless ratio l_D/l_B is now varied in the same manner that l_D/l_B was varied for the backspan model. The range of l_D/l_B in existing cable stayed bridge designs is from 0.40 to 0.65 and the stability curves for $l_D/l_B = 0.40$ and $l_D/l_B = 0.65$ are plotted in Figure 5.55. There is only a very small variation with l_D/l_B , and the stability factor of safety for the standard model varies from 11.2 to 12.4 which is $\pm 5\%$ from the standard value of 11.9.

Just as in the previous model, altering the initial cable tautness f in the normal range of 5 to 10, does not affect the model behaviour. The two new ratios of $A_{C_a}/\sum A_C$ and $E_T I_T/EI$ are also varied in the same manner as l_D/l_B . The normal ranges of $A_{C_a}/\sum A_C$ and $E_T I_T/EI$ are 0.4 to 0.6 and 25 to 100 respectively, and the model behaviour is only slightly affected within these ranges, as shown in Figures 5.56 and 5.57.

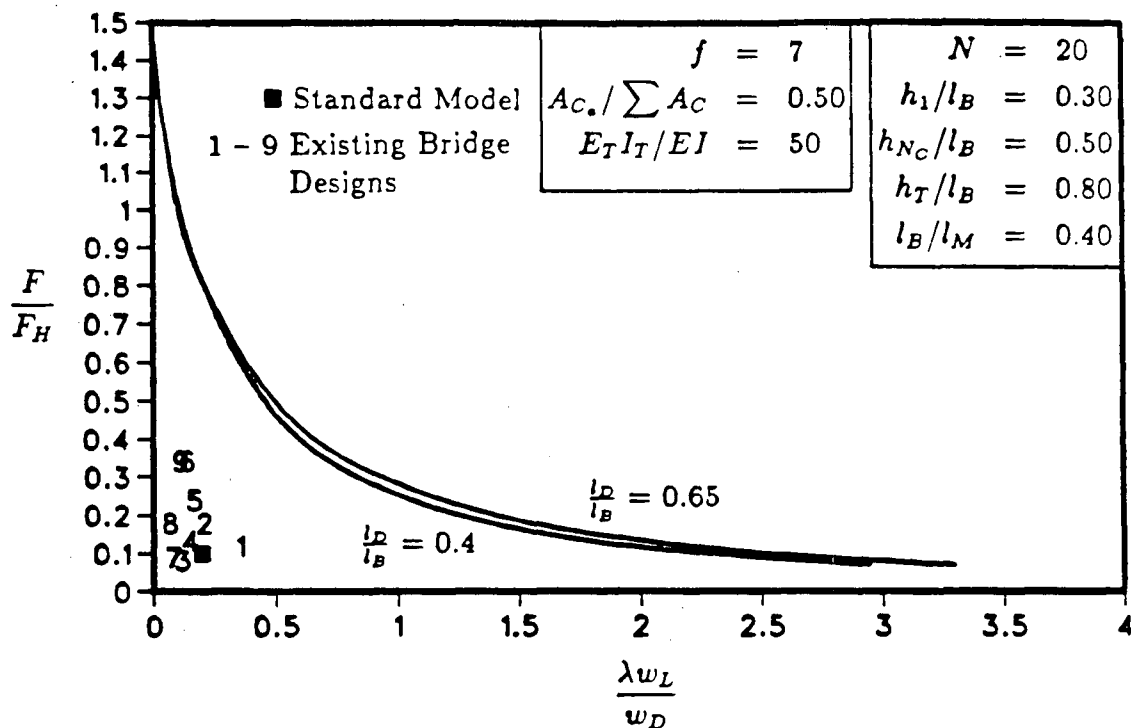


Figure 5.55: Stability of full bridge model— l_D/l_B varied.

The stability factor of safety varies from 11.2 to 12.4 for the variation of $A_{C^*} / \sum A_C$ which is $\pm 5\%$ from the standard value of 11.9. For the variation of $E_T I_T / EI$ the factor of safety ranges from 11.2 to 12.4 as well, and is again a $\pm 5\%$ variation from the standard.

The remaining dimensionless ratios, which are all based on the model geometry, are not investigated.

5.3 Deflection and Moment

The choice of deflection and moment functions to represent the full bridge model is based on the same rationale used in Chapters 3 and 4. The mainspan deflection and moment is investigated as well as the backspan deflection and moment. This is necessary because the maximum deflection will be in the mainspan and the maximum

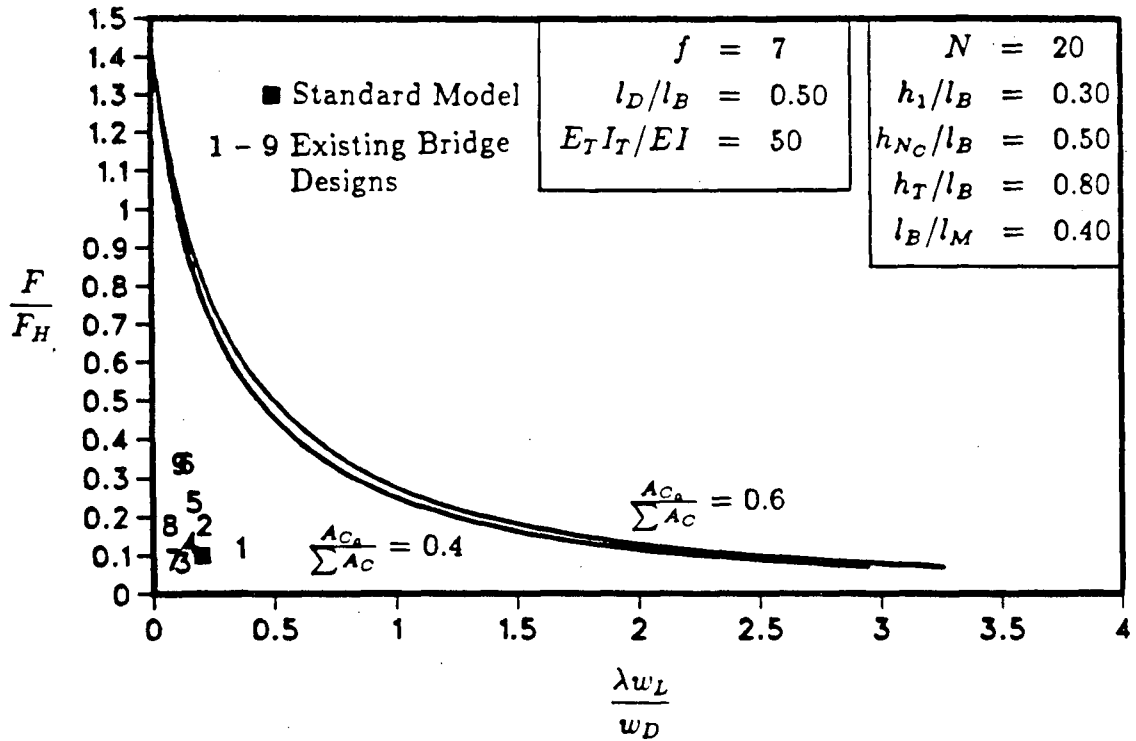


Figure 5.56: Stability of full bridge model— $A_{C_a}/\sum A_C$ varied.

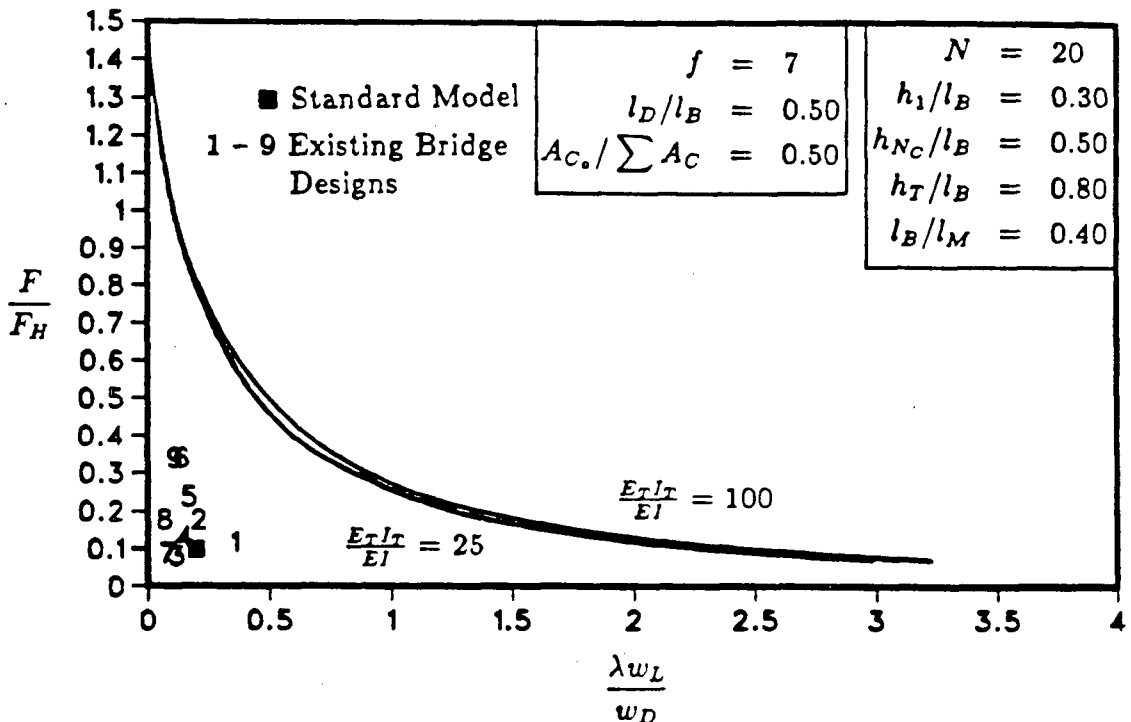


Figure 5.57: Stability of full bridge model— $E_T I_T / EI$ varied.

moment will be in the backspan. For the sake of continuity and consistency the deflections and moments for both the backspan and mainspan will be compared to that of a simply supported beam on an elastic foundation without axial load.

The definition of the full bridge model backspan deflection in terms of independent parameters is

$$\delta_B = \mathcal{F}_B[EI, E_T I_T, A_{C_{N/2}} E_C, A_{C_a}, l_B, l_M, h_1, h_{N_C}, h_T, N, w_{C_{N/2}}, w_D, w_L]$$

and the maximum nondimensional backspan deflection of the bridge model is described by the function:

$$\frac{\delta_B}{\delta_H} = \mathcal{F}_B \left[N, \frac{h_1}{l_B}, \frac{h_{N_C}}{l_B}, \frac{h_T}{l_B}, \frac{l_B}{l_M}, \frac{E_T I_T}{EI}, \frac{A_{C_a}}{\sum A_C}, f, \frac{l_D}{l_B}, \frac{w_L}{w_D}, \frac{F}{F_H} \right]$$

The maximum nondimensional mainspan deflection of the model is described by a function that uses exactly the same ratios as the backspan function, but the functions themselves will be different. The mainspan deflection function is

$$\frac{\delta_M}{\delta_H} = \mathcal{F}_M \left[N, \frac{h_1}{l_B}, \frac{h_{N_C}}{l_B}, \frac{h_T}{l_B}, \frac{l_B}{l_M}, \frac{E_T I_T}{EI}, \frac{A_{C_a}}{\sum A_C}, f, \frac{l_D}{l_B}, \frac{w_L}{w_D}, \frac{F}{F_H} \right]$$

With δ_H defined by Eq. 3.12 and

$$k = \frac{N A_{C_{N/2}} E_C \sin^3 \theta_{N/2}}{l_B h_{N/2}}$$

these functions will show the magnification of the maximum deck deflection due to the deck axial load. All other ratios in these functions are the same as the ones defined for the stability analysis of this model.

The definition of the bridge model backspan moment in terms of independent parameters is

$$M_B = \mathcal{F}_B[EI, E_T I_T, A_{C_{N/2}} E_C, A_{C_a}, l_B, l_M, h_1, h_{N_C}, h_T, N, w_{C_{N/2}}, w_D, w_L]$$

and the maximum nondimensional backspan moment of the bridge model is described by the function:

$$\frac{M_B}{M_H} = \mathcal{F}_B \left[N, \frac{h_1}{l_B}, \frac{h_{N_C}}{l_B}, \frac{h_T}{l_B}, \frac{l_B}{l_M}, \frac{E_T I_T}{EI}, \frac{A_{C_a}}{\sum A_C}, f, \frac{l_D}{l_B}, \frac{w_L}{w_D}, \frac{F}{F_H} \right]$$

Just as for deflection, the maximum nondimensional mainspan moment is described by the same ratios but a different function. The mainspan moment function is

$$\frac{M_M}{M_H} = \mathcal{F}_M \left[N, \frac{h_1}{l_B}, \frac{h_{NC}}{l_B}, \frac{h_T}{l_B}, \frac{l_B}{l_M}, \frac{E_T I_T}{EI}, \frac{A_{Ca}}{\sum A_C}, f, \frac{l_D}{l_B}, \frac{w_L}{w_D}, \frac{F}{F_H} \right]$$

With M_H defined by Eq. 3.13 these functions will show the magnification of the maximum deck moment due to the deck axial load.

5.3.1 Results of Deflection Analysis

The same standard full bridge model is used for maximum deflection analysis as that for the stability analysis. However, different load cases are necessary in order to get the maximum deflection in the backspan and mainspan. The envelope of maximum deflection influence lines is determined using ULA, and the maximum backspan and mainspan deflection influence lines are shown in Figure 5.58 along with the resulting live load distributions and the locations of the maximum deflections.

It should be noted that influence lines are only valid for linear structures. The cable stayed bridge being studied herein is nonlinear in that $P-\Delta$ effects and catenary cables are included in the analysis; therefore, the influence line analysis is only approximate. It turns out, however, that the deflection influence lines work very well for this structure because the load patterns for maximum deflection cover long sections of the deck and would not change, no matter how nonlinear the cable stayed bridge is.

The deflection of the standard model (magnified 200 times) under the maximum backspan deflection load case with $w_L/w_D = 0.20$, is shown in Figure 5.59 with the Hetényi deflection superposed on the left backspan. The δ_B/δ_H ratio is equal to 3.155 which is a significant deviation from the Hetényi deflection and cannot be entirely attributed to magnification due to the deck axial load. In fact the majority of the backspan deflection is due to the mainspan deck flexibility which allows the tower to move; thus, allowing greater backspan deflections than in the previous models.

The model deflected shape under the maximum mainspan deflection load case is

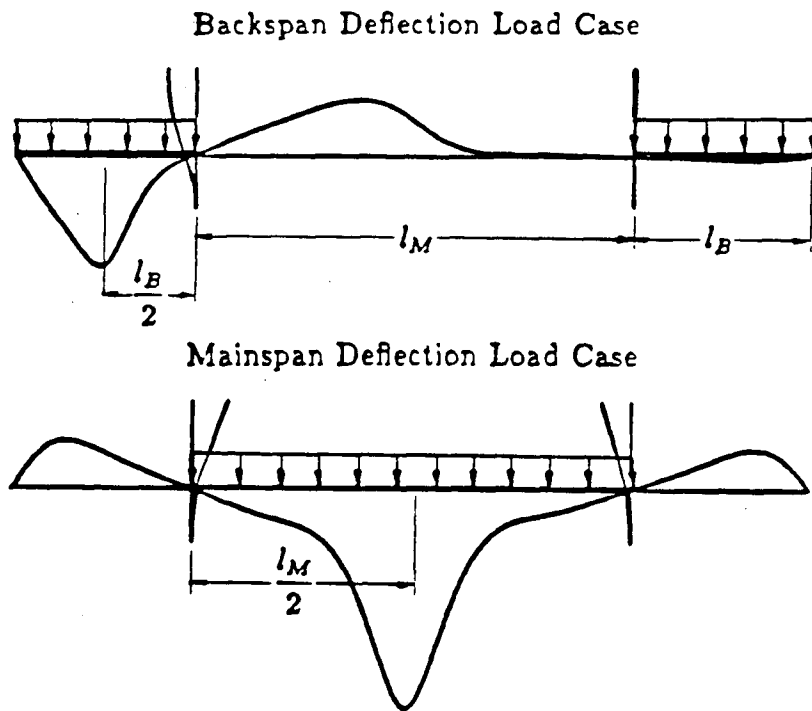


Figure 5.58: Load cases for maximum backspan and mainspan deflection.

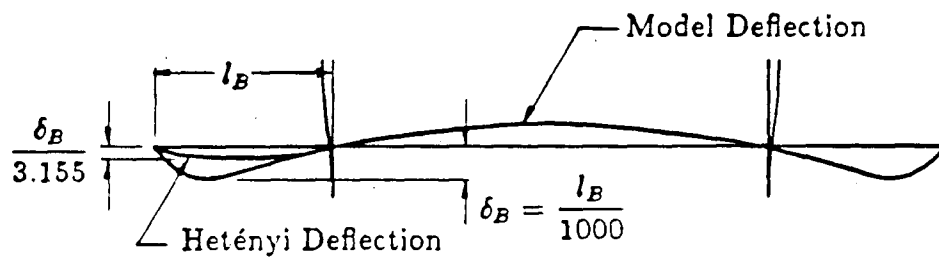


Figure 5.59: Maximum backspan deflection (magnified 200 times) of standard full bridge model.

shown in Figure 5.60. The Hetényi deflection is again superposed on the left backspan and the deflections are magnified 200 times. The δ_M/δ_H ratio is equal to 7.177. This is more than twice the value for δ_B/δ_H which is mostly attributable to the mainspan being 2.5 times as long as the backspan. The bridge deflection does not resemble a beam on an elastic foundation deflection because of the tower movements which are made possible by the flexible backspans.

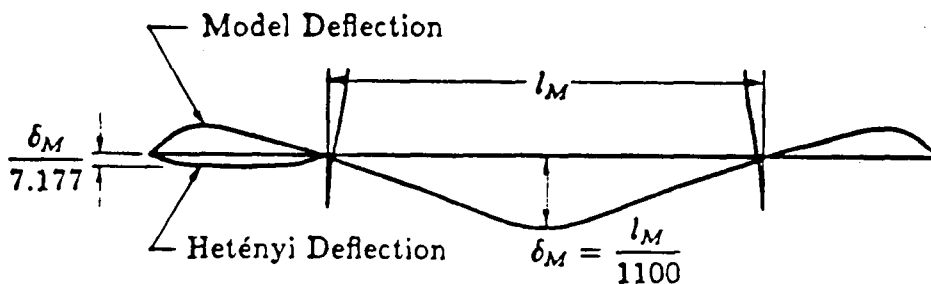


Figure 5.60: Maximum mainspan deflection (magnified 200 times) of standard full bridge model.

The maximum live load deflection versus span ratios, δ_B/l_B and δ_M/l_M are $1/1000$ and $1/1100$ respectively, which are well within the recommended value of $1/500$.

The standard model is now varied by altering the F/F_H ratio while keeping all other ratios constant. The maximum deflection is then determined from a computer analysis of the maximum backspan deflection load case and the maximum mainspan deflection load case. The δ_B/δ_H and δ_M/δ_H ratios from their respective load cases are plotted against F/F_H in Figure 5.61 for a range of F/F_H values. The mainspan curve governs and the backspan curve is shown for interest sake.

In the δ_M/δ_H ratio, the “ δ_M ” is the magnified maximum deflection of the deck due to the presence of axial load in the deck. The “ δ_H ” is Hetényi’s maximum deflection of a beam on an elastic foundation without axial load. Thus, the δ_M/δ_H ratio is expected to

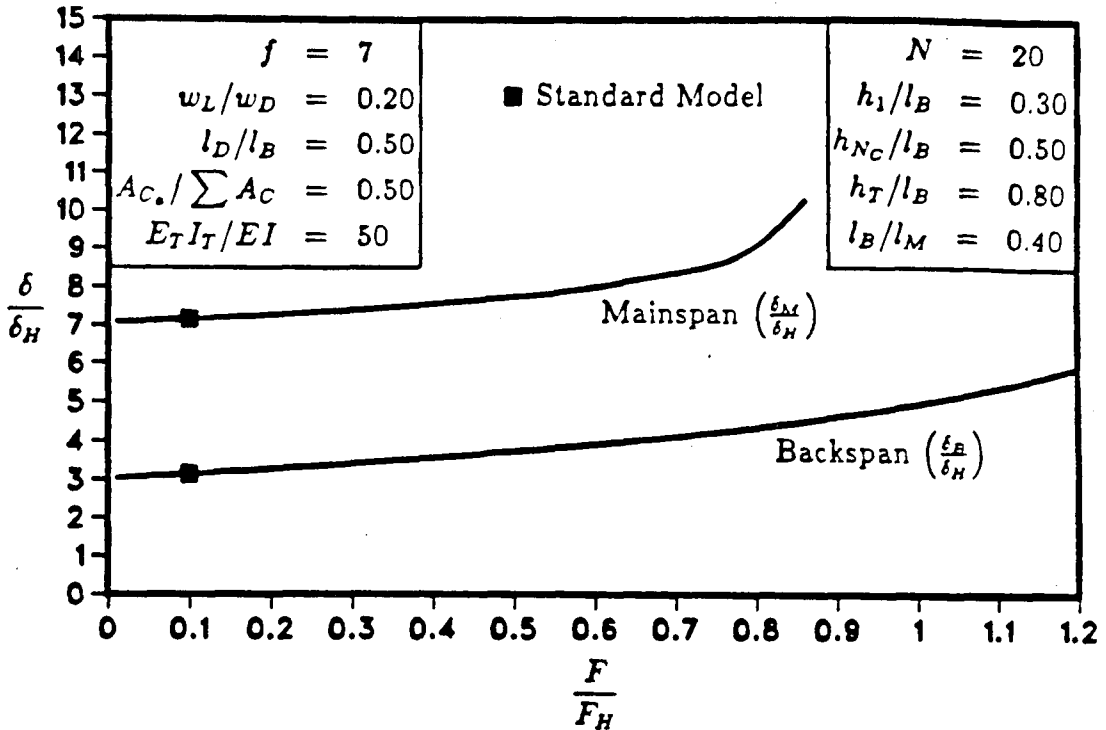


Figure 5.61: Magnification of maximum deflection.

be equal to 1.0 for F/F_H equal to zero, and as F/F_H increases the δ_M/δ_H ratio should deviate from 1.0, showing the magnification behaviour. The ordinate intercept is 7.1, not 1.0. This high initial deflection can be attributed to the relatively soft foundation at the mainspan midpoint and the flexible towers. It must also be noted that the model mainspan deflection is still being compared to a Hetényi beam of span l_B not l_M . The deflection magnification with increasing F/F_H is visible in Figure 5.61 but the increase is not very rapid because of the low deck axial load at the midspan. The deflection increases rapidly after F/F_H reaches 0.75 due to the large deflections of the backspan at this point which allows the mainspan to sag. As expected from Figure 5.52, the bridge becomes unstable at $F/F_H = 0.87$.

The deflection plot as a function of dimensionless decay length l_D/l_B is shown in Figure 5.62. It can be seen that δ_M/δ_H is highly dependent on l_D/l_B and this is especially true in the normal range of l_D/l_B from 0.40 to 0.65 for cable stayed bridges.

If Figure 5.61 were to be used for design purposes it would be necessary to plot a series of mainspan deflection curves, each with a different value of l_D/l_B .

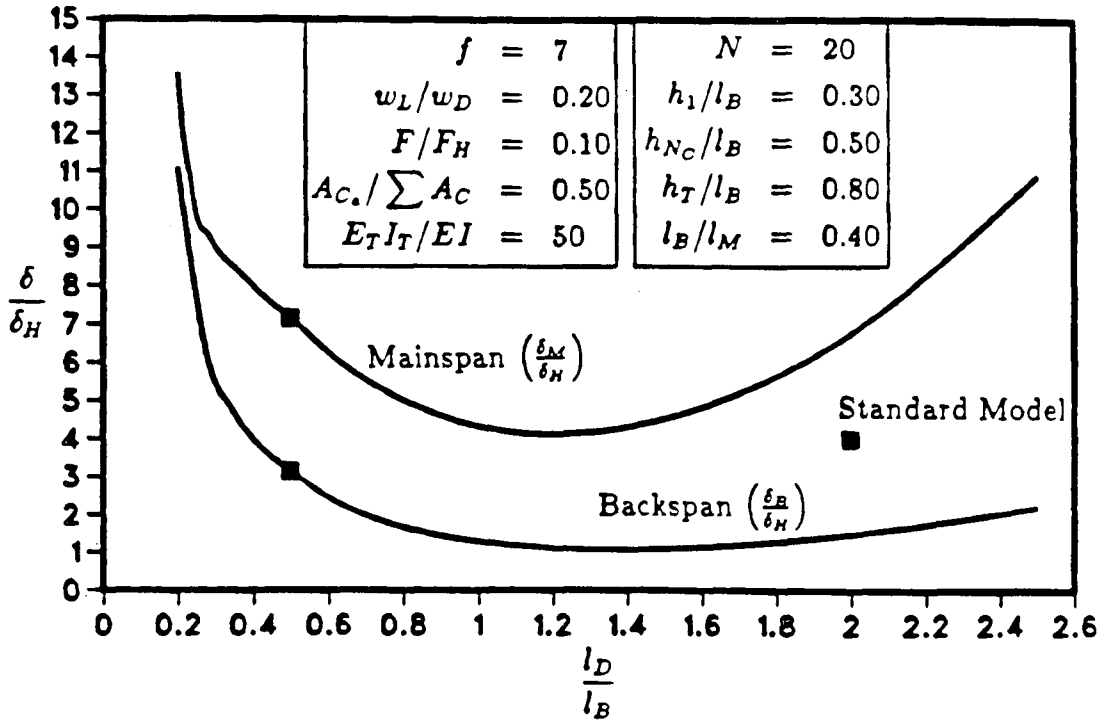


Figure 5.62: Dimensionless deflection versus dimensionless decay length.

The cable tautness graph is shown in Figure 5.63. The cable tautness has very little effect on the mainspan deflection in the normal range of f . However, the importance of having tight cables is demonstrated by the rapid increase of the deflection for low values of f .

Figure 5.64 shows the influence of the live load to dead load ratio w_L/w_D . It can be seen that the maximum deflection of the standard full bridge model is not affected by this ratio.

The deflection plot as a function of the ratio of anchor cable area to backspan cable area $A_{C_s}/\sum A_C$ is shown in Figure 5.65. It can be seen that δ_M/δ_H is also quite dependent on $A_{C_s}/\sum A_C$ in the normal range of $A_{C_s}/\sum A_C$ from 0.40 to 0.60. If Figure 5.61 were to be used for design purposes it would be necessary to have a series of

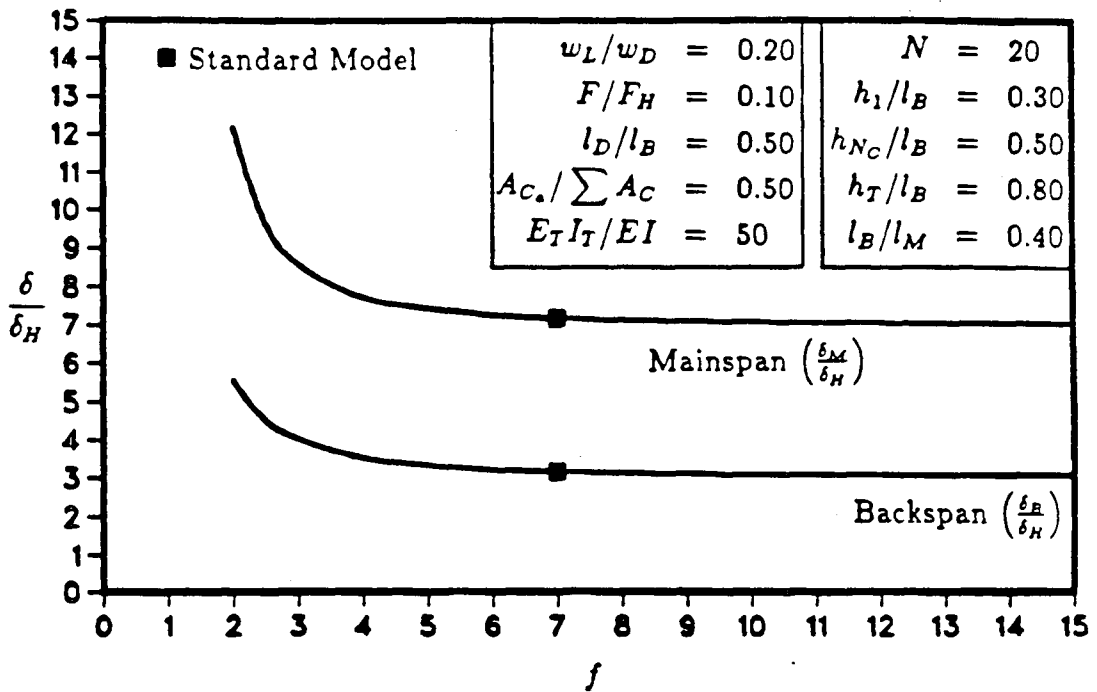


Figure 5.63: Dimensionless deflection versus dimensionless cable tautness.

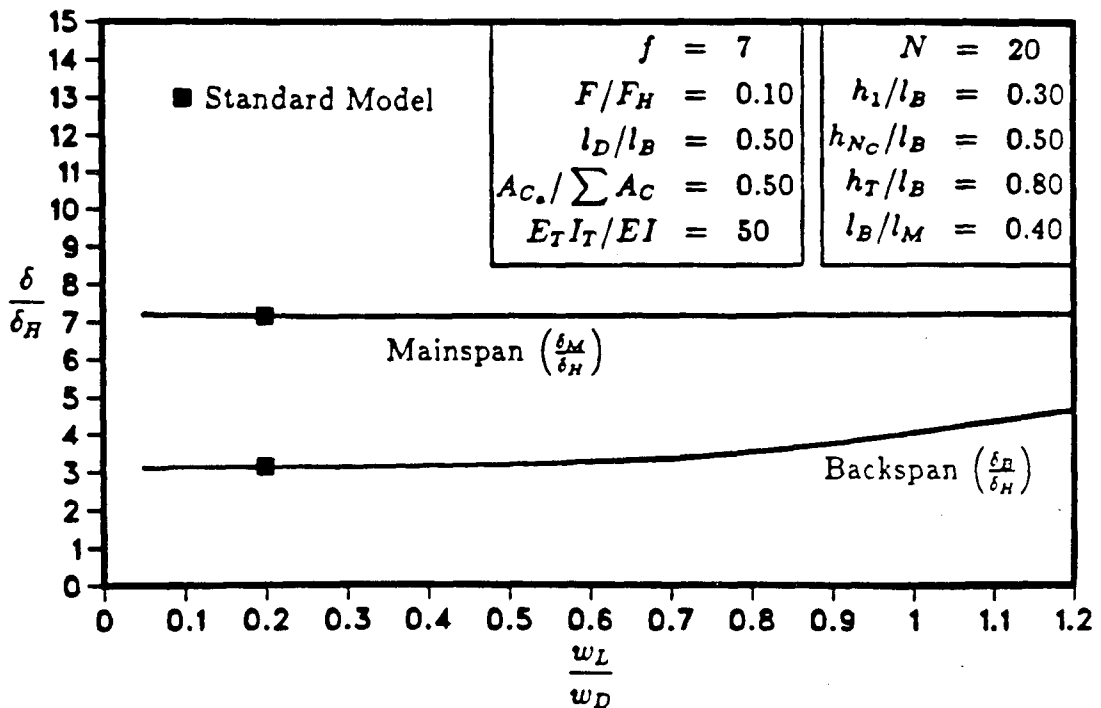


Figure 5.64: Dimensionless deflection versus dimensionless load.

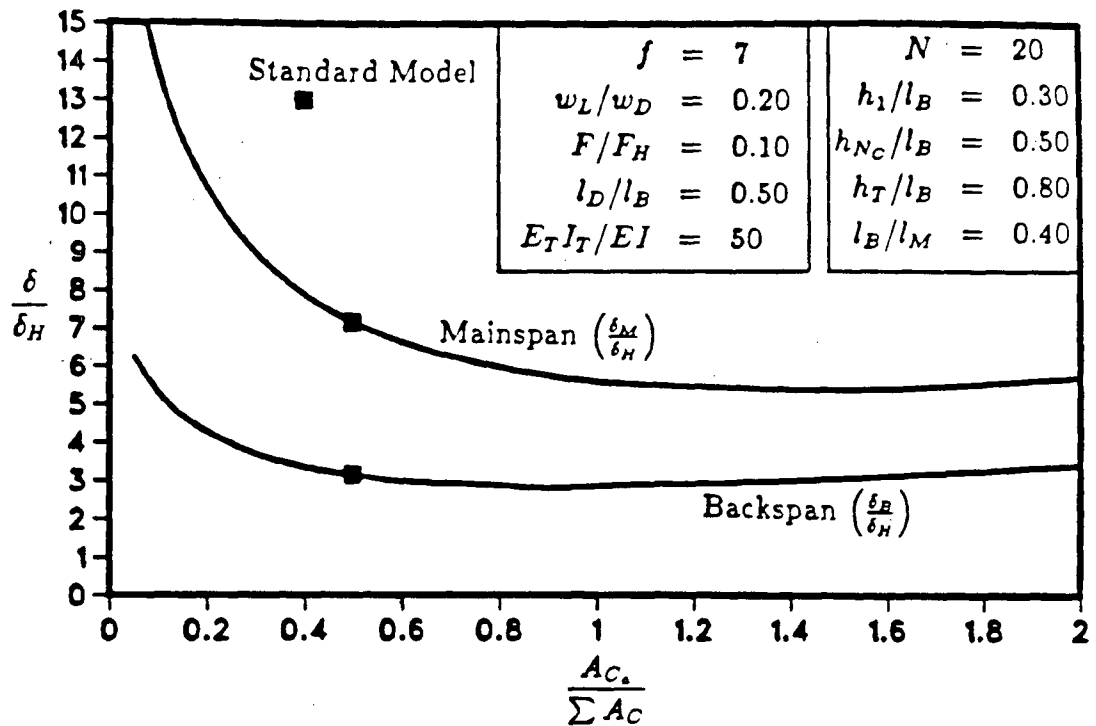


Figure 5.65: Dimensionless deflection versus dimensionless cable area.

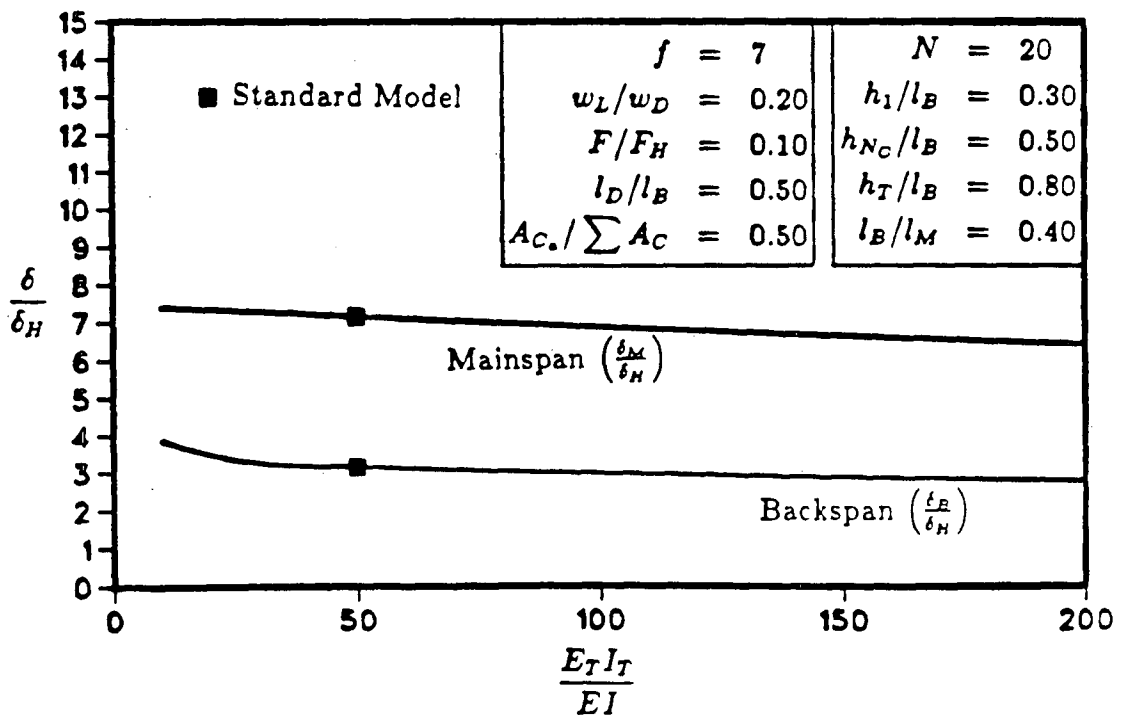


Figure 5.66: Dimensionless deflection versus dimensionless tower stiffness.

figures. Each figure would be valid for a specific value of $A_{C_a}/\sum A_C$ and on the figure would be a series of mainspan deflection curves, each with a different value of l_D/l_B .

The final graph of the tower stiffness effect is shown in Figure 5.66. The tower stiffness has very little effect on the mainspan deflection, which means that the cable stayed bridge stiffness is dependent on the anchor cables and not the towers.

5.3.2 Results of Moment Analysis

The same standard full bridge model is used for maximum moment analysis as that for the deflection analysis. However, different load cases are again necessary in order to get the maximum moment in the backspan and mainspan. The envelope of maximum moment influence lines is determined using ULA, and the maximum backspan and mainspan moment influence lines are shown in Figure 5.67 along with the resulting live load distributions and locations of the maximum moments.

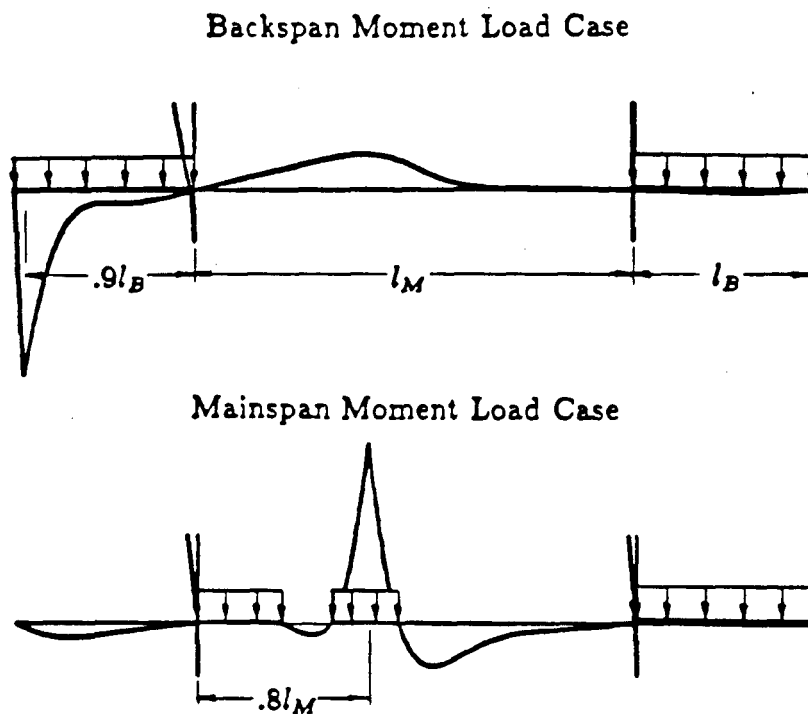


Figure 5.67: Load cases for maximum backspan and mainspan moment.

The fact that the influence line analysis is only approximate for this structure is more of a concern here than for deflections. This is particularly true for the maximum mainspan moment load case. The length of the short segments of loaded deck in the mainspan are not expected to remain constant to produce the maximum moment as the nonlinear analysis of the bridge model progresses. As the standard model is altered by varying the dimensionless ratios, large nonlinearities are expected and unusual phenomenon may appear in the mainspan moment plots. However, the mainspan moment does not govern, and the structure is not too nonlinear at service load levels, so the influence lines are still applicable for the standard model.

The moment of the standard model under the maximum backspan moment load case with $w_L/w_D = 0.20$, is shown in Figure 5.68 with the Hetényi moment superposed on the left backspan. The M_B/M_H ratio is equal to 3.513. The reason for this large deviation from the Hetényi moment is twofold: 1) the mainspan deck flexibility allows the towers to move which allows large backspan deflections and 2) the large backspan deflections occur in a relatively soft foundation region which allows a more severe curvature than the Hetényi model.

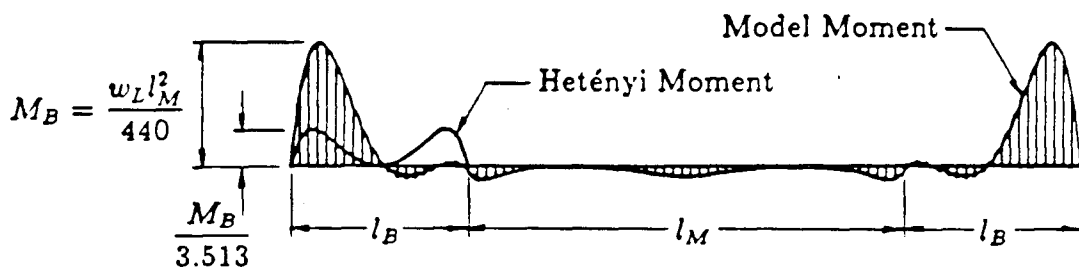


Figure 5.68: Maximum backspan moment of standard full bridge model.

The model moment diagram under the maximum mainspan moment load case is shown in Figure 5.69. The Hetényi moment is again superposed on the left backspan.

The δ_M/δ_H ratio is equal to 2.718. This is less than the value for M_B/M_H which is perhaps attributable to the anchor cable pulling back on the left tower which limits the curvature of the deck. That is, the backspan curvature is limited by the mainspan cables pulling on the towers but the mainspan curvature is restrained by the anchor cables which is a much stiffer system.

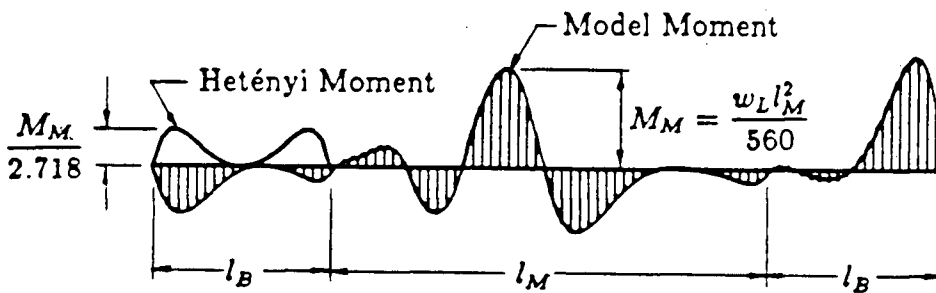


Figure 5.69: Maximum mainspan moment of standard full bridge model.

The maximum backspan live load moment is $w_L l_B^2/70$ and the maximum mainspan live load moment is $w_L l_B^2/90$. These results can be compared to the moment of $w_L l_B^2/140$ obtained for the backspan model. It is more common, however, to express the maximum live load moment in terms of the bridge mainspan length. For suspension and three-hinged arch bridges the linear live load moment is approximately $w_L l_M^2/60$. The maximum nonlinear cable stayed bridge backspan and mainspan moments for the ratio of $l_B/l_M = 0.4$ are $w_L l_M^2/440$ and $w_L l_M^2/560$, respectively. This is a sevenfold reduction in live load moment from other long span bridges and is a major testament to the economy of cable stayed bridges.

The standard model is now varied by altering the F/F_H ratio while keeping all other ratios constant. The maximum moment is then determined from a computer analysis of the maximum backspan moment load case and the maximum mainspan moment load case. The M_B/M_H and δ_M/δ_H ratios from their respective load cases are plotted

against F/F_H in Figure 5.70 for a range of F/F_H values. The backspan curve governs and the mainspan curve is shown for reference.

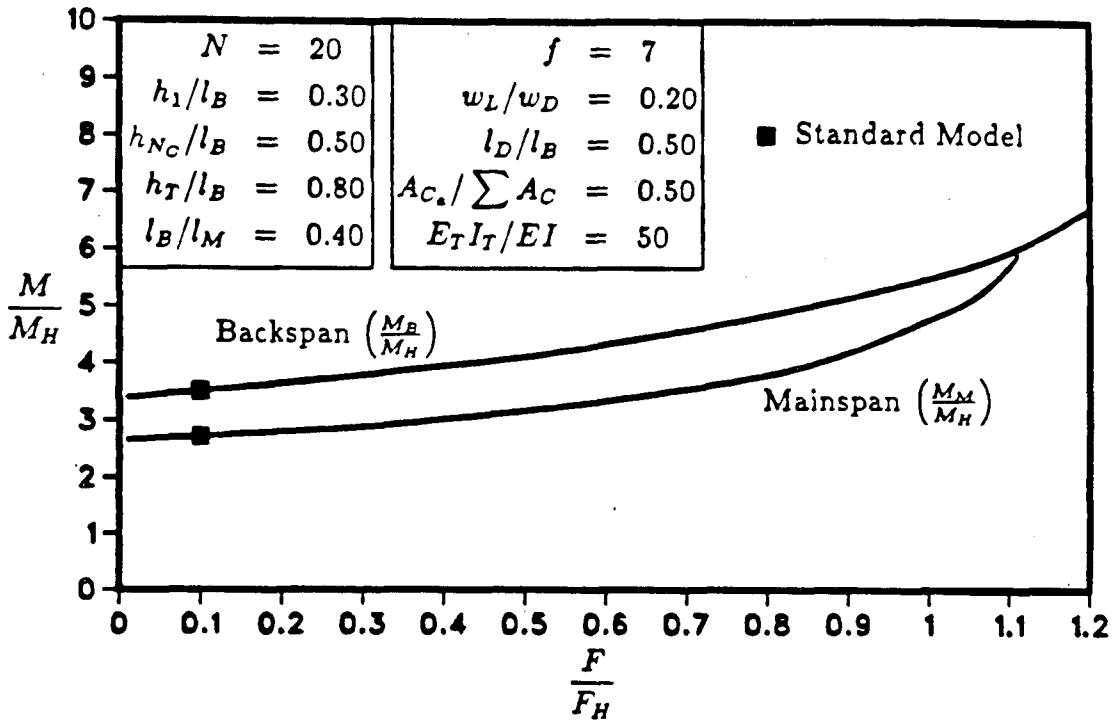


Figure 5.70: Magnification of maximum moment.

The moment magnification is evident in that the M_B/M_H ratio increases with increasing F/F_H . The mainspan moment behaves similarly to the backspan moment except that the load pattern used for the mainspan moment causes instability at a lower F/F_H ratio than for the backspan moment load case. Even though the mainspan moment increases rapidly just before buckling, it never exceeds the backspan moment. The slightly different behaviour of the mainspan moment curve from the backspan curve suggests that the load case used to produce the maximum mainspan moment should be altered as F/F_H varies.

The moment plot as a function of dimensionless decay length l_D/l_B is shown in Figure 5.71. It can be seen that M_B/M_H is highly dependent on l_D/l_B ; however, in the normal range of l_D/l_B from 0.40 to 0.65 the curve is much less steep than for

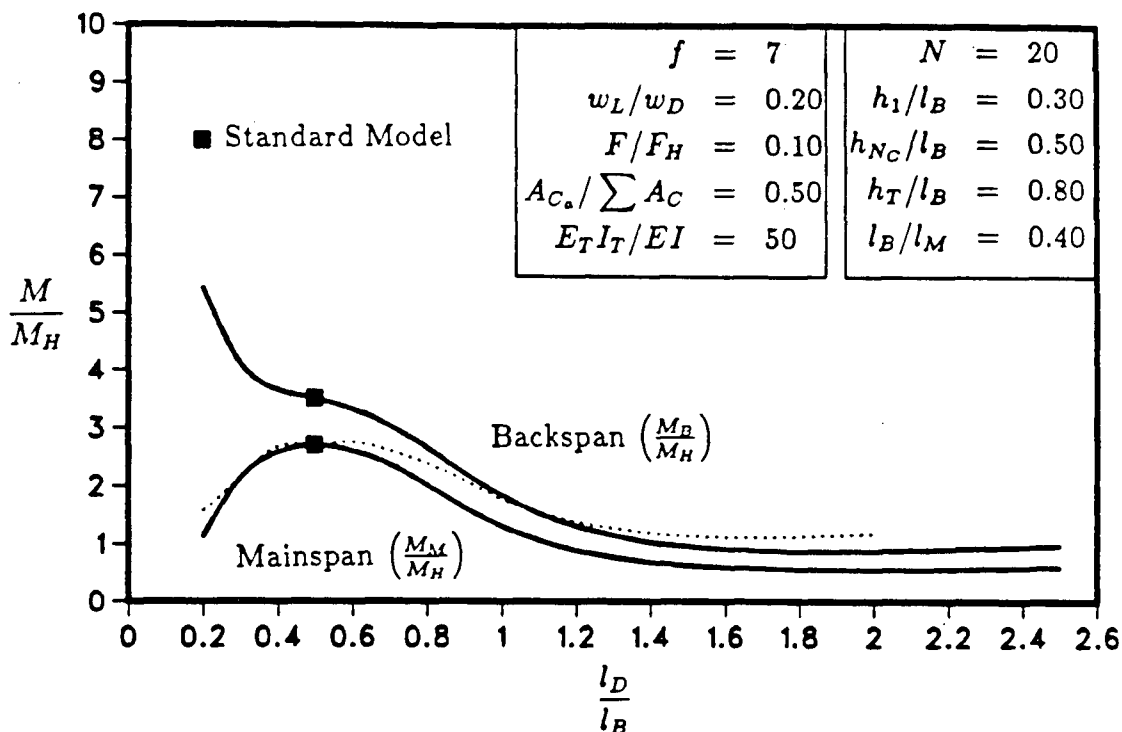


Figure 5.71: Dimensionless moment versus dimensionless decay length.

surrounding values of l_D/l_B . The curve for mainspan moment also exhibits a plateau for the normal range of l_D/l_B with steep sections on either side of this section, but it does not mimic the backspan curve as is the case for all other plots. This suggests that the load pattern must change for changing l_D/l_B in order to truly obtain the maximum moment. To this end, influence lines are obtained for various values of l_D/l_B and the appropriate load patterns are applied to get new M_M/M_H ratios. The corrected curve is plotted in Figure 5.71 as the dotted line. The corresponding curve for the maximum backspan moment is exactly that already plotted because the load pattern does not change with l_D/l_B in this case.

The fact that the new curve is different from the original M_M/M_H curve shows that using the load pattern obtained for one l_D/l_B ratio is not the load pattern that will produce the maximum mainspan moment for other values of l_D/l_B . The new curve actually governs for l_D/l_B greater than 1.2. A last point that should be brought up

is that for low values of l_D/l_B the moment distribution follows a jagged path rather than a smooth one as in Figure 5.69, and the cable layout used in this model may not produce the maximum moment possible. To get the maximum moment, more cables could be used in the model or the existing cables could be attached to different points on the deck. In any case, the discussion on M_M/M_H vs l_D/l_B is academic because the backspan moment governs for all practical cases.

The cable tautness graph is shown in Figure 5.72. The cable tautness has very little effect on the mainspan moment in the normal range of f . However, the importance of having tight cables is again demonstrated by the rapid increase of the moment for low values of f .

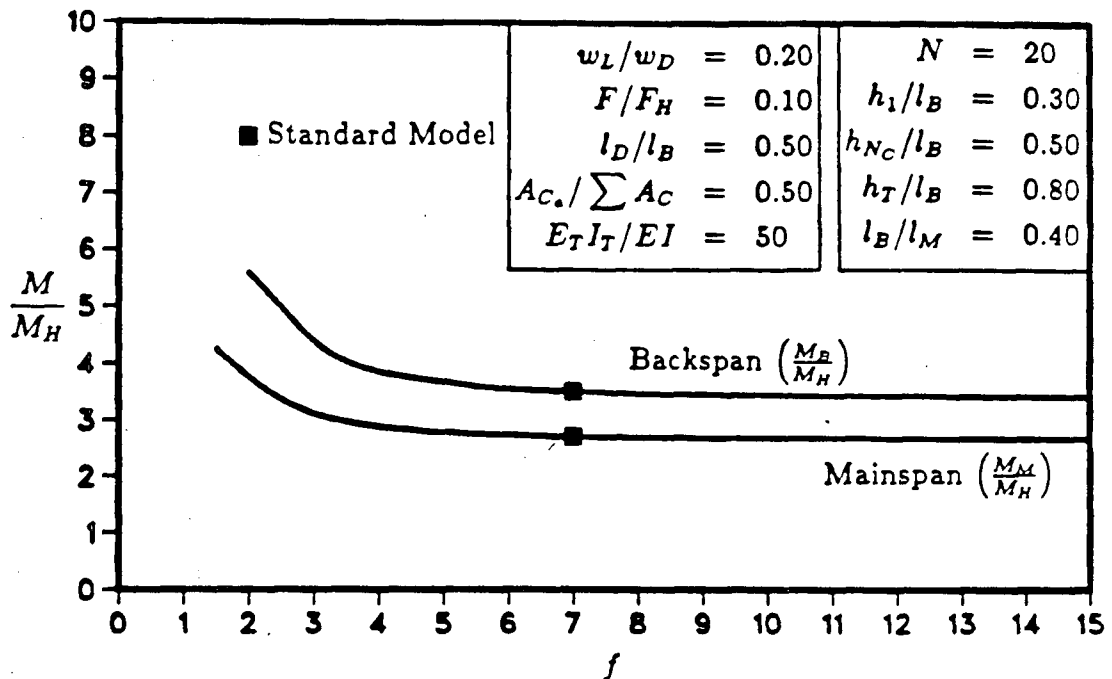


Figure 5.72: Dimensionless moment versus dimensionless cable tautness.

Figure 5.73 shows the influence of the live load to dead load ratio w_L/w_D . The influence of w_L/w_D on the maximum backspan moment is negligible in the normal range of w_L/w_D . There is a marked increase in M_B/M_H , however, for w_L/w_D greater.

than 0.8.

The moment plot as a function of the ratio of anchor cable area to backspan cable area $A_{C_a}/\sum A_C$ is shown in Figure 5.73. It can be seen that dependence of M_B/M_H to $A_{C_a}/\sum A_C$ is not as great as for deflection. However, the importance of heavy anchors is demonstrated by the large increase in backspan moment for $A_{C_a}/\sum A_C$ values less than 0.3.

The effect of varying the tower stiffness is shown in Figure 5.75. The tower stiffness has very little effect on the maximum backspan moment, which means that the towers act in their most efficient capacity; i.e., as axial members vertically supporting the cables, not as bending members tying the cables back.

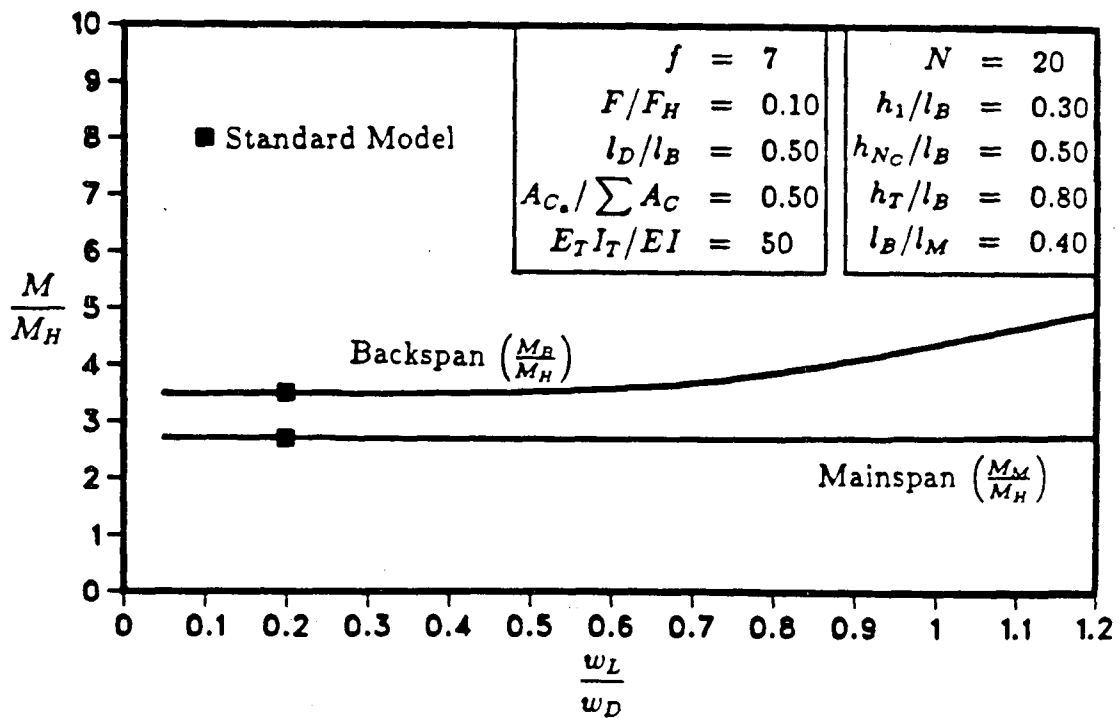


Figure 5.73: Dimensionless moment versus dimensionless load.

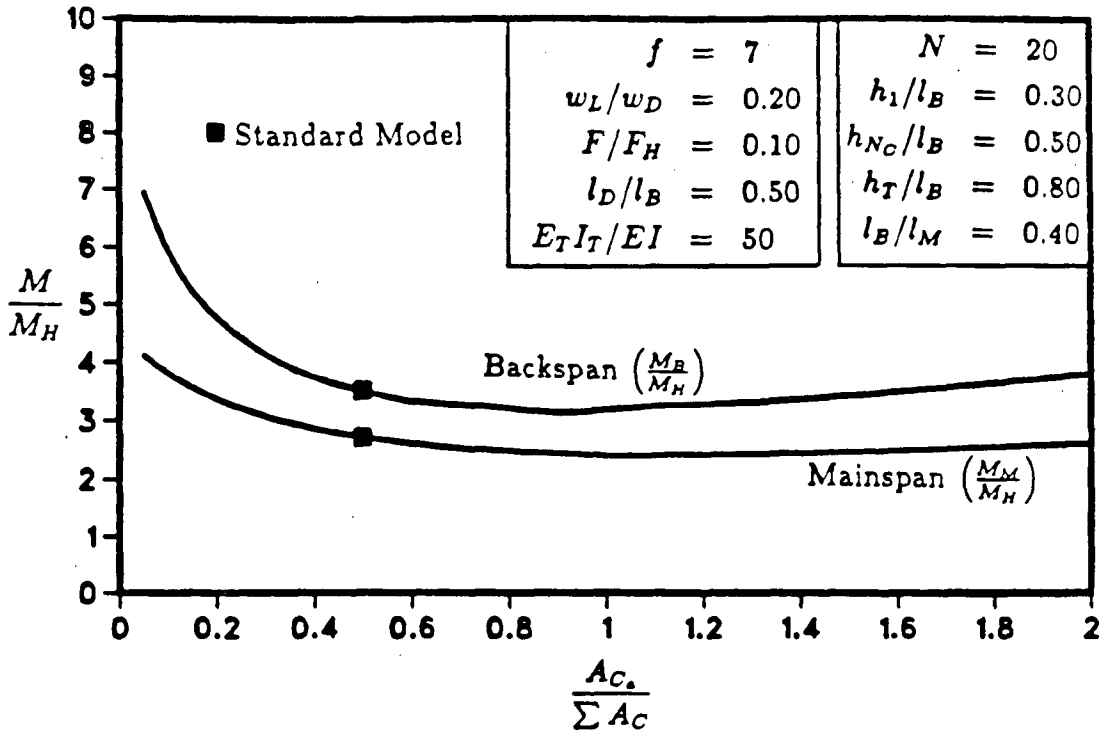


Figure 5.74: Dimensionless moment versus dimensionless cable area.

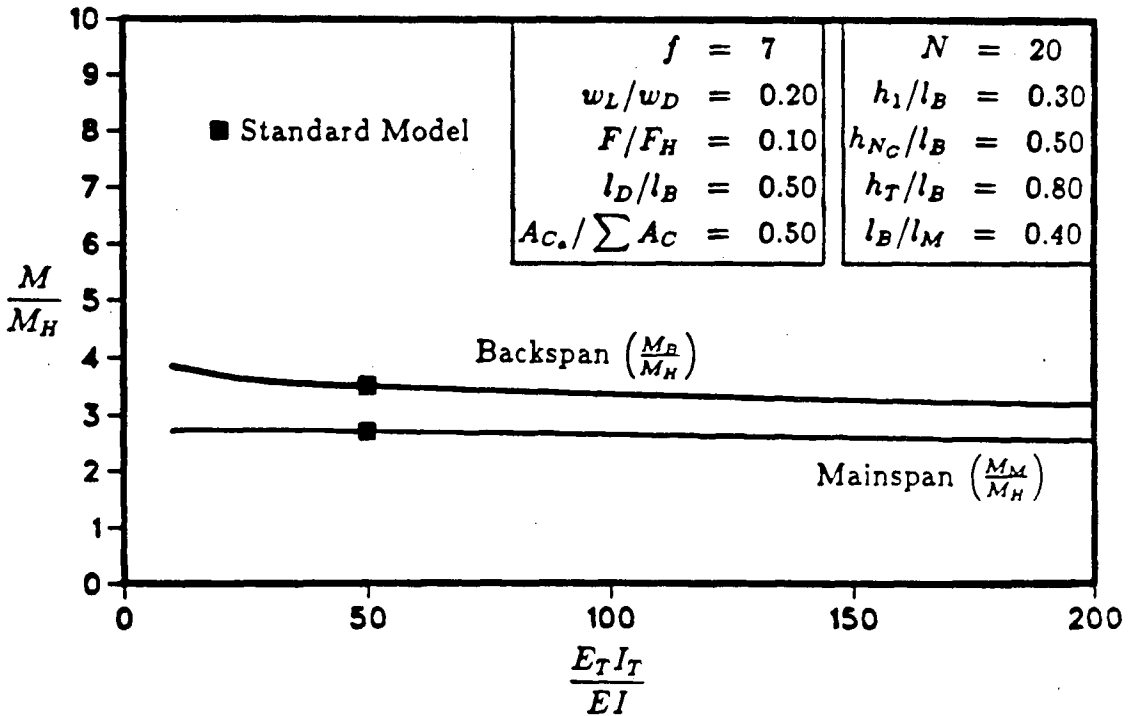


Figure 5.75: Dimensionless moment versus dimensionless tower stiffness.

Chapter 6

Application

The dimensionless stability, moment and deflection plots of Chapter 5 can be used for a preliminary design and analysis aid of cable stayed bridges. A procedure for finding the factor of safety against elastic stability failure and maximum service deck deflection and moment is outlined in this chapter.

A conceptual design could determine the materials to use, the tower and deck sizes, and the number and sizes of cables. However, the mainspan length and the live load are usually determined before the bridge design proceeds (bridges are designed to carry specified loads over fixed spans), so a suggested starting point for the conceptual design is to use $M_B = w_L l_M^2 / 440$ and $\delta_M = l_M / 500$ to obtain preliminary values for the deck E and I .

Once the bridge design is more detailed and ready for computer analysis, a great saving of effort can be made by utilizing the results of this thesis to analyze and reanalyze progressive bridge designs, instead of modelling and analyzing several different designs by computer. When the analysis of the bridge designs utilizing the dimensionless ratio models has served its usefulness, a more detailed analysis could then be performed by computer.

6.1 The Model

The dimensional analysis model has constant deck and tower stiffnesses and a uniform distribution of cable areas such that each cable has the same dead load stress. The cables are at a constant spacing along the deck and tower. A representative geometric model is used and it is assumed that the model behaviour is independent of the number

of cables as long as at least four or five are within the decay length of the model deck.

The model representative cable is taken as the one (or average of two) attached to the center deck section of the bridge backspan. The area, height and angle of this cable are used in the model as the representative values for the bridge. The deck moment of inertia of the bridge backspan center section is taken as the constant moment of inertia of the model deck, and the model dead load is determined from the bridge deck cross section at this point. The tower moment of inertia of the model is an equivalent one, such that the free standing tower deflections of the bridge and model are the same for a unit lateral load at the top.

Once the representative parameters are determined, the dimensionless ratios are calculated as given in Chapter 5, Section 5.2.1. Note that the cable area ratio is not calculated using the representative cable area; rather, the actual bridge anchor and backspan cable areas are used. Also, the maximum dead load axial force F in the model deck is calculated using representative values, i.e.,

$$F = \frac{w_D l_M}{2 \tan \theta_{N_C/2}}$$

6.2 Procedure

Once the eleven ratios have been given a preliminary estimate, it is necessary to determine if the parameters of the bridge to be analyzed falls into the domain of the procedure described in the next sections. That is, the geometric dimensionless ratios h_1/l_B , h_{N_C}/l_B , h_T/l_B and l_B/l_M should be reasonably close to the values of 0.30, 0.50, 0.80 and 0.40, respectively. The number of cables over the decay length must also be greater than four. In other words, l_D/l_B should be greater than $4/N$. The decay length is given by

$$l_D = \pi \sqrt{2} \sqrt[4]{\frac{EI}{k}}$$

where

$$k = \frac{N A_{C_{N/2}} E_C \sin^3 \theta_{N/2}}{l_B h_{N/2}}$$

6.2.1 Stability

The stability factor of safety is found by first determining the critical live load to dead load ratio $\lambda w_L/w_D$ from Figure 5.52 for the value of F/F_H calculated for the bridge to be analyzed. The factor of safety on the live load is calculated as the ratio of the final and original live to dead load ratios. i.e.,

$$\frac{\left(\frac{\lambda w_L}{w_D}\right)}{\left(\frac{w_L}{w_D}\right)}$$

6.2.2 Deflection and Moment

The procedure for determining the maximum backspan and mainspan deflection is slightly more complicated than that for stability because of the influence of l_D/l_B , $A_{C_a}/\sum A_C$ and to a lesser degree F/F_H .

The first step is to obtain the δ/δ_H ratio from Figure 5.62 corresponding to the bridge l_D/l_B ratio. This δ/δ_H ratio is valid if $F/F_H = 0.10$ and $A_{C_a}/\sum A_C = 0.50$. To adjust δ/δ_H for a different value of $A_{C_a}/\sum A_C$, for example, simply multiply by the δ/δ_H ratio from Figure 5.65 corresponding to the bridge value of $A_{C_a}/\sum A_C$, then divide by the δ/δ_H value for the standard model. This assumes a linear relationship, and in symbolic form is

$$\frac{\delta}{\delta_H} = \frac{\left[\left(\frac{\delta}{\delta_H}\right)_{\frac{l_D}{l_B}}\right] \left[\left(\frac{\delta}{\delta_H}\right)_{\frac{A_{C_a}}{\sum A_C}}\right]}{\left(\frac{\delta}{\delta_H}\right)_{\square}}$$

This adjustment is repeated in a similar manner for nonstandard values of F/F_H , $E_T I_T/EI$, f and w_L/w_D although they may not be necessary because they are of relatively smaller influence.

Once the bridge δ/δ_H ratio is determined, the maximum deflection can be calculated by multiplying the ratio by δ_H as given by Equation 3.12 or Figure 3.14.

The procedure for determining the maximum backspan and mainspan moment is exactly the same as that for deflection, using the appropriate corresponding moment graphs. The beam on an elastic foundation moment is given by Equation 3.13 or Figure 3.20.

6.3 Examples

Two cable stayed bridge designs are taken as examples of the analysis procedure and then compared to computer runs of the actual bridge models. The ALRT steel and concrete designs are used for this purpose.

The representative parameters and ratios are given for these two bridges in Appendices C.5 and C.6. Before proceeding with the analysis, the geometric ratios are checked to see if they are close to the standard model ratios. Table 6.1 shows the percent deviations of the two designs from the standard model values, along with the check on the number of cables within the decay length. There is a sufficient number of cables for both bridges and the geometric ratio deviations are small except for the ratio that defines the shape of the cable layout, h_1/l_B . The ALRT steel design is close to being a radiating shape and the ALRT concrete design is more of a fan shape. The effects of the two different cable layouts is assumed to be small, and the analysis procedure is deemed to be applicable to the two bridge designs.

	h_1/l_B	h_N/l_B	h_T/l_B	l_B/l_M	$l_D/l_B > 4/N$
Standard Model	.3	.5	.8	.4	
ALRT Steel	.478 59%	.548 10%	.841 5%	.419 5%	.418 > .364
ALRT Concrete	.234 22%	.516 3%	.819 2%	.406 2%	.423 > .333

Table 6.1: Check on applicability.

6.3.1 Stability

The stability analysis using the suggested procedure and the computer analysis of the actual bridges are summarized in Table 6.2. The simple analysis gives conservative

factors of safety. The live load factors are 16% and 38% lower than the computer analysis for the concrete and steel bridges, respectively. The radiating cable layout of the steel bridge may be the reason the simple analysis is further away from the computer analysis than the concrete bridge.

	w_L/w_D	F/F_H	Simple Analysis		Computer Analysis
			$\lambda w_L/w_D$	Factor of Safety	Factor of Safety
Standard Model	.20	.10	2.4	11.9	11.9
ALRT Steel	.36	.12	2.1	5.83	9.33
ALRT Concrete	.17	.24	1.1	6.47	7.69

Table 6.2: Summary of stability analysis.

An attempt to improve the correlation between the simple analysis and the computer analysis can be made by adjusting the simple analysis factors according to the actual values of l_D/l_B , $A_{C_a}/\sum A_C$ and $E_T I_T/EI$. However, for these two bridges the adjustments counter one another and the net effect would be minimal.

6.3.2 Deflection and Moment

The deflection analysis using the simple procedure and the computer analysis of the actual bridges is summarized in Table 6.3. The δ/δ_H ratios are calculated for the steel bridge as

$$\frac{\delta_B}{\delta_H} = \frac{\left[(3.8) \frac{l_D}{l_B} = .418 \right] \left[(3.0) \frac{A_{C_a}}{\sum A_C} = .595 \right]}{(3.155)_{\square}} = 3.61$$

$$\frac{\delta_M}{\delta_H} = \frac{\left[(7.8) \frac{l_D}{l_B} = .418 \right] \left[(6.7) \frac{A_{C_a}}{\sum A_C} = .595 \right]}{(7.177)_{\square}} = 7.28$$

and for the concrete bridge as

$$\frac{\delta_B}{\delta_H} = \frac{\left[(3.8) \frac{l_D}{l_B} = .423 \right] \left[(3.4) \frac{F}{F_H} = .24 \right]}{(3.155)_{\square}} = 4.10$$

$$\frac{\delta_M}{\delta_H} = \frac{\left[(7.8) \frac{l_D}{l_B} = .423 \right] \left[(7.3) \frac{F}{F_H} = .24 \right]}{(7.177)_{\square}} = 7.93$$

	Standard Model	Simple Analysis		Computer Analysis	
		ALRT Steel	ALRT Concrete	ALRT Steel	ALRT Concrete
l_B	—	138	138	138	138
l_M	—	329	340	329	340
F/F_H	.1	.12	.24	.12	.24
$A_{C_a}/\sum A_C$.5	.595	.502	.595	.502
l_D/l_B	.5	.418	.423	.418	.423
w_L	—	16	16	16	16
k	—	211.5	279.3	—	—
$\delta k/w_L$	—	1.07	1.07	—	—
δ_H	—	.0809	.0613	—	—
δ_B/δ_H	3.155	3.61	4.10	—	—
δ_M/δ_H	7.177	7.28	7.93	—	—
δ_B	—	.292	.251	.254	.261
δ_M	—	.589	.486	.661	.603
δ_B/l_B	1/1000	1/473	1/550	1/544	1/530
δ_M/l_M	1/1100	1/559	1/700	1/498	1/564

Table 6.3: Summary of deflection analysis.

The simple analysis gives unconservative maximum mainspan deflections. The mainspan deflection ratios are 11% and 19% lower than the computer analysis for the steel and concrete bridges, respectively. The corresponding backspan ratios are 15% higher and 4% lower, which indicates that the simple analysis gives conservative results for the maximum backspan deflections.

The moment analysis using the simple procedure and the computer analysis of the actual bridges is summarized in Table 6.4. The M/M_H ratios are calculated for the steel bridge as

$$\frac{M_B}{M_H} = \frac{\left[(2.7) \frac{l_D}{l_B} = .418 \right] \left[(2.6) \frac{A_{C_a}}{\sum A_C} = .595 \right]}{(2.718)_\square} = 2.58$$

$$\frac{M_M}{M_H} = \frac{\left[(3.6) \frac{l_D}{l_B} = .418 \right] \left[(3.3) \frac{A_{C_a}}{\sum A_C} = .595 \right]}{(3.513)_\square} = 3.38$$

and for the concrete bridge as

$$\frac{M_B}{M_H} = \frac{\left[(2.7) \frac{l_D}{l_B} = .423 \right] \left[(2.8) \frac{F}{F_H} = .24 \right]}{(2.718)_\square} = 2.78$$

$$\frac{M_M}{M_H} = \frac{\left[(3.6) \frac{l_D}{l_B} = .423 \right] \left[(3.7) \frac{F}{F_H} = .24 \right]}{(3.513)_\square} = 3.79$$

	Standard Model	Simple Analysis		Computer Analysis	
		ALRT Steel	ALRT Concrete	ALRT Steel	ALRT Concrete
l_B	—	138	138	138	138
l_M	—	329	340	329	340
F/F_H	.1	.12	.24	.12	.24
$A_{C_s}/\sum A_C$.5	.595	.502	.595	.502
l_D/l_B	.5	.418	.423	.418	.423
w_L	—	16	16	16	16
$M_H/w_L l_B^2$	—	.0035	.0035	—	—
M_H	—	1066	1066	—	—
M_M/M_H	2.718	2.58	2.78	—	—
M_B/M_H	3.513	3.38	3.79	—	—
M_M	—	2750	2963	2807.8	2751.1
M_B	—	3603	4040	3731.0	3480.1
$M_M/w_L l_M^2$	1/560	1/630	1/624	1/617	1/672
$M_B/w_L l_M^2$	1/440	1/481	1/458	1/464	1/531

Table 6.4: Summary of moment analysis.

There is fairly close agreement between the simple analysis moments and the computer analysis maximum moments, and any significant deviations are on the conservative side. The backspan moment ratios are 4% lower and 16% higher than the computer analysis for the steel and concrete bridges, respectively. The corresponding mainspan ratios are 2% lower and 8% higher than the computer analysis.

The power in the simple procedure is in being able to change the design and get the effect of the change without computer analysis. Thus, many concepts and alterations can be tested quickly and cheaply. Once the cable stayed bridge design has been sized

via the iterative use of the simple procedure, the bridge can then be modelled for computer analysis. At this stage in the design process, the designer would also have a good understanding of the bridge behaviour and be better prepared to interpret the computer analysis results.

Chapter 7

Conclusion

The elastic stability of cable stayed bridge decks, as well as the deflection and moment of the deck are successfully modelled and analyzed using the computer program ULA (Ultimate Load Analysis). The computer analysis includes $P-\Delta$ effects and true catenary cables. The dimensional analysis used to study the the general behaviour of cable stayed bridges shows that the comparison to a beam on an elastic foundation is a valid one to make. Eleven dimensionless ratios are used to describe the model. Five are geometric ratios and are set to representative values and kept constant for this study. The remaining six ratios describe the material properties, structural elements and the loading of the model. These six ratios are varied from the standard and the effect on the cable stayed bridge model is observed.

The elastic stability of cable stayed bridges is governed by the laws that govern a beam-column on an elastic foundation. The direct correlation is seen when the critical section of deck is isolated and examined. The critical load case for stability is identified and the factor of safety on the live load against elastic failure for the standard model is 11.9. This factor of safety is dependent on the maximum axial load in the deck under dead load only (F/F_H) and the magnitude of the servive live load (w_L/w_D). The remaining ratios have little ($\pm 5\%$) or no effect over the normal range of values.

Deck stability could be the governing criterion if load factors are applied to the dead load, for example, $2.0w_D + 6.7w_L$ is a load case more severe than the standard $w_D + 11.9w_L$. Thus, the elastic stability of a cable stayed bridge could sometimes be the limiting design criterion.

The maximum deflection and moment of the cable stayed bridge model is compared

to that of a beam on an elastic foundation. The maximum live load deflection versus span ratios, δ_B/l_B and δ_M/l_M are 1/1000 and 1/1100 respectively, which are well within the recommended value of 1/500. The maximum nonlinear cable stayed bridge model backspan and mainspan moments are $w_L l_M^2/440$ and $w_L l_M^2/560$, respectively. This is a sevenfold reduction in live load moment from other long span bridges and is a major testament to the economy of cable stayed bridges. Both the deflection and moment are dependent on the decay length of the deck and on the anchor cable size. Magnification of deflection and moment is observed for increasing deck dead load axial force. It is also important to note that the cable tautness has no effect on the model response as long as the cables do remain tight. The cable stayed bridge response is also independent of the tower stiffness which is also a cost saving feature because the towers do not have to be designed for heavy bending and the tower foundations do not have to transfer large moments, except perhaps during erection.

A simple analysis procedure is developed based on using the charts in this study. Two example analyses are carried out and compared to actual computer runs. For the two examples, the simple procedure is up to 40% conservative compared to the computer runs for elastic stability. The maximum mainspan deflection is up to 20% unconservative and the maximum backspan moment is up to 20% conservative for the two examples used. The large deviations of the simple analysis results from the computer results indicate that caution must be used in interpreting the simple analysis results, especially when the cable layout differs significantly from the standard model layout. However, the simple procedure can still be used to compare geometrically similar cable stayed bridge designs.

7.1 Further Research

Research on the effect of the geometric dimensionless ratios, in particular the ratio that defines the cable layout (h_1/l_B) would complement this study. Research on single tower

cable stayed bridges would be interesting as would a space frame analysis on bridges with A-frame towers.

Further research on the elastic stability of cable stayed bridges is still called for, however, the real mechanism of cable stayed bridge collapse would involve the formation of plastic hinges in the deck. Therefore, plastic analysis of cable stayed bridges would be a more urgent topic of research. This involves the addition of two more parameters, namely the plastic moment capacity M_p of the deck and—for the moment-axial interaction—the deck cross sectional area A . This then requires two more dimensionless ratios say,

$$\frac{M_p l_M}{EI}$$

and

$$\frac{A}{\sum A_C}$$

It turns out that $M_p l_M / EI$ is approximately equal to 0.6 and $A / \sum A_C$ is approximately equal to 10 for steel deck bridges. Using these values of $M_p l_M / EI$ and $A / \sum A_C$ and the model values of l_M , EI and $\sum A_C$ values for M_p and A are input into ULA. The plastic stability analysis under load case 4 is carried out and a plastic hinge forms at $6.76w_L/w_D$ which causes the bridge to become unstable. The factor of safety on the live load for this case is 6.76 which is a 43% drop from the elastic stability factor of safety. The deflected shape of the failed bridge is shown in Figure 7.76. This is a catastrophic mode of failure because the bridge collapses as soon as one hinge forms—there is no warning of imminent failure.

The single hinge mode of failure occurs because the axial load in the deck is high enough to cause a $P-\Delta$ stability failure of the bridge with a hinge in it. A more likely mode of failure is plastic hinge formation with the post hinge structure remaining stable. Additional loading would then cause more hinges to form until enough hinges are in the structure to form a mechanism. This occurs for the maximum backspan moment load case, for example. Hinges form at both ends of the bridge at $5.76w_L/w_D$

and the bridge is still able to carry even heavier loads until at $9.25w_L/w_D$ another hinge forms at the center of the mainspan. The bridge is still stable at this point but cannot carry heavier loads. The deflected shape of the deck with three plastic hinges is shown in Figure 7.77. If the formation of the first hinge is defined as failure, the factor of safety against failure is 5.76, which is lower for this mode than the plastic stability mode. However, this mode of failure may be preferred because there is a warning of collapse.

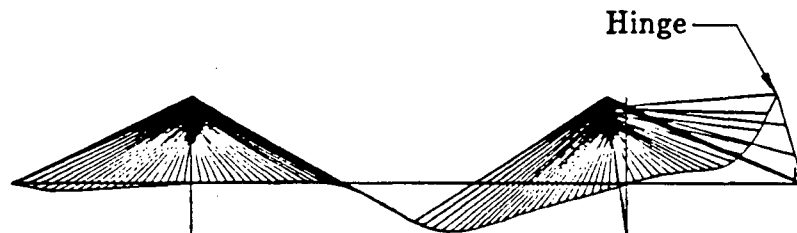


Figure 7.76: Plastic stability failure of bridge model.

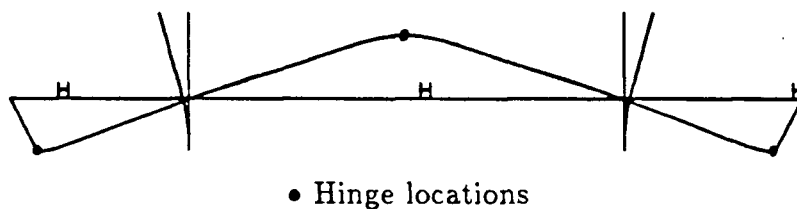


Figure 7.77: Plastic hinge failure of bridge model.

Bibliography

- [1] Leonhardt, F. and Zellner, W., "Cable-Stayed Bridges: Report on Latest Developments," Canadian Structural Engineering Conference, 1970, Canadian Steel Industries Construction Council, Toronto, Canada.
- [2] Troitsky, M. S., *Cable-Stayed Bridges, Theory and Design*, Crosby Lockwood Staples, London, England, 1977.
- [3] Dischinger, F., "Hängebrücken für schwerste Verkehrslasten," *Der Bauingenier*, March 1949, pp. 65, 107.
- [4] Leonhardt, F. and Zellner, W., "Cable-Stayed Bridges," *IABSE Surveys S-13/80*, *IABSE Periodica 2/1980*, May 1980, pp. 21-48.
- [5] Tang, M. C., "Buckling of Cable-Stayed Girder Bridges," *Journal of the Structural Division*, ASCE, Vol. 102, No. ST9, September 1976, pp. 1675-1684.
- [6] Gimsing, N. J., *Cable Supported Bridges, Concept and Design*, John Wiley & Sons Ltd., Chichester, England, 1983.
- [7] Smith, B. Stafford, "The Single Plane Cable-Stayed Girder Bridge: A Method of Analysis Suitable for Computer Use," *Proceedings of the Institution of Civil Engineers*, Vol. 37, May 1967, pp.183-194.
- [8] Smith, B. S., "A Linear Method of Analysis for Double-Plane Cable-Stayed Girder Bridges," *Proceedings of the Institution of Civil Engineers*, Vol. 39, January 1968, pp. 85-94.
- [9] Troitsky, M. S., and Lazar, B. E., "Model Analysis and Design of Cable-Stayed

- Bridges," *Proceedings of the Institution of Civil Engineers*, March 1971, pp. 439-464.
- [10] Lazar, B. E., "Stiffness Analysis of Cable-Stayed Bridges," *Journal of the Structural Division*, ASCE, Vol. 98, No. ST7, July 1972, pp. 1605-1612.
- [11] Tang, M. C., "Analysis of Cable-Stayed Girder Bridges," *Journal of the Structural Division*, ASCE, Vol. 97, No. ST5, May 1971, pp. 1481-1496.
- [12] Kajita, T. and Cheung, Y. K., "Finite Element Analysis of Cable-Stayed Bridges," *IABSE Publication 93-II*, 1973.
- [13] Rajaraman, A., Loganathan, K. and Raman, N. V., "Nonlinear Analysis of Cable-Stayed Bridges," *IABSE Proceedings P-37/80*, IABSE Periodica 4/1980, November 1980, pp. 205-216.
- [14] Como, M., Grimaldi, A. and Maceri, F., "Statical Behaviour of Long-Span Cable-Stayed Bridges," *International Journal of Solids and Structures* Vol. 21, No. 8, pp. 831-850, 1980, pp. 831-850.
- [15] Hegab, H. I. A., "Energy Analysis of Cable-Stayed Bridges," *Journal of Structural Engineering*, ASCE, Vol. 112, No. 5, May 1986, pp. 1182-1195.
- [16] Ernst, H. J., "Der E-Modul von Seilen unter Berücksichtigung des Durchhanges," *Der Bauingenieur*, Vol. 40, No. 2, February 1965, pp. 52-55.
- [17] Ito, M. and Maeda, Y., Discussion, "Commentary on the Tentative Recommendations for Cable-Stayed Bridge Structures," *Journal of the Structural Division*, ASCE, Vol. 104, No. ST2, February 1978, pp. 372-374.
- [18] Mill, A. J., "Ultimate Load Analysis of Fixed Arches," M.A.Sc. Thesis, The University of British Columbia, 1985.

- [19] Weaver, W. and Gere, J. M., *Matrix Analysis of Framed Structures*, D. Van Nostrand Company, New York, 1980.
- [20] Hooley, R. F., "Cable Equations for Cable Stayed Bridge," Unpublished notes, The University of British Columbia, 1986.
- [21] Goodier, J. N., "Dimensional Analysis," in *Handbook of Experimental Stress Analysis*, Ed. M. Hetényi, John Wiley & Sons, New York, 1950.
- [22] Hetényi, M., *Beams on Elastic Foundations*, Ann Arbor: The University of Michigan Press, 1944.
- [23] By Committee, "Tentative Recommendations for Cable-Stayed Bridge Structures," *Journal of the Structural Division*, ASCE, Vol. 103, No. ST5, May 1977, pp. 929-939.
- [24] By Committee, "Recommended Design Loads for Bridges," *Journal of the Structural Division*, ASCE, Vol. 107, No. ST7, July 1981, pp. 1161-1213.

Appendix A

Catenary Cable

For the free-body diagram of Figure A.78 which is an element from the catenary cable shown in Figure A.79, the sum of the forces in the vertical direction produces the governing differential equation.

$$Hy' + w dc = H(y' + dy')$$

where w is the load per unit of cable length.

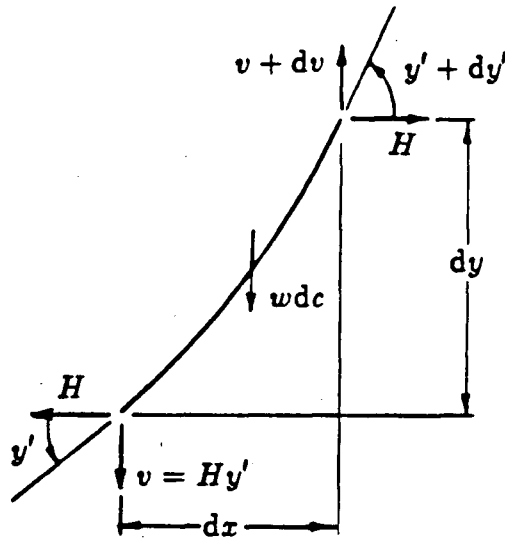


Figure A.78: Catenary cable element.

Simplifying and using $dc = \sqrt{dx^2 + dy^2}$ yields

$$y'' = \frac{w}{H} \sqrt{1 + y'^2}$$

Integration yields

$$y' = \sinh \left(\frac{wx}{H} + A \right)$$

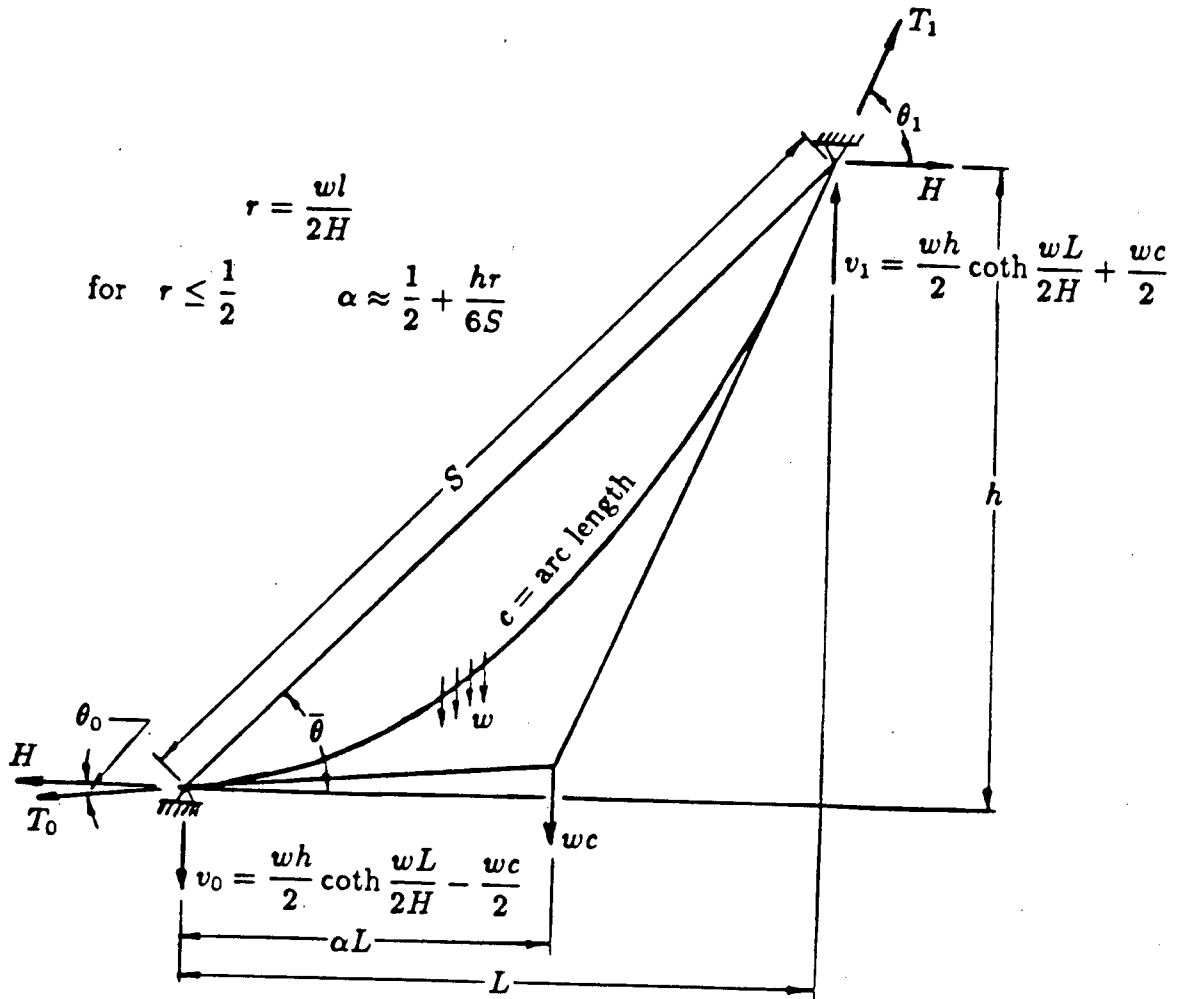


Figure A.79: Catenary cable.

and integrating again yields

$$y = \frac{H}{w} \cosh \left(\frac{wx}{H} + A \right) + B$$

where A and B are constants of integration.

With the boundary conditions at $x = 0$; $y = 0$ and at $x = L$; $y = h$ the constants of integration are evaluated as

$$A = \sinh^{-1} \left(\frac{wh}{2H \sinh \frac{wL}{2H}} \right) - \frac{wL}{2H}$$

and

$$B = -\frac{H}{w} \cosh A$$

The cable arc length c is obtained by integrating the elemental cable length through the length of the cable.

$$c = \int_0^c dc = \int_0^L \frac{dc}{dx} dx = \int_0^L \sqrt{1 + y'^2} dx$$

Appropriate substitutions and simplifications yield

$$c = \sqrt{h^2 + \frac{4H^2}{w^2} \sinh^2 \frac{wL}{2H}}$$

Using the fact that $\tan \theta = y'$ the vertical components of cable tension v_0 and v_1 can be determined and from equilibrium of moments, the point of application αL of the total cable weight wc can be evaluated. The results are shown on Figure A.79.

The elastic elongation Δ_e of the cable is

$$\int_0^c \frac{T}{AE} dc = \int_0^L \frac{H \sec \theta}{AE} \sec \theta dx$$

which reduces to

$$\Delta_e = \frac{HL}{AE} \left(\frac{wh^2}{2HL} \coth \frac{wL}{2H} + \frac{1}{2} + \frac{H}{2wL} \sinh \frac{wL}{H} \right)$$

The above expressions are exact but inconvenient to work with. For tight cables, where $r = wL/2H \leq 1/2$ it is convenient to expand the hyperbolic functions as power

series. The series below are used and terms up to and including r^4 are retained.

$$\begin{aligned}\sinh r &= r + \frac{r^3}{6} + \frac{r^5}{120} + \dots \\ \cosh r &= 1 + \frac{r^2}{2} + \frac{r^4}{24} + \frac{r^6}{720} + \dots \\ \coth r &= \frac{1}{r} + \frac{r}{3} - \frac{r^3}{45} + \frac{2r^5}{945} - \dots\end{aligned}$$

From these expressions and using $\sqrt{1+r} = 1 + r/2 + r^2/8 + \dots$ the final results are

$$c = S \left[1 + \frac{\cos^2 \bar{\theta}}{6} r^2 + \left(\frac{\cos^2 \bar{\theta}}{45} - \frac{\cos^4 \bar{\theta}}{72} \right) r^4 \right]$$

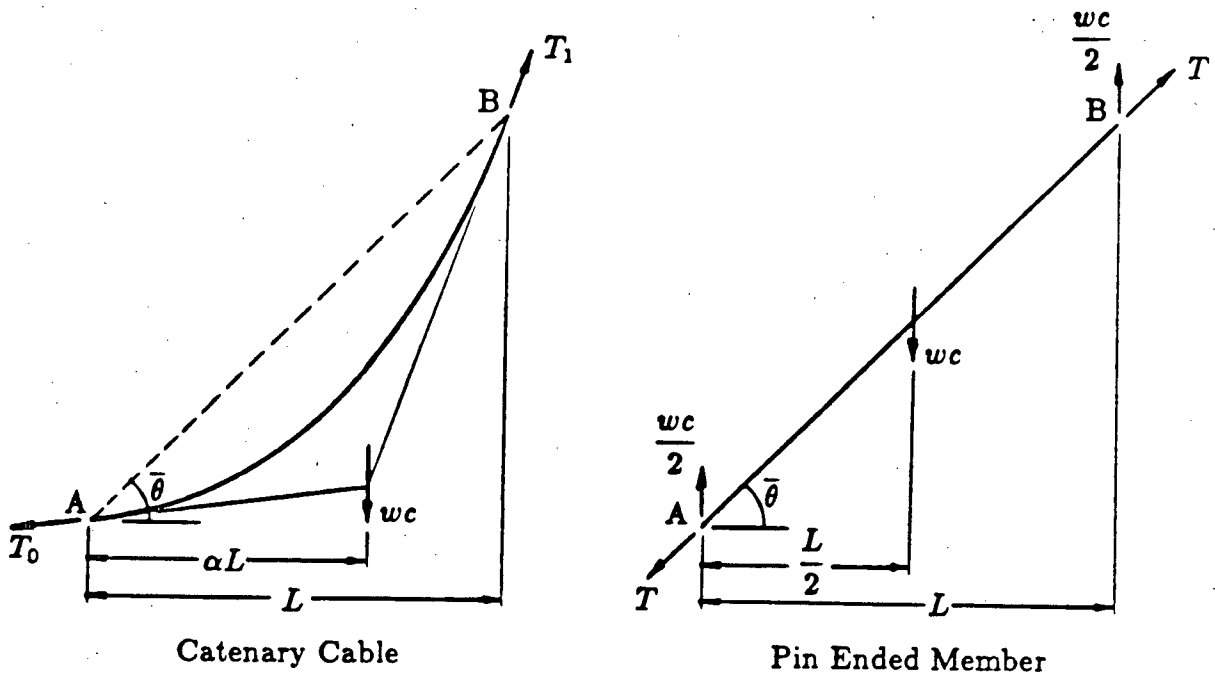
and

$$\Delta_c = \frac{HL \sec^2 \bar{\theta}}{AE} \left[1 + \frac{r^2}{3} - \left(1 - 4 \frac{L^2}{S^2} \right) \frac{r^4}{45} \right]$$

In most computer structural analysis the catenary cable is modelled with a straight line member that lies along the chord of the cable and is pin-connected at both ends. The cable behaviour is then duplicated by making use of the equations for c and Δ_c .

Free body diagrams that show how the catenary cable and the bar are made equivalent are given in Figure A.80. In the cable, the tensions T_0 and T_1 include the force necessary to support the cable self-weight; consequently, the cable tension is not constant along the cable. The cable tension force is, of course, in-line with the catenary shape of the cable. For the bar, the self-weight is made the same as that for the cable, but the application of this weight is at the center of the bar, and the support for this weight is provided by equal external reactions at the member ends. Thus, if the weight of the cable is applied at the two member ends as a dead load force equal to $wc/2$, the cable tension becomes constant and acts in-line with the chord. The only approximation made is in placing half the dead load of the cable at each end instead of in true proportion according to α , where for tight cables, $\alpha = .5 + hr/6S$. It only remains to duplicate relative motion of B with respect to A in both the cable and the bar.

The relative motion of B with respect to A is split into the motions parallel and perpendicular to the chord line. The parallel motion is shown in Figure A.81. When the



Catenary Cable

Pin Ended Member

Figure A.80: Pin ended member equivalent to catenary cable.

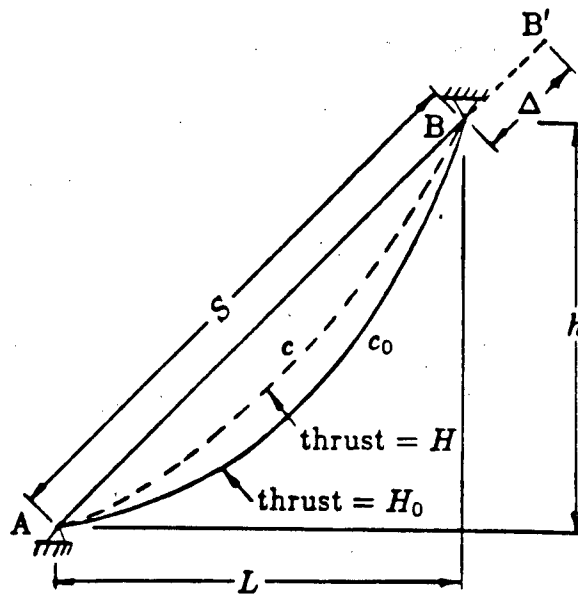


Figure A.81: Elongation of catenary cable.

horizontal end thrust changes from H_0 to H , point B moves to B' for an elongation Δ . This chord line elongation is accounted for by assigning an equivalent area to the bar, so that the calculation for the elastic elongation of the bar gives the actual elongation of the cable due to a change in sag as well as the elastic elongation of the cable.

In order to calculate Δ , the unstressed length of a cable USL is introduced. The USL is the length of an unloaded cable layed horizontally and straight on a uniform continuous surface.

$$\begin{aligned} USL &= c - \Delta_e \\ USL &= S \left(1 + \frac{r^2}{6} \cos^2 \bar{\theta} \right) - \frac{HL}{AE} \sec^2 \bar{\theta} \left(1 + \frac{r^2}{3} \right) \\ USL &= S - \frac{HL}{AE} \sec^2 \bar{\theta} + \frac{Sr^2}{6} \cos^2 \bar{\theta} - \frac{HLr^2}{3AE} \sec^2 \bar{\theta} \end{aligned}$$

Neglecting the $HLr^2 \sec^2 \bar{\theta} / 3AE$ term because it is second order compared to the $Sr^2 \cos^2 \bar{\theta} / 6$ term, and substituting for r and the trigonometric terms results in

$$USL = S + \frac{w^2 L^4}{24SH^2} - \frac{HS^2}{AEL}$$

Ignoring the elastic elongation of the cable between B and B' the elongation of the cable is given as the relative displacement of points A and B in direction S, as shown in Figure A.81.

$$\begin{aligned} \Delta &= USL_0 - USL \\ \Delta &= \left[S + \frac{w^2 L^4}{24SH_0^2} - \frac{H_0 S^2}{AEL} \right] - \left[S + \frac{w^2 L^4}{24SH^2} - \frac{HS^2}{AEL} \right] \\ \Delta &= \frac{S^2}{AEL} \left(H - \frac{w^2 L^5 AE}{24S^3 H^2} \right) - \frac{S^2}{AEL} \left(H_0 - \frac{w^2 L^5 AE}{24S^3 H_0^2} \right) \end{aligned}$$

If two new parameters are introduced

$$\beta^3 = \frac{w^2 L^5 AE}{24S^3}$$

and

$$\gamma = \frac{S^2}{AEL}$$

the elongation is expressed as

$$\Delta = \gamma \left(H - \frac{\beta^3}{H^2} \right) - \gamma \left(H_0 - \frac{\beta^3}{H_0^2} \right)$$

Gathering all the known initial condition terms along with a known cable elongation and equating them to the unknown final horizontal thrust terms gives

$$\frac{\Delta}{\gamma} + H_0 - \frac{\beta^3}{H_0^2} = H - \frac{\beta^3}{H^2}$$

To express this in dimensionless terms let $H = f\beta$ where f is a dimensionless variable which is a measure of the cable tautness. After simplification this yields

$$\frac{\Delta}{\gamma\beta} + f_0 - \frac{1}{f_0^2} = f - \frac{1}{f^2}$$

Let G equal the left hand side and the final result is

$$G = f - \frac{1}{f^2}$$

Thus, given G , the parameter f can be found and then the final horizontal thrust H of an elongated catenary cable can be calculated.

The reduced area \bar{A} of a pin ended member to give the same elongation Δ with this final thrust H is now derived. Figure A.82 shows the bar extension with a change in tension. The elastic elongation is

$$\Delta = \frac{(T - T_0)S}{AE}$$

or

$$\Delta = \frac{(H - H_0)S^2}{L\bar{A}E}$$

which gives

$$\bar{A} = \frac{(H - H_0)S^2}{LE\Delta} \quad (\text{A.16})$$

This equivalent area is used as the bar area in the next cycle of calculations to produce the elongation of the cable.

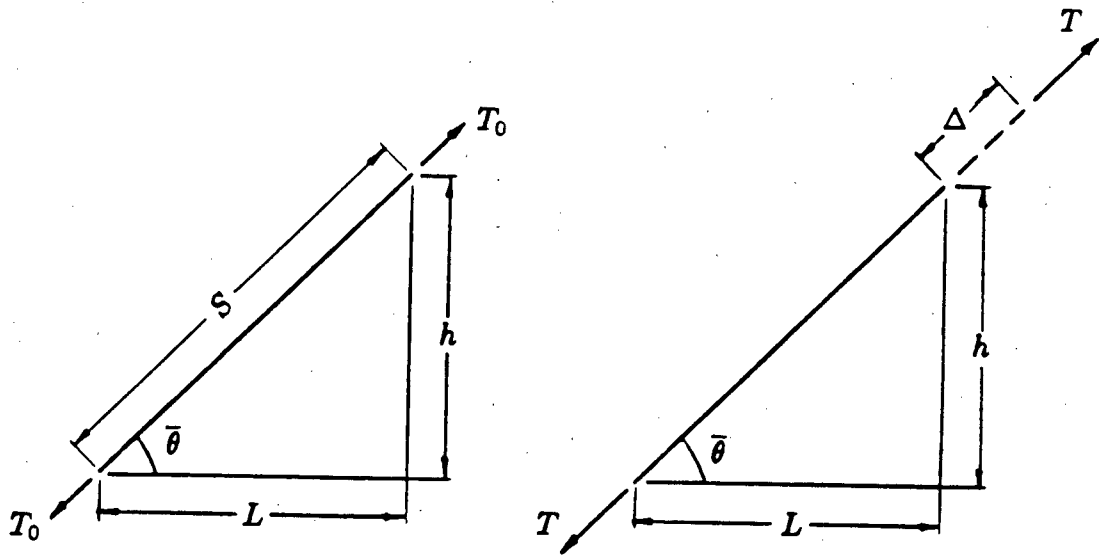


Figure A.82: Bar extension under a change in tension.

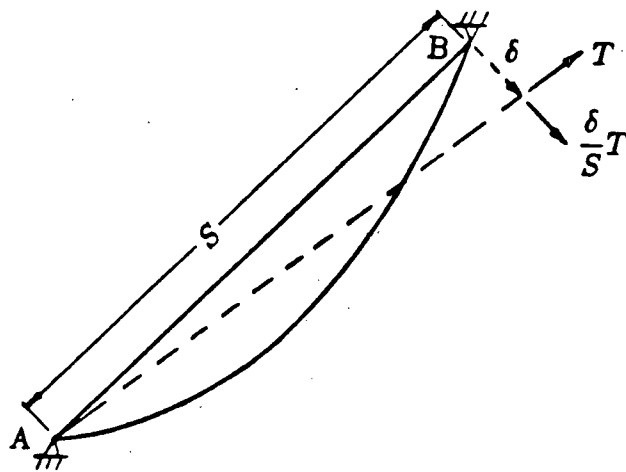


Figure A.83: Relative motion perpendicular to cable chord.

The relative motion perpendicular to the cable chord is shown in Figure A.83. The effect of the lateral motion δ is handled by augmenting the member stiffness matrix with the stability functions for a pin ended member. The 6 by 6 member matrix is augmented by the following matrix:

$$\begin{bmatrix} 0 & 0 & 0 & 0 & 0 & 0 \\ 0 & T/S & 0 & 0 & -T/S & 0 \\ 0 & 0 & 0 & 0 & 0 & 0 \\ 0 & 0 & 0 & 0 & 0 & 0 \\ 0 & -T/S & 0 & 0 & T/S & 0 \\ 0 & 0 & 0 & 0 & 0 & 0 \end{bmatrix}$$

The implementation of catenary cables in the computer program ULA is described in Appendix B.

Appendix B

ULA Implementation of Catenary Cable

The equation relating cable deflection to cable thrust using dimensionless parameters as derived in Appendix A is

$$G = f - \frac{1}{f^2} \quad (\text{B.17})$$

A graphical representation of this equation is given in Figure B.84.

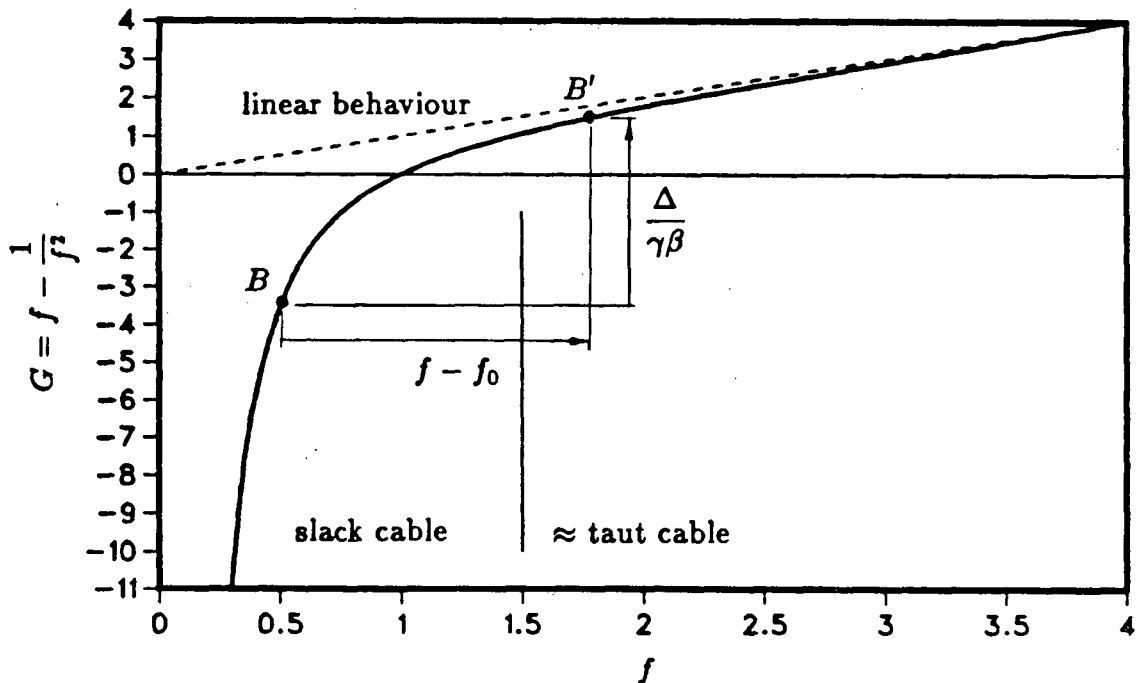


Figure B.84: Behaviour of catenary cable under load changes.

It can be seen that for large values of f the curve is linear with $G \approx f$ and for small values of f the curve equation essentially becomes $G = -1/f^2$. These observations are important because it will be necessary to calculate f from a known value of G . Note:

as point B goes to B' in Figure A.81, the cable action goes from B to B' on the graph of Figure B.84 to show how the cable tautness changes with the cable elongation.

A table look up procedure is necessary due to the nature of the equation being solved. The table should extend from $G = -\infty$ to $+\infty$, however, the previous observations suggest that the table can be cut off. The cut off points used are $G = -4$ and 3 which limit the error in calculating f from the approximate equations (after four iterations) to 0.0001%. The values used in the table look up procedure are calculated from Equation B.17 and are as follows:

G	f	Error
-4	.473	.035%
-3	.532	.017%
-2	.618	.005%
-1	.755	.016%
0	1.000	0%
1	1.466	.029%
2	2.206	.019%
3	3.104	.006%

The calculation of f is carried out as follows:

- If $G < -4$ then $f = 1/\sqrt{-G}$ then iterate on $f = 1/\sqrt{-G + f}$ four times.
- If $-4 \leq G \leq 3$ then use the table look up and interpolation procedure.
- If $G > 3$ then $f = G$ then iterate on $f = G + 1/f^2$ four times.

The implementation of catenary cables in ULA is necessarily an iterative one. The first iteration calculates forces and displacements for all members based on their original member stiffness matrices. If $P-\Delta$ effects are neglected, this single iteration would produce good results for most members. For a cable however, the highly nonlinear effect of the change in sag must be accounted for, and this is done by substituting

an effective stiffness into the cable stiffness matrix. Either E or A can be altered to produce an effective stiffness EA . A will be used as a matter of convenience only, due to the data requirements of ULA.

The procedure for catenary cable calculations in ULA is as follows:

1. Cable constants β and γ are calculated. (w is calculated using the input cable area and density. Absolute values of distances are used.)
2. Set $\bar{A} = A$.
3. Build the stiffness matrix using \bar{A} .
4. Solve the system of equations.
5. Calculate $\Delta = TS/\bar{A}E$ where T is the change in cable tension.

6. Calculate G where

$$G = \frac{\Delta}{\gamma\beta} + \frac{H_0}{\beta} - \frac{\beta^2}{H_0^2}$$

$$H_0 = \frac{|L|}{S} P_0$$

$$P_0 = \text{input cable prestress load (+ tension).}$$

7. Calculate f .
8. Calculate reduced area AA to look after the loss of stiffness due to sag.

$$AA = \left(\frac{S}{|L|} f\beta - P_0 \right) \frac{S}{E\Delta}$$

For a very small change in cable tension this equation becomes indeterminant in the form 0/0. To avoid this, a test is made such that

$$\text{if } \left| \frac{S}{|L|} f\beta - P_0 \right| < .03P_0 \text{ then } AA = A$$

where A is the original input area.

9. Set $\bar{A} = AA$.
10. Calculate the error $(AA - \bar{A})/\bar{A}$ and print it on the terminal screen.
11. If the error is too large, continue the calculations at step 3.

Appendix C

Data From Existing Cable Stayed Bridge Designs

This appendix contains the data acquired from four steel deck and five concrete deck cable stayed bridges. The data was obtained from design blueprints kindly provided by Bush, Bohlman and Partners.

The bridges and the design dates are as follows:

- Steel Deck Bridges

- ALRT – Advanced Light Rail Transit Bridge; Vancouver, British Columbia; February 1986.
- AF – Alex Fraser Bridge; Vancouver, British Columbia; September 1983.
- Q – Quincy Bridge; Quincy, Illinois; May 1983.
- S – Sunshine Skyway Bridge; Tampa Bay, Florida; May 1982.

- Concrete Deck Bridges

- ALRT - Advanced Light Rail Transit Bridge; Vancouver, British Columbia; January 1986.
- AF - Alex Fraser Bridge; Vancouver, British Columbia; September 1983.
- Q - Quincy Bridge; Quincy, Illinois; May 1983.
- WS - Weirton-Steubenville Bridge; Weirton, West Virginia - Steubenville, Ohio; February 1983.
- EH - East Huntington Bridge; East Huntington, West Virginia; October 1980.

C.1 Backspan Data from Bridge Designs for Simplified Backspan Model

	Steel Deck				
	ALRT	AF	Q	S	
E	200.	200.	200.	200.	1,000,000 kN/m^2
E_C	195.	195.	195.	195.	1,000,000 kN/m^2
γ_C	77.	77.	77.	77.	kN/m^3
I	.030	.281	.171	.180	m^4
$A_{C_{cent}}$.00235	.00466	.00656	.00478	m^2
l_B	138.00	182.75	134.00	146.80	m
h_{cent}	70.6	68.7	44.7	75.5	m
w_D	44.	135.	76.	127.	kN/m
w_L	16.	28.	9.33	18.66	kN/m
F	4847.	29929.	14069.	16494.	kN
θ_{cent}	51.4	39.5	35.9	48.5	deg
N	11	20	7	10	

	Concrete Deck					
	ALRT	AF	Q	WS	EH	
E	28.	28.	28.	28.	28.	1,000,000 kN/m^2
E_C	195.	195.	195.	195.	195.	1,000,000 kN/m^2
γ_C	77.	77.	77.	77.	77.	kN/m^3
I	.297	1.470	1.730	5.866	.636	m^4
$A_{C_{cent}}$.00350	.00420	.00656	.00668	.00355	m^2
l_B	138.00	195.25	134.00	209.70	185.3	m
h_{cent}	58.3	62.4	44.0	83.8	72.1	m
w_D	96.	196.	112.	270.	87.	kN/m
w_L	16.	28.	9.33	18.66	9.33	kN/m
F	14009.	52097.	19916.	59873.	16988.	kN
θ_{cent}	43.4	36.3	37.0	43.4	43.5	deg
N	12	30	12	21	14	

C.2 Backspan Ratios from Bridge Designs for Simplified Backspan Model

	Steel Deck				Concrete Deck					Value used
	ALRT	AF	Q	S	ALRT	AF	Q	WS	EH	
N	11	20	7	10	12	30	12	21	14	20
$\sin \theta_{cent}$.782	.636	.586	.749	.687	.592	.602	.687	.688	.7
h_{cent}/l_B	.512	.376	.334	.514	.422	.320	.328	.400	.389	.4
n	3.52	2.95	2.32	2.62	3.49	3.51	2.50	2.79	3.56	3
f	5.62	5.99	6.65	8.69	8.08	7.31	5.78	8.12	7.22	7
F/F_H	.063	.103	.069	.073	.134	.199	.060	.104	.131	.1
w_L/w_D	.36	.21	.12	.15	.17	.14	.083	.069	.11	.2

l_D/l_B	.402	.480	.610	.540	.405	.403	.566	.507	.397	(.47)
-----------	------	------	------	------	------	------	------	------	------	-------

C.3 Backspan Data from Bridge Designs for Backspan Model

	Steel Deck				
	ALRT	AF	Q	S	
E	200.	200.	200.	200.	1,000,000 kN/m^2
I	.030	.281	.171	.180	m^4
$A_{CN/2}$.00235	.00466	.00546	.00478	m^2
l_B	138.00	182.75	134.00	146.80	m
h_1	65.9	44.5	35.7	64.1	m
h_N	75.6	95.0	53.6	81.6	m
$h_{N/2}$	70.0	66.7	43.2	75.5	m
w_D	44.	135.	76.	127.	kN/m
w_L	16.	28.	9.33	18.66	kN/m
F	5520.	33800.	14760.	18100.	kN
$\sin \theta_{N/2}$.74	.59	.57	.72	
N	11	20	7	10	

	Concrete Deck					
	ALRT	AF	Q	WS	EH	
E	28.	28.	28.	28.	28.	1,000,000 kN/m^2
I	.297	1.470	1.730	5.866	.636	m^4
$A_{CN/2}$.00350	.00350	.00546	.00627	.00365	m^2
l_B	138.00	195.25	134.00	209.70	185.3	m
h_1	32.3	28.5	35.0	45.7	58.0	m
h_N	71.25	89.9	53.0	103.6	83.9	m
$h_{N/2}$	55.7	56.0	43.0	83.1	71.4	m
w_D	96.	196.	112.	270.	87.	kN/m
w_L	16.	28.	9.33	18.66	9.33	kN/m
F	15960.	59800.	23450.	71670.	20400.	kN
$\sin \theta_{N/2}$.64	.54	.54	.62	.62	
N	12	30	12	21	14	

$$E_C = 195,000,000 kN/m^2$$

$$\gamma_C = 77 kN/m^3$$

C.4 Backspan Ratios from Bridge Designs for Backspan Model

	Steel Deck				Concrete Deck					Value used
	ALRT	AF	Q	S	ALRT	AF	Q	WS	EH	
N	11	20	7	10	12	30	12	21	14	20
h_1/l_B	.478	.244	.266	.437	.234	.146	.261	.218	.313	.3
h_N/l_B	.548	.520	.400	.556	.516	.460	.396	.494	.453	.5
f	5.47	6.08	8.15	8.50	8.20	9.41	7.05	8.55	6.94	7
F/F_H	.077	.13	.082	.085	.17	.27	.09	.15	.18	.1
w_L/w_D	.36	.21	.12	.15	.17	.14	.083	.069	.11	.2
l_D/l_B	.418	.503	.645	.557	.423	.440	.640	.554	.426	.5

C.5 Bridge Data from Bridge Designs for Full Bridge Model

	Steel Deck				
	ALRT	AF	Q	S	
E	200.	200.	200.	200.	1,000,000 kN/m^2
E_T	28.	28.	28.	28.	1,000,000 kN/m^2
I	.030	.281	.171	.180	m^4
I_T	9.25	49.3	14.0	58.5	m^4
$A_{CN/2}$.00235	.00466	.00546	.00478	m^2
A_{CN}	.01466	.04153	.00896	.02652	m^2
ΣA_C	.02463	.08292	.03392	.04534	m^2
l_B	138.00	182.75	134.00	146.80	m
l_M	329.	462.	274.	366.	m
h_1	65.9	44.5	35.7	64.1	m
h_N	75.6	95.0	53.6	81.6	m
h_T	116.0	143.5	69.5	135.0	m
$h_{N/2}$	70.0	66.7	43.2	75.5	m
w_D	44.	135.	76.	127.	kN/m
w_L	16.	28.	9.33	18.66	kN/m
F	8630.	46780.	15000.	29050.	kN
$\sin \theta_{N/2}$.74	.59	.57	.72	
$\tan \theta_{NC/2}$.838	.667	.694	.800	
N	11	20	7	10	
N_C	13	24	7	12	

	Concrete Deck					
	ALRT	AF	Q	WS	EH	
E	28.	28.	28.	28.	28.	1,000,000 kN/m^2
E_T	28.	28.	—	—	—	1,000,000 kN/m^2
I	.297	1.470	1.730	5.866	.636	m^4
I_T	28.7	202.4	—	—	—	m^4
$A_{CN/2}$.00350	.00350	.00546	.00627	.00365	m^2
A_{C_a}	.01863	.04456	—	—	—	m^2
$\sum A_C$.03714	.10572	—	—	—	m^2
l_B	138.00	195.25	134.00	209.70	185.3	m
l_M	340.	463.	—	—	—	m
h_1	32.3	28.5	35.0	45.7	58.0	m
h_N	71.25	89.9	53.0	103.6	83.9	m
h_T	113.0	150.0	—	—	—	m
$h_{N/2}$	55.7	56.0	43.0	83.1	71.4	m
w_D	96.	196.	112.	270.	87.	kN/m
w_L	16.	28.	9.33	18.66	9.33	kN/m
F	22720.	74360.	23900.	87160.	38800.	kN
$\sin \theta_{N/2}$.64	.54	.54	.62	.62	
$\tan \theta_{N_C/2}$.718	.610	.642	.694	.706	
N	12	30	12	21	14	
N_C	15	35	12	24	16	

C.6 Bridge Ratios from Bridge Designs for Full Bridge Model

	Steel Deck				Concrete Deck					Value used
	ALRT	AF	Q	S	ALRT	AF	Q	WS	EH	
N	11	20	7	10	12	30	12	21	14	20
h_1/l_B	.478	.244	.266	.437	.234	.146	.261	.218	.313	.3
h_N/l_B	.548	.520	.400	.556	.516	.460	.396	.494	.453	.5
h_T/l_B	.841	.785	.519	.920	.819	.768	—	—	—	.8
f	5.47	6.08	8.15	8.50	8.20	9.41	7.05	8.55	6.94	7
F/F_H	.12	.18	.083	.136	.24	.34	.09	.18	.34	.1
w_L/w_D	.36	.21	.12	.15	.17	.14	.083	.069	.11	.2
l_D/l_B	.418	.503	.645	.557	.423	.440	.640	.554	.426	.5
l_B/l_M	.419	.396	.489	.401	.406	.400	—	—	—	.4
$E_T I_T / EI$	43.2	24.6	11.5	45.5	96.6	137.7	—	—	—	50
$A_{C_s} / \sum A_C$.595	.501	.264	.585	.502	.422	—	—	—	.5

$$A_{C_s} = \sum_{i=N}^{N_C} A_{C_i}$$

$$\sum A_C = \sum_{i=1}^{N-1} A_{C_i}$$

$$A_{C_s} / \sum A_C = \frac{\sum_{i=N}^{N_C} A_{C_i}}{\sum_{i=1}^{N-1} A_{C_i}}$$

Appendix D

Maximum Deflection and Moment

The maximum deflection and moment is expressed in terms of the span length for deflection and $w_L l^2$ for moment. The actual data from the computer analyses are used. (The actual values are not chosen to reflect real bridges—they are dictated by the dimensionless ratios.) The following table lays out the data and calculations for the maximum deflection and moment for the standard models:

	Simplified Backspan	Backspan	Full Bridge		
			Backspan	Mainspan	
l	180.	180.	180.	441.	m
w_L	32.7	27.2	19.0	19.0	kN/m
δ^*	0.0873	0.114	0.177	0.403	m
M^*	4039.	6000.	8734.	6759.	$kN-m$
δ^*/l	1/2062	1/1579	1/1017	1/1094	
$M^*/w_L l^2$	1/262	1/147	1/70	1/547	